Summer 2022

Structural History of the Bald Mountain Mining District, Nevada, USA

David Paul Ryan
Western Washington University, david.dpr.ryan@gmail.com

Structural History of the Bald Mountain Mining District, Nevada, USA

By

David Paul Ryan

Accepted in Partial Completion
of the Requirements for the Degree
Master of Science

ADVISORY COMMITTEE

Dr. Elizabeth R. Schermer, Chair

Dr. Sean Mulcahy

Dr. Cristina Garcia Lasanta

GRADUATE SCHOOL

David L. Patrick, Dean

Master's Thesis

In presenting this thesis in partial fulfillment of the requirements for a master's degree at Western Washington University, I grant to Western Washington University the non-exclusive royalty-free right to archive, reproduce, distribute, and display the thesis in any and all forms, including electronic format, via any digital library mechanisms maintained by WWU.

I represent and warrant this is my original work and does not infringe or violate any rights of others. I warrant that I have obtained written permissions from the owner of any third party copyrighted material included in these files.

I acknowledge that I retain ownership rights to the copyright of this work, including but not limited to the right to use all or part of this work in future works, such as articles or books.

Library users are granted permission for individual, research and non-commercial reproduction of this work for educational purposes only. Any further digital posting of this document requires specific permission from the author.

Any copying or publication of this thesis for commercial purposes, or for financial gain, is not allowed without my written permission.

David Paul Ryan

June 2022

Structural History of the Bald Mountain Mining District, Nevada, USA

A Thesis
Presented to
The Faculty of
Western Washington University

In Partial Fulfillment
of the Requirements for the Degree
Master of Science

by
David Paul Ryan
June 2022

Abstract

The Bald Mountain Mining district, like much of central Nevada, has experienced a complex deformation history. The mining district is considered here as a southern extension of the well-studied Carlin trend of gold deposits to the north. In order to gain a better understanding of how the Bald Mountain Mining District structural style relates to other structural models developed to the north in the Carlin trend, I completed a mapping and structural domain analysis in the district, with a focus on the North Mooney basin area where a high spatial concentration of Carlin-type gold deposits occur. The identification of structural domain boundaries and classes utilized a compiled database of historical mapping and structural measurements along with new mapping and cross section work. The domain analysis revealed four different classes of structural domains, of which monoclinal folds were determined to play the strongest role in gold mineralization.

Using the structural domain designations in addition to an analysis of the geometry of commonly occurring structures, I identified five structural styles at Bald Mountain: 1) kilometer-scale NNE- to NE-striking reverse faults and NNE- to NE-trending open to overturned folds; 2) kilometer-scale WNW- to NW-striking normal faults with oblique separation; 3) decameter- to kilometer-scale NNW-trending open folds, NNW-striking reverse faults, and N-striking thrusts; 4) meter- to decameter-scale NW-trending tight to close folds; 5) meter- to kilometer-scale N- to NE-striking normal faults. Evidence for structural reactivation and observations of the cross-cutting relationships between the five structural styles inform a relative sequence of deformational events at Bald Mountain.

These five structural styles were then considered with respect to regional tectonic events and their kinematic and timing relationships in order to assign deformational phases: 1) NNE- to

NE-striking reverse faults and NNE- to NE-trending open to overturned folds associated with episodic ESE- to SE-directed shortening through the Paleozoic to early Mesozoic; 2) WNW- to NW-striking strike-slip and tear faulting in the Late Jurassic to Cretaceous; 3) NNW-trending open folds, NNW-striking reverse faults, and N-striking thrusts with ENE-directed shortening through the Late Cretaceous to Eocene; 4) NW-trending tight to close folds with sinistral tranpression on WNW- to NW-striking faults during a mid-Eocene event associated with exhumation of the Ruby Mountain core complex; 5) N- to NE-striking normal faulting with NW-SE directed Basin and Range extension from the Miocene.

The five structural styles were then compared to previous work including structural models developed in north-central Nevada. Deformation events are similar between the northern Carlin trend and Bald Mountain. Primary differences between the Bald Mountain structural history and the structural models in the northern Carlin trend include the documented Eocene folding event, and a major WNW-striking basement-seated feature with parallel structures that have a significant strike-slip component and partition Bald Mountain into discrete kilometer scale structural domains. Further work to add value to targeting and exploration should place an emphasis on identifying major WNW- to NW-striking faults and understanding their kinematics. Knowledge of these structural boundaries along with how structural styles change across them will help to constrain targeting and lend insight to the significant role that strike-slip faulting played in the Bald Mountain Mining District's complex deformational history.

Acknowledgements

Thanks to Kinross Gold Corporation for funding this study and to the crew of Bald Mountain exploration geologists for giving me a crash course on 500 million years of rocks in the largest mining claim in the country. This study relies on decades of work done by many great geologists, and I am grateful to be able to stand of the back of those giants. My advisory committee provided valuable feedback in the writing process, and special thanks to Liz who helped guide me through the scientific process while ensuring rigor. Further financial support for this study was provided by the Geological Society of America and Western Washington University.

Table of Contents

List of Tables and Figures

List of Tables:

List of Figures:

1. Introduction

The Carlin trend of Nevada, USA is the type area for Carlin-type gold deposits (Figure 1). These deposits comprise the world's largest hydrothermal gold resource, having produced over 85 million ounces of gold through 2017 and containing 179 Mt of proven and probable reserves as of 2020 (Carlin Complex-Mining Data Online, 2022). Carlin-type gold deposits (CTGD) are characterized as being disseminated, stratabound, carbonate-hosted ore bodies with strong lithologic and structural controls on mineralization (Cline et al., 2005). The structural and stratigraphic features that allow for the prolific gold endowment in the Carlin trend developed throughout the Neoproterozoic to Eocene tectonic history of central Nevada and included abundant carbonate sedimentation followed by the formation of regional fold-thrust belts and magmatism (Figure 1). Previous studies (e.g., Teal and Jackson, 1997; Cline et al., 2005; Muntean et al., 2007; Rhys et al., 2015) have identified key structural features and stratigraphic horizons that concentrate Au-bearing fluids in Carlin-type systems into economically mineable deposits in the Carlin trend west of Elko (Figure 1). While models relating Carlin-type gold mineralization to structure and stratigraphy have been developed in the Carlin trend (Teal and Jackson, 1997; Rhys et al., 2015), uncertainties remain in how well these models correlate with other occurrences of CTGD in Nevada.

The Bald Mountain Mining District (BMMD) is owned by Kinross Gold Corporation and is the largest private mining package in the United States, containing 798 koz of proven and probable gold reserves as of December 2021 (Bald Mountain-Operations, 2022). BMMD is located 130 kilometers from the Carlin trend along a postulated southeast projection and hosts similar Carlin type gold mineralization despite the geographic separation (Figure 1). While the BMMD shares a partial tectonic history with the Carlin trend (Nutt et al, 2000), its geographic separation can be expected to result in differences of tectonic influence and incongruencies with structural models derived in north-central Nevada (e.g., Rhys et al. 2015). Some of these primary geographic differences include the BMMD being located to the east

of the Roberts Mountain thrust, within the Antler foreland basin, and situated near the boundary of the Central Nevada Thrust Belt and Eastern Nevada Fold Belt in the Sevier orogeny hinterland (Long et al., 2015) (Figure 1).

Exploration models and tectonic history derived for the Carlin trend in northern Nevada (e.g., Rhys et al., 2015) need to be compared in the apparent southeast extension of the trend at BMMD in order to address questions of how deformation changes across the region and how this may affect the structures that control Carlin-type mineralization. The present study in the BMMD addresses local deformation and the resulting structural framework as it relates to hydrothermal gold mineralization. In order to address the incomplete understanding of how BMMD structurally relates to the Carlin trend and exploration models therein, I completed a mapping and structural domain analysis in the district, with a focus on the North Mooney basin (NMB) area where a high spatial concentration of Carlin type gold deposits occur (Figure 2). Structural domains identified in the BMMD are interpreted with respect to regional tectonic events and are compared with structural features that have been identified in exploration models to play a key role in Carlin-type mineralization to the north (Rhys et al., 2015; Griesel et al., 2020). Comparing the geometry, kinematics, and timing of mapped structures at Bald Mountain with the Rhys et al. (2015) structural model to the northwest in the Carlin trend will yield insight to variations in deformation style across northern and eastern Nevada and aid in further exploration efforts.

Geologic History of Central Nevada and the Bald Mountain Mining District

The Great Basin physiographic province, spanning the entirety of Nevada, contains a prolific gold endowment that accounts for about 83% of U.S. gold production and makes the state of Nevada the fifth largest gold producer in the world (Perry and Vishner, 2019). This high gold productivity is due to abundant sedimentation, a complex deformation history, and a resulting structural architecture primed to move and trap gold bearing fluids. The tectonic history of east-central Nevada is summarized in this

section to provide a context for structural development at Bald Mountain and for comparison to structural models in the Carlin trend (Figure 3).

Beginning in the Neoproterozoic, rifting of the Rodinian supercontinent established a steeply dipping normal fault basement architecture that controlled subsequent passive margin stratigraphy and is thought to control regional-scale gold trends in northern Nevada (Embso et al., 2006; Muntean et al., 2007). A post-rifting passive margin was established by the middle Cambrian and miogeoclinal sedimentation continued through the Late Mississippian along the continental margin (Figures 3 and 4) (Poole et al., 1992; Miller et al., 1992; Dickinson, 2006). Miogeoclinal shelf sedimentation was interrupted in the Late Mississippian with the Antler Orogeny and emplacement of the Roberts Mountain allochthon above the Roberts Mountain thrust (RMT) (Figures 1, 3, and 4) (Speed and Sleep, 1982). To the west of the BMMD and in the Carlin trend, the RMT (Figure 1) placed Ordovician to Devonian deep marine, sedimentary, and volcanic rocks over younger shelf carbonates (Figure 3). In the BMMD, influence of the Antler orogeny is recorded by deposits filling the Antler foreland basin (Figures 1,3). These basin-filling deposits conformably overlie the Lower Mississippian deposits at Bald Mountain in a succession of 3100' (945 m) of Mississippian subaerial siliciclastic sediments which include the Chainman and Diamond Peak formations (Figures 3, 4) (Poole, 1974; Sandberg and Poole, 1977). The Antler foreland continued to evolve into the Middle Pennsylvanian as northwest-southeast directed compression resulted in thin-skinned folding, faulting, and uplift (Trexler et al., 2015). The Antler Overlap Sequence (Figures 3 and 4) unconformably overlies deformed rocks associated with the RMT and Antler Foreland Basin (Saller and Dickinson, 1982). This unconformity is noted in the southern BMMD at Buck Mountain (Figure 2) below Pennsylvanian carbonates (Ely Limestone, Figure 4; Pp and Pe Units, Figure 7) (Cashman and Sturmer, 2021).

The Late Permian-earliest Triassic Sonoma orogeny emplaced the Golconda allochthon over the Roberts Mountain allochthon and Antler Overlap sequence along the Golconda thrust (Figures 1 and 3). Whether deformation related to the Sonoma orogeny extends as far east as the Carlin trend and BMMD is

debated (Rhys et al. 2015), however three possibly Sonoma-related late Paleozoic to early Mesozoic thin-skinned fold sets have been identified in Antler foreland deposits of the northern Carlin trend near Elko, NV. (Trexler et al., 2015). Rocks at Buck Mountain exhibit fold geometries that differ from later Mesozoic geometries and may record a post-Antler and pre-Sonoma deformation event (Whitmore, 2011) (Figure 2).

Later orogenic events include the Early to Middle Jurassic Elko Orogeny which is coeval to the Luning-Fencemaker fold and thrust belt (Figures 1 and 3). The Elko Orogeny deformation is dated by Late Jurassic intrusion cross-cutting deformed rocks and is associated with ESE-directed folds and thrusts as far east as Utah (Thorman, 1991) and SE-directed recumbent fold nappes in the RMCC (Price, 2010). Workers continue to debate the significance of deformation from the Late Mississippian initiation of the Antler orogeny to the earliest Mesozoic with respect to distinct orogenic events vs. a continuum of shortening (Decelles and Coogan, 2006; Rhys et al., 2015; Trexler et al., 2015; Thorman et al., 2020).

During the Late Jurassic, the area of BMMD was in a continental back-arc setting and undergoing east-directed shortening (Dickinson, 2006; Nutt and Hofstra, 2007) (Figure 3 and 4). Numerous regional plutons were emplaced from Late Jurassic to Early Cretaceous, including the Bald Mountain pluton and associated dike swarm (Ji) (Figures 3 and 4). The Bald Mountain pluton has been dated at 159 Ma (Mortenson et al., 2000), is quartz monzonite to granodiorite in composition, and spatially associated with reduced intrusion-related gold deposits in BMMD that predate the CTGD (Nutt and Hofstra, 2007). The pluton is emplaced within a regional-scale NW- to WNW-trending structure known as the Bida trend (Figure 2). Based on magnetotelluric data, the Bida trend is interpreted by Wannamaker et al. (2002) to be related to a basement structure and the pluton to extend to a depth of up to 12 km.

Bald Mountain lies in the hinterland of the Late Jurassic to Eocene Sevier fold and thrust belt of central Utah which is partly coeval with the Middle Jurassic to Early Cretaceous Luning-Fencemaker thrust belt to the west of BMMD (Figures 2 and 3), and the two belts may share a common mid crustal detachment (Wyld, 2002). BMMD lies at the boundary of two temporally overlapping middle to Late

Cretaceous age fold/thrust belts termed the Central Nevada/Eureka Thrust Belt (CNTB) and the Eastern Nevada Fold Belt (ENFB) (Figure 2) (Long et al., 2004; Long; 2012; Long, 2015). These deformation belts are thought to represent hinterland components of the Sevier fold and thrust belt in western Utah (Taylor et al., 2000; Long et al., 2014) (Figure 3). Druschke et al. (2009) and Long et al. (2015) cite depositional, structural, and thermochronological evidence that the Sevier hinterland in the area of BMMD may have experienced localized zones of episodic synconvergent extension, temporally overlapping Sevier foreland shortening to the east.

The Great Basin transitioned from localized extensional domains to a broadly extensional tectonic regime in the early Cenozoic (e.g., Dickinson, 2006). Initial exhumation of the Ruby Mountain core complex (RMMC) (Figure 1) began in the Paleocene to Eocene and was followed by rapid uplift in the Oligocene and Miocene (McGrew and Snee, 1994; Nutt and Hofstra, 2000). BMMD is located to the south of the RMCC (Figure 1), and large magnitude extension associated with the core complex is not recognized at BMMD, which lacks the metamorphic signature and exposure of Archean rocks (Nutt et al., 2000). Various workers (e.g., Ketner and Alpha, 1988; Nutt and Good, 1998; Nutt et al., 2000) have documented local folds in Eocene sediments which are uncomformably overlain by volcanics. This latest recorded shortening is interpreted to be related to initial unroofing of the Ruby Mountain core complex which resulted in transpression at the margins of the range (Nutt and Good, 1998). The extensional tectonic regime resulted in steeply dipping normal faults and the formation of half-grabens throughout northern Nevada (Henry et al., 2011).

Low-angle detachment faults associated with extension, also referred to as attenuation faults, have also been noted by previous workers in BMMD (e.g., Nutt et al., 2000; Nutt and Hofstra, 2007; Mach et al., 2015). While these detachment faults may not control mineralization directly, they cut and translate sections of deposits across the district and are locally intruded by Jurassic dikes indicating these low angle structures range from pre-159 Ma to post-40 Ma in age (Nutt et al., 2000; Mach et al., 2015). In late Miocene time the direction of extension rotated from NE-SW to NW-SE in the northern Basin and

Range (e.g., Wernicke, 1992), and extension in this direction continues to present day. Carlin-type gold mineralization deposits throughout Nevada are associated with the initial onset of extension and resultant volcanism between ~42 and 36 Ma (Ilchik, 1990; Nutt et al., 2000; Cline et al., 2005).

Carlin-Type Gold Deposits Overview

Sediment-hosted Carlin-type gold deposits are Eocene in age and dominantly found in the east and south portions of BMMD (Figure 2). Carlin-type gold deposits have magmatic-hydrothermal fluid origins. Weakly acidic Au-bearing fluids react with carbonate bearing rocks in a process of dissolution and decalcification, and the resulting Au mineralization is widely disseminated and liberated as sub-micron-sized gold in the form of arsenian pyrite (Hofstra and Cline, 2000; Cline et al., 2005; Muntean, 2011). Deposits are typically stratabound at intersections of high angle normal faults with wide damage zones (Hammond and Evans, 2003) and at lithological contacts with changes in porosity and permeability (Nutt et al., 2000; Rhys et al., 2015). The Carlin-type mineralization appears to track with a northeast to southwest sweeping magmatic arc and shift to regional extension. The Carlin-type mineralization throughout northern and eastern Nevada occurred between 42 and 35 Ma (Ressel, 2006; Muntean et al., 2011). Mineralization is also coeval with local volcanism and other metasomatic alteration (Rhys et al., 2015).

Summary of the Rhys et al. (2015) Structural Model of the Carlin Trend

Comparison of structural domains and features at BMMD to other deformation models in the Carlin trend is useful in understanding parallels between exploration strategies. Rhys et al. (2015) provide a classification of major regional tectonic events and associated structural geometries as they relate to gold mineralization in the northern Carlin district of Nevada. The following is a brief summary of the northern Carlin trend structural model after Rhys et al. (2015): The model classifies structures by

orientation and kinematics with respect to major tectonic phases, with Phases I-III being contractional, and Phase IV being extensional (Table 1).

Phase I corresponds to the Antler orogeny and emplacement of the Roberts Mountain allochthon in the northern Carlin trend. The RMA plays a key role in Au mineralization as it creates a relatively impermeable boundary against which mineralizing fluids rising toward the surface through fault conduits are impeded and forced outward into reactive carbonate strata (Muntean, 2011). Most gold deposits in the Carlin trend have been discovered in structural windows through the impermeable upper plate of the Roberts Mountain Thrust (RMT) into the reactive carbonates of the lower plate (Figure 3).

Phase II deformation was developed during the Late Paleozoic to Early Triassic Humboldt and Sonoma orogenies and includes the Golconda Thrust (GT) (Figure 1) associated with the latter. Deformation of Phase II may extend into the Mesozoic and record multiple superposed events. This phase locally folds and offsets Phase I structures, and it is generally defined by the development of north to northeast-trending and east-vergent folds along with west to northwest dipping reverse faults. The folds can be several kilometers in scale and often have short or structurally truncated steeply dipping to overturned eastern limbs and gently dipping upright western limbs (Rhys et al., 2015 and references therein).

Phase III deformation is characterized by northwest-trending upright folds and conjugate sets of moderate to steeply southwest- and northeast-dipping reverse faults (Rhys et al., 2015). Phase III structures are associated with the Laramide and Sevier orogenies and lack a consistent vergence direction. Some Phase II reverse faults were remobilized during Phase III. The timing of Phase III deformation is difficult to constrain, but associated structures generally cut Jurassic dikes and Eocene dikes cut across structures suggesting a post-Jurassic, pre-Eocene age of deformation (Rhys et al., 2015 and references therein).

Phase IV is characterized by a regional shift to an extensional tectonic regime that spans the Cenozoic. Major extension-related normal faults have dominantly northwest, north, and northeast strikes with moderate to steep dips. Normal fault strikes oblique to these dominant directions are likely inherited and reactivated from earlier contractional or strike-slip phases. Normal fault kinematic indicators often overprint and mask earlier reverse fault kinematic indicators making differentiation of newly established and reactivated structures difficult. Apparent stratigraphic displacement across major northern Carlin trend northerly-striking normal faults is locally >1 km, and these major faults often offset north-trending Phase II folds (Rhys et al., 2015).

Rhys et al. (2015) note that Carlin-type gold mineralization targets in the Carlin trend occurs in structural culminations and intersections of folds and faults which formed throughout the four phases. One such common target occurs with fault-propagation-related asymmetric anticlines in which the steeper fold limb is typically steeply down faulted, and where the fold hinges may act as traps for gold-bearing fluids. The present study places emphasis on identifying similar structural domains within the BMMD.

North Mooney Basin Area

This study focuses on North Mooney Basin (NMB) area (Figures 2, 5 and 6) due to its high spatial concentration of CTGD that share common structural features and stratigraphic horizons (Figures 3-7). Major trends and structural features that are within and bound the NMB are described below. Many of these structural features are also represented in the BMMD area. The NMB is a ~1 km long NNE trending graben that hosts seven open pit mined Carlin-type gold deposits along its horst block margins (Figure 2).

Stratigraphy of the North Mooney Basin

The stratigraphic section that comprises the North Mooney basin is approximately 4,750' (1,448 m) thick, however Carlin type gold mineralization always occurs within a narrow 600' (183 m) band (Figure 4). All the CTGD of the NMB host mineralization at the Guilmette/Pilot (Dg/Mp), Pilot/Joana (Mp/Mj), or Joana/Chainman (Mj/Mc) stratigraphic horizons (Figures 4 and 5). Favorable carbonate stratigraphy in conjunction with structure is necessary in controlling Carlin-type mineralization. Additionally, rheological contrasts between thick bedded limestone and shale units and the development of jasperoids influence structural development. Note that the mining industry in the United States typically uses the Imperial system of measurement which this study includes as unit thicknesses measured in feet. Detailed stratigraphic descriptions of units in the NMB are provided in Appendix 1.

Structural Overview of the North Mooney Basin

An initial comparison of historically mapped structures in the NMB (Kinross Gold Corp. and previous owners, unpublished mapping; Nutt et al., 2000) suggests broad similarities in the style and geometry of structural features between the NMB and those described in the Carlin trend by Rhys et al. (2015).

Folds in the NMB typically trend from NW (Figure 6), plunge gently to the north or south, have upright to steeply east-dipping axial planes, and have open to tight interlimb angles. Fold shape and style varies strongly by lithology and competency contrasts between units. NW- to N-trending folds have axial traces on the order of tens of meters, while NNE- to NE-trending folds tend to be meter-scale and discontinuous. Decameter-scale folds in the NMB typically occur adjacent to trend-parallel faults, and this parallel relationship of fault strike to fold trend occurs on a larger kilometer-scale throughout the BMMD (Figure 5).

Both normal and reverse faults occur in the NMB, and many faults display kinematic indicators of multiphase movement. Normal faults in the NMB have dominantly NW and NE strikes with moderate to steep dips. There is a complex and often mutually cross cutting relationship between NE- and NW-striking normal faults. These normal faults are primary ore controlling structures, and they also define the graben feature that is the Mooney Basin (Figures 5 and 6).

2. Methods

I completed field work at Bald Mountain over the summer of 2019 and 2020. Initial time was spent becoming familiar with the district geology through guided tours by Kinross geologists, logging reverse circulation and diamond core drill holes, and compiling historical to recent geologic data in both hard copy and digital formats. Later work focused on field mapping, field checking historical data, geodatabase organization, and updating compilation mapping.

Relevant structural data spans nearly fifty years of geology work in the BMMD with much of the historical data being unutilized. Digital mapping and structural data in AcQUIRE and ArcGIS geodatabases were compiled, validated for database entry completeness, and locally spot checked in the field for accuracy. Additional paper mapping with relevant structural data was digitized and incorporated into the databases. A final digital compilation consisted of ≥ 8900 spatially referenced structural point data features of predominantly bedding and fault measurements throughout the district. I created a geodatabase and map package which contains all the compiled structural and mapping data used in this thesis. This geodatabase may be accessed with permission from Kinross Gold Corp., Bald Mountain: *(Data Supplement 1, an ArcGIS Pro map package (NorthMooneyMapping_Base.mmpk).*

To better view and analyze, the surface bedding measurements (N ≥ 6200) were characterized into 32 bins according to their dip direction and dip magnitude. Dip directions were divided into eight equal azimuthal sub-bins (1-8) of 45 degrees each. Dip magnitudes were divided into sub-bin ranges of 0°- 20°, 20°- 40°, 40°- 60°, and 60°- 90° (A-D). The two sub-bins for each bedding measurement were concatenated into one of 32 possible bins to be symbolized in ArcMap (Figure 9). Larger arrow symbols were used for larger dip magnitudes to visualize and test the hypothesis of steep monocline limbs being associated with mineralization. A final compilation of the of the district symbolized bedding map is shown in Plate 1. Note my updated mapping (outlined in Figure 3) may not agree or align with mapping done by other workers outside of my areas of focus. Also note, some previous workers rounded dip measurements to the nearest five-degree increment which affects the grouping of poles to bedding on some stereonets.

After compiling the structural dataset, I completed a structural domain analysis using the compiled structural measurement data visualized as dip domain maps (Figure 10; Plate 1) (e.g., Long, 2015). Structural domains were identified through which patterns were recognized, analyzed, and compared to structural models proposed by previous workers at BMMD and in nearby districts (e.g., Nutt and Hofstra, 2000; Muntean, 2010; Rhys et al., 2015; Mach et al., 2015; Long, 2015). Structural domains are defined here as structurally homogeneous areas with respect to a structure type. Structural domain selection consisted of picking surface data representing recognized structural features and their general trends; domains are described in the Results section and Tables 2 and 3. Domain selection was an iterative process of choosing bedding measurements at pit to district scales, then plotting those data on a stereonet and using statistical deviation (Kamb) contouring (Allmendinger and Cardozo, 2012) to quantify distributions. Additionally, *Stereonet v.10* is used to calculate fold axes (FA) using the Bingham Axial Distribution function and to calculate fold axial planes (AP) using the Axial Plane Finder tool and a picked representative pole to each fold limb. Both analyses assume a cylindrical fold shape. Stereonets with contoured plots of poles to bedding planes, geologic unit map patterns, mapped folds and faults, and

cross sections are used to determine if the selected domain meets the criteria of the structural domain definition. Later stages of domain selection were further iterated with drawn domains being reassessed and redefined based on my cross-section construction and field mapping.

Resulting structural domains (Tables 2 and 3) are further constrained by their commonality throughout the BMMD, occurrence at a scale of decameter or larger, and domain bounding features e.g., a single cylindrical fold domain is defined by a single fold axis orientation, while parasitic fold domains include antiform/synform pairs with a consistent fold axis orientation at various scales. Fault domains are bounded by mapped faults and contain either fault parallel or discordant bedding. Homoclinal domains include a sequence of strata with uniform dip direction and local minor variations in dip magnitude. Roll over domains are monoclines with abrupt, steep limb roll over. Detachment domains are uniformly dipping blocks that are bounded by a low angle younger over older normal fault (Table 2, Figure 10, Plate 1). Emphasis for follow up study and field mapping was given to structural domains exhibiting fault and fold relationships such as monoclines with abrupt steep limb rollover, asymmetric folds possibly related to fault propagation folding, and anticlinal hinges cut by faults (Tables 2 and 3). Additionally, the vergence of first, second, and third-order folds was used to determine folding wavelength and symmetry of regional folds that can be associated with distinct orogenic events to help determine the deformation history.

Final mapping products are a compilation of integrated subsurface drilling data, cross sections, and revised field mapping done by the author. My mapping served to spot check previous mapping efforts for accuracy and consistency as well as to infill map areas of interest in greater detail. Work was focused on existing deposits and open pits as well as areas identified to be of significance using compiled structural data and domain identification techniques described above. The included map figures and ArcGIS Pro map package (*Data Supplement 1)* are both observational and interpretive in nature, and they integrate various datasets including historical mapping, drill hole lithologies at surface below cover, high resolution aerial photos and digital elevation models, and iterative cross sections.

In areas with poor exposure or ambiguity, drill logs were used to identify the pre-Quaternary units that are closest to surface from drilling collars (the borehole location at the surface). These drill collar lithologies were used in the map creation to effectively strip away cover, providing a bedrock map, and to aid in the drawing unit contacts as well as in the interpretation of structures. Note that due to ambiguity in previous mapping and the lack of a consistent standard over time, depositional unit contacts are included without symbols that define the contact as definite, approximate, inferred, or concealed. Faulted contacts were drawn as either "inferred" or "measured" with dashed and solid lines, respectively (Figure 8). Where faults are inferred, the traces are drawn to project across topography in accordance with nearby fault measurements and drill collar lithology changes. My mapping of structures does not always agree with existing and historically mapped structures. To differentiate the two, my structures are symbolized by thicker black lines while historically mapped structures are in blue (Figures 5-8). Cross sections using my surface mapping, geometrically corrected drillhole traces, and drill logs were constructed in order to interpret subsurface geology and inform surface mapping based on the unit the drillhole collared in. Inclined drill holes were geometrically corrected using surface traces constructed from down-hole surveys. This geometric correction used the length of the surface trace and angle between the surface trace and the cross section line to calculate the plotted apparent dips of the drill holes in cross section view and the unit depths. Drill holes that were selected to be included in cross sections have an inclination azimuth approximately parallel to the cross section line and collared within 200 meters of the section line. Cross section lines assume a slice thickness which is wide enough to contain the drill holes plotted in each section.

All maps use a UTM NAD 27 zone 11N coordinate system, and as the Imperial system is the standard used within the United States mining industry all map contour and cross section elevations are listed in feet (‘). Note that field mapping notation for planar orientations used dip/dip azimuth (xx/xxx) and linear features therefore use a trend/plunge (xxx/xx) notation in this study to avoid confusion. Labels are provided when dip/dip azimuth is converted to strike/dip.

3. Results

Structural Domain Analysis

The following section describes select structural domains that were identified throughout the entire BMMD (Tables 2 and 3) (Plate 1). Other identified domain outlines and labels are included in *Data Supplement 1*.

Domain Class A:

Class A domains are composed of large areas of homoclinal bedding, major fault blocks, and detachment fault hanging walls (Table 2). The northern portion of the BMMD can be broadly divided into large structural blocks that dip ~10-30° west to southwest (SWB01) (Figures 11 and 12) or east to southeast (SEB01) (Figures 13 and 14) (Table 3). These km-scale blocks, with minor, local internal variations, are bounded by both high and low angle normal faults. Where these homoclinal domain blocks are cut by internal faults, similar orientations of bedding on either side of the faults suggests the faults are steep and non-rotational. Silurian and younger rocks on the west side of the North Mooney Basin are dominated by gently east dipping stratigraphy as highlighted by SEB01 (Figure 13). Differences in east vs. west dipping homoclinal blocks of Silurian and younger strata may be a result of the Ordovician Eureka Quartzite acting as a detachment surface, along which attenuation faulting occurred (Nutt and Hofstra, 2007).

Domain Class A also contains smaller scale blocks with east and west dip directions that are bounded by steeply dipping, km-scale strike length, normal faults (TOP01/02) (Table 3). Examples of these blocks are noted in the Top deposit area (Figures 3 and 10, Plate 1) and are inferred to be related to block rotation along the West Top and Bida trend related faults (Figures 15 and 16). TOP01 is a gently

W- to WSW-dipping block that is bounded by a NW-trending Bida structure and NNE-trending Dynasty fault related structures. TOP02 contains a fault block on the north side of the Top pit. This east-dipping block is bounded by the West Top fault to the west and by the Dynasty fault to the east, while the NE and SW boundaries are controlled by NW- to WNW-trending Bida trend structures. Similarly juxtaposed east- and west-dipping blocks are noted to the south along strike of the steeply east-dipping Dynasty fault. Revised mapping and the significance of the Dynasty fault are discussed below.

Domain Class B:

Domain Class B structures are classified as upright, gentle, km-scale anticline and syncline pairs that are sub horizontal to gently plunging NW to NNW or SE to SSE. These folds are identified in the southwest of the BMMD in the Buck Pass area (Figure 3) where they deform Mississippian through Permian units in Domains BUC05/06 (Table 3) (Figures 10, 17, and 18). The general fold trend in the southern district, including the Yankee and Vantage deposits, is most clearly represented in the Buck Pass area (Figure 17) (Rigby, 1960; Nutt, 2000). NW- to NNW-trending folds are also identified in the North Mooney Basin area (Figure 6), although they tend to be at a smaller (decameter) scale and more discontinuous in comparison to the southern district. NNW-trending folds are also noted in the Snake Eyes, Galaxy, Winrock, and Royale areas, and are discussed below.

Domain Class C:

Domain Class C structures are classified as N to NNE-trending, horizontal to gently plunging, moderately inclined, close to tight, asymmetric folds. These N-S trending folds of Domain Class C are locally associated with thrust faults. One example is noted in the LJ pit (Figure 3) where the Hamburg formation (Ch) is thrust over the Dunderberg formation (Cd) and folding occurs in the hanging wall (R. Morrell, pers. comm., 2020). Another km-scale example includes Alligator Ridge along with mapping by

Nutt and Good (1998) shows a thrust fault exposed on the NE side. The Alligator Ridge domain contained in GAT01 (Figure 19) contains steeply dipping to overturned beds on the east side of the N-S trending anticline of Alligator Ridge and is interpreted to be part of a km-scale east vergent fault propagation fold (Figure 19).

Domain Class D:

Domain class D is characterized by monoclines that have a limb that abruptly rolls over to a steep dip. The limb roll-over is variably accompanied by a strike-parallel fault near the fold hinge. The roll-over may be associated with normal faults parallel to bedding strike, flexural slip at a significant rheological contrast between units, fault bend folding, or possibly with underlying structures such as a fault propagation fold. Example domains include SNK04, GAL01, RYL01, and WIN01(Table 3) which are described in detail below.

Structure of the North Mooney Basin Area

After completing the structural domain analysis, I focused mapping and investigation on Class D domain areas in the North Mooney area, in part because the Rhys et al. (2015) deformational model of the northern Carlin trend notes the importance of fault-propagation-related asymmetric anticlines in which the steeper fold limb is typically steeply down faulted, and where the fold hinges may act as traps for gold bearing fluids. With the exception of the Class C GAT01 domain and a fault propagation anticline revealed through drilling in the Red Bird deposit (Mach et al., 2015), it is difficult to identify with certainty folds that are directly related to thrust fault propagation and share the N-S to NNE trend of mapped reverse faults along Alligator Ridge and the Mooney Basin. Monoclinal folds with steep roll over are abundant in the North Mooney Basin. The most similar mineralization-related structural geometries at BMMD to those described by Rhys et al. (2015) are the monoclines within the North Mooney basin area

noted in Domain Class D. Areas within the North Mooney basin that contain Domain Class D features are described below.

Snake Eyes Area

The Snake Eyes area is an active exploration area east of the Poker Flats open pit in the North Mooney basin (Figures 3 and 6), however minable mineralization in the area has not yet been identified. The area contains well exposed outcrops of the Dg/Mp contact along a haul road cut and of variably silicified Mj limestone and jasperoid cropping out to the east of the road (Figure 4). Two SNK domains, SNK03 and SNK04, were analyzed, and are classified as domain Classes B and D, respectively (Figure 20).

Folds

Folding in the Snake Eyes area occurs on two scales, the first is captured within the SNK03 domain. Domain SNK03 contains a series of Gently NNW plunging folds (349/04) (trend/plunge), with steeply inclined axial planes, open interlimb angles, as sub-cylindrical anticline and syncline pairs on a decameter scale (Figure 20 and Figure 21A). The larger scale fold occurs as a Class D monocline rollover ~500 m long, captured in the SNK04 domain (Figure 20 and 21B). The SNK04 domain (Figure 21B) contains an anticlinal limb that rolls over abruptly with steeply east dipping to sub-vertical Dg limestone and Mp siltstone. The bedding rolls over at the north-striking Dg/Mp contact. Up section and to the east, the steeply dipping fold limb shallows back to moderately east dipping Mp, Mj, and Mc (Figure 20). Drill logs defining the Mp/Dg and Mj/Mp contacts at depth are discordant with surface outcrop bedding orientations, possibly indicating the presence of underlying inter-unit and intra-unit detachment surfaces (Figures 22-25).

Faults

A generally north striking, west-vergent series of imbricate thrust faults is identified in the Snake Eyes area (Figure 20). The primary thrust fault cuts up the stratigraphic section of the footwall from north to south. In the northernmost A-A' cross section (Figure 22), a thrust fault is inferred to place Mp over Mp north of where the surface Mj pinches out, and an imbricate of the same thrust to the east places Mj jasperoid over Mc. In the B-B' cross section (Figure 23), the Mp and Mj units are overthickened in drilling intercepts. The smaller eastern duplex thrust truncates the eastern syncline limb and places Mp over Mj. Further south to C-C' (Figure 24), the thrust continues to cut up section in the footwall and places thin imbrications of Mj over Mc. Cross section D-D' displays the southernmost stratigraphic repetition recorded in drill logs within the Snakes Eyes area with Mj jasperoid and gouge thrust over Mc siltstone. Below the thrust, the normal stratigraphic sequence omits Mj and drill logs show a brecciated Mc on Mp contact (Figure 25). The presence of a west-vergent thrust fault is further supported by abrupt unit thickness variations recorded in drilling. Drill logging throughout the Snake Eyes area demonstrates wide variations in the thickness of the Mj unit and often includes omission of the unit. In drill logs where Mj is omitted and logged as a Mc/Mp contact, a thin gouge intersection of ~5-10' is typically observed indicating this contact is faulted. The thrust is inferred to have multiple duplexes as the westernmost sole thrust at the Dg/Mp contact ramps up and creates structural repetitions of Mp/Mp, Mj/Mj, and Mj/Mc, identified by drill log lithologies and gouge intervals. Logging and surface mapping suggest the Mj limestone in the hanging wall of the thrust is preferentially silicified to a jasperoid (Tj) with respect to the footwall.

Normal faults in Snake Eyes area occur in three sets with NE, NNE, and NW to NNW strikes (Figure 20). NE-striking normal faults are short, discontinuous, display an *en echelon* pattern, and are cut by all other fault orientations with the exception of the NE1 fault (Figure 20). This mutually cross cutting relationship may indicate two phases of NE-striking fault formation. NNE-striking normal faults bound the east end of the Snake Eyes area from the west edge of the Mooney Basin. The primary NNE-striking

fault is locally parallel to the strike of the thrusts. NW-striking faults locally bend or merge into NNW-striking faults and NNW-trending folds, whereas NE- to NNE-striking fault orientations are distinct and discontinuous. Both the NE-striking normal faults and the thrusts described above are cut by NW-striking normal faults. The NNW- to NW-striking normal faults labeled NNW1 and NNW2 on the Snakes Eyes geology map (Figure 20) are the primary through-going faults of the Snake Eyes area. Based on mapping and drilling data, the NW- to NNW- striking normal faults are moderately to steeply dipping with the hanging wall downthrown variably to the NE or SW. NNW1 dips to the ENE while NNW2 dips to the SSW and a complex NNW trending fold set occurs within the graben-like feature and relay faults between them (Figures 20, 22, and 23). The NW- to NNW-trending faults form grabens and half grabens in the Snake Eyes area with displacements on the order of tens of meters (Figures 22 and 23). Bedding dip differences between footwall and hanging wall within the grabens are complicated by earlier folding, however apparent stratigraphic offset suggests the graben bounding faults to be steep and non-rotational e.g., the graben between NNW1 and NNW2 in Figure 22.

The Snake Eyes area is fault bounded to the north, east, and south (Figure 20). A north-dipping normal fault occurs at the far north of the Snake Eyes mapping area, north of A-A' (Figure 20). The fault cross cuts all units and structures, and it effectively divides the Snake Eyes area from the Duke prospects to the north. This fault has right-lateral separation based on offsets of the north-striking thrusts. North of this fault, drilling penetrated Tertiary volcanic units that do not crop out within the Snake Eyes area. This suggests the timing of the fault is post-Tertiary with the Tv unit being eroded from the Snake Eyes area and preserved in the hanging wall of the E-W fault. The east side of the Snake Eyes mapping area is marked by an east-dipping normal fault that cuts off the thrust hanging wall and down drops Mc, Mdp, and Tv to the east, bounding the west side of the Mooney basin (Figure 20). In the Snake Eyes area, this basin bounding fault appears to cross cut all other fault orientations and is mapped by abrupt increases in Mc and Qal thickness in drill logs toward the center of the Mooney Basin to the east (Figures 20, 23, and 24). The latest movement on the NNE-striking basin bounding fault to the south of the Snake Eyes area in

the Galaxy area is complicated as it appears to be offset by NE-striking normal faults (Figure 26). In the area between Snake Eyes and Galaxy there is a change in the dominant cross-cutting fault orientation from a NW to a NE strike. While less common at Snake Eyes, NE-striking faults have a mutually cross cutting relationship with NNW-striking faults and associated NNW-trending folds. NE-striking faults, as mapped by other workers (D. Schwarz, unpublished internal mapping, 2012; K. Conway, unpublished internal mapping, 2020), are common at Galaxy, offset all other structural orientations, and may effectively make the Galaxy area structurally distinct from the Snake Eyes area (Figure 26).

Interpretation

The geometry of folds and faults identified in surface mapping and drilling suggests bedding-parallel slip or detachment along the rheologically contrasting Dg/Mp contact. This detachment interpretation is supported by angular discordance between surface bedding orientations and contacts defined by drilling at depth (Figures 22-24). Disharmonic relationships are noted in the Snake Eyes area where folds with tight interlimb angles are constrained to low competency units like Mp which are bounded by open to gentle folds in thick, high competency units like Dg (Figures 22 and 23). Faulted detachment folds between units of high competency contrast commonly display varied fold shapes with the wavelength controlled by the thickness of dominant units (Mitra, 2002). In this interpretation, shallow west-vergent thrusts in the eastern Snake Eyes area may be structural imbrications related to flexural slip along the broadly folded Mp/Mj contact. A flexural slip interpretation integrates evidence of both stratigraphic repetition and omission of the Mj unit in drilling, while an alternative interpretation of west-vergent thrusting cannot account for younger over older stratigraphic discontinuities separated by gouge intervals. Out of sequence thrusting may also account for younger over older stratigraphic discontinuities and can be considered as an alternative interpretation for follow up work.

Galaxy Area

The Galaxy deposit lies directly south of the Snake Eyes area (Figure 26). Mineralization occurs primarily at the Dg/Mp contact in the form of a decalcified and silicified Mp breccia (Mp brxs). The deposit can be classified as occurring in a Class D domain and is encompassed by GAL01 (Figure 27). Gently east dipping Dg to the west of the deposit abruptly rolls over to steeply normal faulted Mp and steeply east dipping Mj limestone/jasperoid to the east of the deposit (Figures 26 and 27). Like the Snake Eyes area, bedding roll over is recorded in dip measurements and indicated in increased drilling intercept thicknesses in vertical holes.

Folds

The monocline contained within GAL01, with the hinge marked by the yellow line in Figures 26 and 27, is the primary fold in the Galaxy area. The fold trace is ~1 km long and generally NNW-trending with local NNE-trending segments.

In the northeast corner of the Galaxy pit the Mp siltstone features a series of meter-scale angular to open folds that plunge shallowly to the NW (325/16, T/P) and display asymmetric "Z" limbs indicating vergence to the SW (Figures 27 and 28A). The "Hematite" Fault, a NNE-striking, steeply ESE-dipping normal fault, cuts along the hinge of a NNE-trending anticline on the southeast side of the Galaxy pit (Figures 27 and 28B). While poorly preserved, bedding in the footwall of the Hematite fault appears to be parasitic to the larger Hematite Fault-cut-anticline and suggests fold vergence to the ESE (Figure 28B). Pit wall and pre-pit bedding measurements obtained from historical mapping indicate that mineralization may have been hosted in an accompanying syncline to the west of the Hematite Fault and fold (Figures 27 and 29A) that was subsequently cross-faulted and mined out.

While minor fold hinges measured in the Galaxy pit are broadly consistent with the dominant northerly trends throughout the North Mooney (Figures 27, 28, 29), m to dm-scale fold hinges generally occur in two sets which trend NNE or NW. Differences in vergence between the NW- and NNE-trending

folds, in addition to bent hinge lines indicating refolding, suggest that two distinct folding events occurred. NNE-trending folds like the anticline cut by the Hematite fault and adjacent pit syncline likely formed in an earlier event associated with the formation of the GAL01 monocline, while discontinuous NW-trending folds may be related to a later transpressional folding event (Nutt et al., 2000), discussed below. All folds are cut by later NE-striking faults with multiphase movement.

Faults

NNE-striking, steeply dipping faults, observed in the north pit wall, are the primary ore controlling structures at Galaxy. Mp siltstone exposed in the northern pit walls is complexly deformed in a semi-ductile shear zone. Silicified blocks are locally caught up in shear zones and intact bedding is rarely preserved. The NNE-striking structures are generally subparallel to bedding strike of adjacent lithologic units and occur in meter-scale spaced sets with their hanging walls stepping down to the east. A range of NE- to NW-striking faults are also mapped throughout the Galaxy area and select fault planes containing slickenline measurements are plotted in Figure 29B. The NE-striking faults appear to cut NW- to NNE-striking faults; however, a timing relationship remains uncertain due to evidence of fault reactivation in slickenlines. A steeply dipping, NE-striking fault surface exposed in the west pit wall displays post-mineralization shallowly plunging slickenlines (<20°) with a right lateral sense of shear (Figure 29B). The NE-striking faults also display differing senses of separation across stratigraphic contacts indicating a dip-slip component on oppositely dipping faults. Additionally, there is more apparent vertical offset on the NE-striking faults than the shallowly plunging slickenlines can account for, implying there was first normal-slip followed by post-mineralization dextral-slip. It is unclear if both the initial normal slip and later dextral slip on the NE-striking faults cut the NW-striking faults, or if only late dextral slip cuts NW orientations.

Slip on a silicified NW-striking fault in the east pit wall is oblique with a reverse-left lateral sense of shear recorded by slickenlines (Figure 29B). This recorded slip vector on a NW-striking fault may be consistent with a late transpressional folding event associated with discontinuous NW-trending folds in the southern BMMD (Nutt et al., 2000). The NE-striking faults have little apparent stratigraphic separation; however, they cut all other orientations in the Galaxy pit and appear to cut the West Basin Bounding fault (Figure 20) of the Snake Eyes area.

Interpretation

Differences in the structural styles and latest throughgoing fault orientation between the Snake Eyes and Galaxy areas may be a function of the structural and stratigraphic levels being exposed and a potential structural domain boundary separated by WNW-striking faults. Monoclinal roll over is traceable along trend between the two areas, however Galaxy may feature more instances of parasitic folding while Snake Eyes features low angle faulting and structural imbrication. The pit syncline and Hematite fault-cut anticline (Figure 27) share a trend with the monocline and may be parasitic to it. This difference may be related to the exposed structural level between the two areas, whereas Galaxy exposes lower levels near the Dg/Mp contact and Snake Eyes higher levels in the Mp/Mj/Mc contacts. In this way, the thrusts at Snake Eyes may be expressed as the NNE-trending folds at Galaxy.

While Snake Eyes contains a single instance of a late NE-striking fault (NE1) (Figure 20), late throughgoing NE-striking normal faults are common at Galaxy (Figure 27). Differences in expression of the late NE-striking normal faults between the two areas may be related their proximity to major WNW-striking faults (Figure 20). A large steeply NNE-dipping normal fault with oblique normal-left lateral separation (WNW1) is parallel to the Bida trend and can be traced from north of the Top deposit to the area between Snake Eyes and Galaxy (Figure 30). Additionally, on the eastern side of the Casino deposit, a km-scale N-striking, steeply E-dipping fault with normal-left lateral separation is inferred to bend into a NW- to WNW-striking orientation north of Galaxy (Figure 30). Nutt et al. (2000) cite major NW- to WNW-striking faults throughout the district that divide it into domains, acting as tear faults during

Mesozoic compression and controlling block rotation during Cenozoic extension. The convergence of two major WNW-striking faults between the Galaxy and Snakes Eyes areas (Figure 30) may effectively separate these areas as distinct structural domains and account for differences in the predominant fault orientations. The NW- to NNW-striking faults at Snake Eyes may be truncated to the south by these WNW-striking faults which act as tear faults, translating similarly styled deformation away from the Galaxy area and functioning as a district-scale structural domain. Additional evidence for these areas being distinct structural domains includes difficulties extending mineralization of the Galaxy deposit to the north as the NNE-trending mineralizing structure appears to be truncated north of Galaxy. (Figure 30).

Royale Area

The Royale area lies in the northeast corner of the Bald Mountain district (Figure 2) and hosts three NNW-elongated pits called here Royale West, Royale Central, and Royale East in addition to the RYL01 domain (Figures 31-33). Mineralization is hosted at both the Dg/Mp and Mj/Mc contacts (Figures 4 and 33). The area can be divided into two km-scale fault blocks separated by a major NNE-striking, steeply east dipping normal fault with a calculated stratigraphic offset of 1367' (413 m), labeled NNE1 (Figures 31 and 34). Domain RYL01 encompasses the hanging wall block of the NNE1 fault and includes the three Royale pits (Figure 31). Bedding within the domain locally rolls over in a monoclinal fold with a calculated fold axis of 349/18 (Figure 32). This decameter-scale roll over is classified as a Class D domain and controls mineralization in the Royale East pit (Figures 31-35).

Folds

The Mj and jasperoid outcropping in the Royale East pit has been described by C. Mach (unpublished written communication) as having "small-scale 'S' folds" in cross section interpretation. These meter-scale tight to isoclinal folds verge west and may account for significant thickness differences

between the Mj jasperoid outcropping in the north and south ends of the east pit (Figures 33 and 35). Reconstructive mapping based on drill collar lithologies shows pre-pit outcrop patterns to be folded around an interpreted NW-trending hinge. This fold interpretation is shown by the dashed red line in Figure 33 and supported by west-dipping strata proximal to the Royale West pit (Figure 36) (K. Conway, 2019, Internal Report). However west-dipping beds are constrained to a narrow zone and may instead be associated with block rotation in the anastomosing NNW3 fault zone (Figure 33). Mineralization of the Royale Central and Royale East pits occurs on the east-dipping limb of the fold, while mineralization in the west pit occurs at the intersection of the NNW3 fault and the proposed NW-trending fold hinge.

A meter-scale fold measured (341/06) within the Mdp of the NNE1 hanging wall has a tight interlimb angle and plunges gently NNW (Figures 31 and 37), matching the geometry and orientations of other discontinuous meter-scale folds throughout the NMB.

Faults

The Royale West pit (Figure 33) contains mineralization at the Dg/Mp contact. The pit is located near an intersection of the NNE1 fault and the major NNW-striking fault (NNW3). The NNW3 fault has approximately 1000’ (305 m) of apparent stratigraphic offset where it is measured 3500’ (1067 m) away along strike to the SSE (Figure 31), however displacement at the Royale West pit is less (Figure 33), on the order of tens of meters. The NNW3 fault anastomoses, and the deposit occurs in a graben-like splay of upper Dg to lower Mp within a Dg hanging wall and footwall (Figure 33).

The Royale Central pit (Figure 33) is mineralized at the Dg/Mp contact in a variably decalcified, silicified breccia of mixed Dg limestone and Mp siltstone. The contact and Dg upper surface are irregular in drilling and in the western pit wall exposure, suggesting an originally karsted surface and/or contact dissolution breccia of the limestone and calcareous mudstone caused by interaction with hydrothermal fluids. While the Royale West and Royale East pits have strong structural controls on mineralization, the

Royale Central pit has a primary lithologic control with minor offset NNW-striking normal faults within the lower Mp possibly accommodating fluid flow.

The Royale East pit (Figure 33) is mineralized near the Mj/Mc contact, above and below a steeply dipping band of Mj jasperoid that forms an abrupt domain Class D monoclinal roll over along a NNW-striking normal fault (Figures 34 and 35). The north pit wall exposure of the Royale East pit exposes moderately to steeply east-dipping Mp mudstone, transitioning to steep, near vertical Mj jasperoid. Steep shear fabric and thickness variations in the upper Mp and Mj jasperoid units are apparent on the north and south pit wall exposures (Figure 35). The primary mineralization structure at which the roll over occurs strikes parallel to the NNW3 fault (Figure 31), and dips near vertical or steeply to the ENE. The mineralizing fault has an approximate apparent offset of 150' (46 m). Smaller normal faults with 2-3 meters of displacement measured within the Mc of the hanging wall of the east pit mineralizing fault are steeply SE-dipping (Figure 33 and 35). These smaller SE-dipping normal faults appear to cut the ENE-dipping mineralizing fault, and both orientations control gold grades. This relationship suggests the ENE-dipping faults formed prior to the SE-dipping faults, and both pre-date gold mineralization. Iron oxide vein sets that strike NE are stacked in an *en echelon* pattern parallel to the SE-dipping normal faults. The en echelon stacking and apparent offset of these iron oxide veinlets indicates a top to the SE sense of shear. If the vein sets are coincident with mineralization, they imply NNW-SSE extensional kinematics and oblique normal-right lateral slip along the steeply ESE-dipping mineralizing fault (Rhys, unpublished report; written communication, 2013).

To the west of the Royale pits, a large displacement west-dipping, NNE- to north-striking normal fault down drops the mineralized sections contained within the three Royale pits (NNE1) (Figure 31 and 34). This west-side-down normal fault contains dolomite in the footwall. The footwall dolomite is either the Devonian Simonson formation (Dsi) or a section of altered Devonian Guilmette (Dg). If it is Guilmette, the limestone has undergone secondary decalcification and dolomitic alteration related to fluids in a 500' (152 m) wide structural shear zone. Unpublished mapping by D. Schwarz (2012) notes a

yellow siltstone facies characteristic of lower Dg in the west wall of the Royale West pit, indicating that the fault-bounded dolomite belongs to the Dsi unit below. However, other workers (K. Conway and C. Mach, written comm.) and cross section work determine the brecciated dolomite to be of the lower Guilmette. Considering the ambiguity of the exact location in the stratigraphic section, apparent stratigraphic offset on this normal fault ranges from the cross section calculated stratigraphic throw of 1367' (417 m) at a minimum, up to 2000' (610 m) at a maximum (Figure 33). The NNE1 fault hanging wall contains patchy weak to pervasively silicified Mississippian Diamond Peak (Mdp) sandstone and conglomerate that is poorly sorted and well rounded. Where pervasively silicified, the Mdp unit is also brecciated.

In the northern Royale area, kilometer-scale NE-striking faults (e.g., NE2; Figure 31) cross cut all other fault orientations. The NE2 fault cuts both the NNW3 and NNE1 fault zone north of their intersection (Figure 31). The relationship of these kilometer-scale NE-striking faults to the minor NE-striking normal faults noted in the Royale East pit is undetermined, however both are apparently late and cut the NNW-striking faults.

Interpretation

Drilling and cross sections suggest large spatial variations in geologic unit thicknesses. The western hanging wall fault block of NNE1, as viewed in cross section E-E' (Figure 34), shows Mp and Mj thinning from W to E. In the western Royale area the varying stratigraphic thicknesses are likely a function of both primary depositional differences and structure. D. Schwarz (unpublished written communication, 2012) notes the possibility of differential compaction in originally water-saturated Mp mudstones as well as the upper Dg surface being regionally karsted, and therefore irregular. Paleotopographic karsted high and lows may have resulted in pseudo basin and range or "egg carton"

topography over which Mp mudstone was differentially deposited. Greater thicknesses of foreland basin related deposits, Mc and Mdp, above exceptionally thin Mp may indicate greater high degrees of dewatering and compaction of mudstones in paleotopographic lows.

In the eastern Royale area, correspondence of fault and fold axis orientations in addition to the scale of the east-dipping stratigraphic package across numerous faults suggest these structures to be primarily related to an early ENE- to NE-directed compression phase rather than later Tertiary extension. The NNW-trending fold in the NNE1 fault hanging wall (Figures 31, 36, 37), and the NNW3 fault in addition to its synthetic NNW-striking pit mineralizing faults (Figure 33) are interpreted to have been established under the same early compressional regime. While the meter-scale NNW trending folds noted above (Figures 31 and 37) share an orientation with the NNW-striking mineralizing faults in the Royale area, adjacent minor faults with SSE-strikes and dip-slip slickenlines indicate that NNW-trending folds and faults in the Royale area were early compressional structures, with the faults later reactivated in extension. The interpreted NNW-trending fold highlighted in Figure 33 is cut by the NNW3 fault near an apparent intersection at the Royale West pit. While the validity of a west-dipping limb of this fold as interpreted by other workers remains uncertain, it is important to note the potential significance of these km-scale fault and fold intersections. If the NNW3 fault and other large displacement normal faults mapped throughout the district were initially reverse faults, then adjacent strike-parallel anticlines may be related to early reverse fault propagation. While the NNW3 fault is interpreted here in cross section as ENE-dipping with normal throw, limited recent drilling along the southern extension of the NNW3 fault at the Dg/Mc contact indicates that the NNW3 fault may be vertical to steeply WSW-dipping, suggesting reverse throw (K. Conway, verbal communication, 2022). Further work is recommended to determine the geometry of the NNW3 fault along its strike length as this may have implications for differential reactivation of originally compressional structures.

While the Royale Central and East pits may be interpreted as occurring on an eastern fold limb, the localized roll over at Royale East pit and its relatively minor decameter-scale throw on the NNW-

striking fault make the roll over unlikely to be caused by a large displacement reverse fault coring it at the pit-scale. More likely, it is a fold feature contained within the Mp and Mj units caused by flexural slip of the Dg/Mp contact during ENE-directed shortening. This flexural slip/faulting during folding is evidenced by high angle bedding-parallel slip and significant thickness differences of Mj across short distances e.g., in the north and south pit wall exposures (Figures 33 and 35). Later extension likely reactivated mechanical weaknesses parallel to the fold hinges and the pre-existing steeply ENE-dipping conduit for mineralizing fluids in the Royale East pit. Alternatively, smaller scale roll over features like the one in the Royale East pit may be parasitic folds on the eastern limb of a larger regional-scale anticline, discussed below.

The timing relationship between the NNE1 fault and the NNW3 fault is inconclusive in the Royale area. Near the intersection of the two faults, the NNW3 fault has far less apparent stratigraphic displacement than along strike to the SSE, while the NNE1 faults bends into the NNW3 fault, and both are offset by late NE-striking faults ~1500' to the north of cross section E-E' (Figure 34). Offset of the NNW3 fault may have been accommodated by the earlier NNE1 fault at their intersection in the Royale area, and the apparent bending of NNE1 into NNW3 may be accounted for as slip interference between the two. The NE2 fault cuts both the NNE1 and NNW3 faults and is the latest through going orientation in the Royale area (Figure 31).

Winrock Area

The Winrock deposit is located ~2.5 km directly east of Snake Eyes on the east side of the North Mooney basin (Figure 2). Mineralization is hosted at the Mj/Mc contact (Figures 4 and 38) and accompanying alteration consists of decalcification, argillization, and silicification. The Joana Limestone

exhibits multiple stages of intense hydrothermal alteration and brecciation in fault controlled and strata-bound jasperoids. The bulk of the accompanying maps (Figures 38 and 39) are modified from mapping done by R. Conelea in 2004 at a scale of 1:2,400 (R. Conelea, unpublished written communication, 2004). Bedding roll over at the Blowout fault is encompassed by the WIN01 polygon as a Class D domain (Figure 38).

Folds

NW-trending folds are mapped in the Winrock area. Abrupt, steeply east dipping bedding roll over is noted in the Mp and Mj units exposed in the northern pit wall of the Blowout pit (Figure 41) and the southern pit wall exposure of the Deer Camp pit. Mineralization in these pits occurs along the axis of this NW-trending fold associated with the Blowout fault, described below. Bedding along the steeply dipping east limb of the fold is locally overturned, implying the fold formed during reverse faulting.

In the Summer of 2020, a new haul road cut was made in the Winrock area. This exposure shows a tight, moderately NW-plunging syncline in the Mdp unit (Figure 38 and 43). Moderately plunging NW fold trends and with tight interlimb geometries at Winrock are consistent with those measured throughout the greater North Mooney Basin area.

Faults

The Winrock area as a whole is interpreted as a west vergent thrust sheet containing upper Dg through Mc emplaced over a footwall of Mdp. Drilling in the west of the deposit area that collars in Mp intercepts Mdp at depth (e.g., WR-017 and WR-018) (Figure 40). The thrust wrapping around the west, southwest, and northwest sides of Winrock (Figure 38) was originally mapped by R. Conelea and corroborated by the published 1:24,000 USGS map of Nutt and Hart (2004). The southern and western margins of the Winrock area are structurally and stratigraphically complex with imbricated stratigraphic units and abundant gouge intervals in drilling. Mineralization in the Blowout and Deer Camp pits

(Figures 38 and 39) is controlled by a NW-striking, steeply NE-dipping fault, termed the Blowout fault. The Blowout fault offsets Mp and mineralized Mj jasperoid in the footwall against mineralized lower Mc calcareous mudstone to micrite (Mcl) in the hanging wall. The Mp, Mj, and Mc units are entrained within a fault zone that is approximately 40' (12 m) wide. With the exception of steeply dipping strata directly within the fault zone, footwall and hanging wall strata both dip moderately to the east (Figures 39 and 40). Deformed Mp and Mj units in the Blowout fault footwall exhibit a strongly asymmetric fold shape with near vertical to overturned bedding in the shear zone (Figure 41).

Previous work (R. Conelea, unpublished written communication, 2004) proposed that structural mineralization controls of the Hilltop deposit to the south of the Blowout fault are high angle, NNE- to N-striking extensional faults that track with jasperoids and elevated gold values (Figure 38). NNE trends are also visible in Au-soil anomalies. The NNE- to NE-striking, steeply dipping normal faults exhibit post-mineralization slickenlines on jasperoids that indicate a small right lateral oblique slip component (Figure 42). The kinematic and cross cutting relationship between the NW-and NNE- to NE-striking faults suggests that at the Blowout and Deer Camp deposits, mineralization is primarily controlled by the NW-trending Blowout fault which is determined to have an oblique-normal offset with a left lateral strike-slip component and dip-slip component of 300' (R. Conelea, unpublished written communication, 2004), while the NNE- to NE-striking oblique normal-right lateral faults are subsidiary dilatant structures that act as relays and link NW-striking left lateral faults.

The new haul road exposure at Winrock shows a steeply SW-dipping reverse fault (Figures 38 and 40). The low angle thrust fault daylighting on the west side of the deposit, as viewed on the SW portion of cross section F-F, is cut by the reverse fault putting the thrust above the current ground surface (now eroded) and places Mdp against Mp (Figure 40).

Interpretation

The Winrock area is interpreted to contain the hanging wall component of a west vergent thrust sheet that places a complete section of Mdp through Dg over a Mdp footwall (Figure 40). The thrust is interpreted to sole in upper Dg as that is the lowest stratigraphic level of the fault hanging wall exposed at the west side of the Winrock area where the thrust surfaces (Figure 38). Deeper drilling in the area may reveal structural repetition of mineralization at favorable stratigraphic horizons in the thrust footwall. The Class D domain rollover of WIN01 at the Blowout fault is interpreted to be the result of fault propagation folding in a later stage of reverse faulting that cross cuts the low angle thrust. Locally overturned bedding in the Blowout fault zone suggests reverse fault kinematics (Figure 41). Another reverse fault parallel to the NW strike of the Blowout fault truncates the low angle thrust on the west side of the Winrock area (Figure 40). The steeper eastern limb of the Blowout fault/fold was later exploited along the fold axis by multiple generations of slip including left lateral-oblique movement and with normal reactivation enhancing the fault propagation fold in the latest extensional tectonic regime. The kinematics and fault orientation pattern of the Winrock deposits suggests the structural control on alteration and mineralization to be a large pull-apart system on a left lateral NW-striking shear where the NE to NNE trends are subsidiary dilatant structures (R. Conelea, unpublished written communication, 2004). I found kinematic support for this interpretation in the analysis of slickenlines on the NE- to NNE-striking faults which indicate a right lateral oblique normal slip component. These kinematics and the discontinuous NW-trending folds (Figure 40 and 43) are consistent with syn- to post-mineralization transpressive structures in the southern BMMD at the western margin of the Ruby Mountain core complex which have been interpreted as Eocene in age (Nutt and Good, 1998). Eocene transpression with an E-W directed σ_1 would result in left lateral separation along the Blowout fault and other pre-existing WNW- to NW-striking faults, and it is consistent with the right lateral slip component on the NNE- to NE-striking faults in the Winrock area.

4. Discussion

Geometry, Kinematics, and Timing of Deformation in the North Mooney Basin and Beyond

Updated mapping and interpretation of structural features in the North Mooney Basin lend insight into the tectonic history of the greater Bald Mountain region. While mineralization is stratabound and in part controlled by favorable carbonate lithologies (e.g., Cline et al., 2005), deposits always occur at the intersections of differently oriented structures, many of which include kinematic indicators of multi-phase movement. The identification of commonalities in the geometry, kinematics, and timing of structures along with an understanding of how specific structural intersections control gold deposits throughout the NMB will aid further exploration efforts. In this section I present an inferred structural and tectonic sequence based on my observations in the NMB and the work of others outside the NMB (Figure 44; Table 4). Early deformation phases created district-scale structures that bound the NMB, while later phases had a greater role in controlling gold mineralization. My structural interpretations in the NMB are largely consistent with those made by other workers throughout the district, and relevant correlations are noted below.

Phase 1

The earliest compressional deformation (Phase 1; Table 4) recorded in NMB and throughout the district includes NNE- to NE-striking reverse faults and m- to km-scale folds (Figures 30, 44, and 45). NNE-trending asymmetric fold geometries are consistent with fault propagation folding by east-vergent reverse faults e.g., Alligator Ridge (Figures 19 and 45). While these features are largely overprinted,

reactivated, or crosscut by normal faults at the scale of the NMB, related district-scale NNE-striking reverse faults bound the basin to the east and west (Figure 44). Many of the NNE- to NE-striking normal faults in the district are inferred to be reactivated, originally forming as reverse faults. Evidence of reactivation includes NNE- to NE-trending folds of various scales sharing an orientation with, and being cut by, normal faults of the same strike.

The NNE-striking Dynasty (DYN) and West Top faults (WTF), located to the west of the NMB, are interpreted to control a series of NNE-trending parasitic folds between the WTF and DYN corridor and the NNE-trending open anticline at the Casino deposit which has subsequently been faulted along its axis and possibly refolded (Figure 44). A continuation to the NNE along the WTF and DYN corridor lines up with the mapped NNE1 fault zone at Royale (Figures 31,34, and 44). A primary difference between the WTF and DYN corridor and NNE1 fault lies in the dip direction of the fault plane, whereas the Dynasty dips steeply east, the NNE1 faults dips steeply west. This difference makes unclear if the NNE1 fault zone is a direct extension of the West Top and Dynasty fault corridor, however this apparent change in the dips of the fault planes may be caused by interference with NNW3 fault in the Royale area (Figure 30, 44).

To the east of the NMB, a km-scale east vergent reverse fault is interpreted to have established the NNE trend of the Mooney Basin, and Nutt et al. (2000) interpret exposures of reverse faults in the southern district such as at Alligator Ridge (Figure 18) to be part of a large reverse fault system that extends through to the northern end of the Mooney Basin (Figure 45). The NNE to NE trend of folds and interpreted east-vergent reverse faults, highlighted in the Dynasty and NMB trends, are kinematically consistent with general ESE-WNW to SE-NW shortening throughout the late Paleozoic-early Mesozoic and the late Antler to Sonoma and Elko orogenies (e.g., Speed and Sleep, 1982; Miller et al., 1992; Price, 2010; Thorman, 2020) (Table 4).

Phase 2

The next deformational phase (Phase 2; Table 4) includes WNW- to NW-striking, steeply-dipping, normal faults with oblique separation. These km-scale faults have a predominant normal and left lateral separation in the northern portion of the district, and a predominant normal and right lateral separation in the southern district (Figure 45). The WNW-striking faults are most prominent in the central portion of the district where they are related to the Bida trend which geographically bounds the NMB to the south and controls Late Jurassic intrusives (Figures 44, 45) (Nutt et al., 2000). Timing of these WNW to NW faults predates 159 Ma as they control the emplacement of the Bald Mountain stock. (Nutt and Hofstra, 2007).

I have identified additional WNW-striking faults that divide the Galaxy from the Snakes Eyes areas (WNW1) and the North Duke from South Duke areas (WNW2) (Figure 44). Cross cutting relations are seen throughout the NMB, most notably to the west of the NMB where the WNW- to NW-strikes appear to both cut and bend into major NNE-striking faults of the Dynasty fault corridor with a local left separation (Figure 44). Left-slip and drag across the WNW-striking faults in the NMB is also interpreted from offset and curved fold hinges (Figure 44). The WNW-striking Bida-parallel faults in the NMB apparently divide the area into distinct structural domains and in part control the predominant cross cutting orientation within those domains. This is evident at WNW1 between Galaxy and Snake Eyes, as discussed above, and at WNW2 between North Duke and South Duke areas which feature NW and NE through going orientations, respectively (Figure 44). In the southern district, Nutt et al. (2000) also note the apparent partitioning of structural domains by km-scale WNW-striking faults and posit that they acted as tear faults during Mesozoic compression while later controlling block rotation during extension (Figure 45). As such, reactivation of the WNW- to NW-striking faults of Phase 2 complicate cross cutting

relationships and is in part coeval with later deformation phases. Evidence for multi-phase oblique movement on the WNW-striking faults is also noted where the faults cut later Phase 3 NW-trending fold hinges with a left-lateral slip sense (Figure 44). Phase 2 deformation is consistent with a rotating of the shortening direction from SE-NW to ENE-WSW and the formation of a NW-striking transtensional tectonic regime that facilitated the emplacement of intrusives by the Late Jurassic (Nutt et al., 2000; Price, 2010).

Phase 3

Phase 3 (Table 4) is marked by ENE-WSW shortening that resulted in in km-scale gently to moderately NW- and NNW-plunging folds and NW- to N-striking reverse and thrust faults (Figure 45). This phase has been determined by cross cutting relationships and varying structural styles across domains bounded by the WNW- to NW-striking faults of Phase 2 (Figures 44, 45). Structural features of Phase 3 are highlighted within the Class B domains (Tables 2 and 3; Figures 44 and 45). The folds of this phase are attributed to broad Mesozoic shortening. The kilometer-scale NW fold trends are most clearly observed in the southern district in the Buck Pass area and are plotted in the BUC05 and BUC06 domains (Figures 17, 18, 45).

In the Snake Eyes area the NNW-trending folds appear to control the orientation of the NNW1 and NNW2 faults which break near fold inflection points between anticline and syncline pairs to form horst and graben features during later extension (Figures 20, 21A, 22, and 23). Broad folding patterns in the NMB suggest that these NW- to NNW-trending folds refold earlier NNE-trending folds in the Duke, Casino, and Poker areas. West of the NW1 fault, which runs through the Casino and Poker pits and apparently merges with WNW1 and WNW2 (Figure 44), fold trends are dominantly NNE-trending and associated with the WTF and DYN corridor. These NNE-trends bend into NW- to NNW-trends as they approach the NW1 fault, and NNW-trends dominate to the east of NW1 (Figure 44).

In the Royale area, the NNW3 fault controls mineralization in the Royale West pit while cutting the Phase 1 Dynasty associated NNE1 fault. (Figure 31). NNW-striking faults, synthetic to the NNW3 fault, that occur at favorable stratigraphy are inferred to be the primary control of mineralization in all three Royale pits (Figure 33). The NNW-trending fold in Figure 33 and the NE-facing monocline from the Royale Central pit continuing to the Mdp unit northeast of the Royale East pit may be linked to this same Phase 3 shortening event.

Northerly striking, low angle west-vergent thrusting occurs at the east and west margins of the North Mooney structural graben, as noted in the Snake Eyes (Figures 20-25) and Winrock areas (Figures 38 and 40). NW-striking, steeply dipping, NE-vergent reverse faults which cut the low angle west-vergent thrust at Winrock are also noted. The timing and kinematics of these buried and reactivated west vs. east vergent compressional structures are difficult to constrain; however, both are interpreted to be broadly coeval in Phase 3. West-vergent thrusting noted throughout the northern district at Winrock, Snake Eyes, and LJ (Figure 2) (R. Morrell, written communication, 2020) features complex imbrication of stratigraphic units and gouge intervals. East-vergent compressional structures are steeply dipping reverse faults accompanied by NE- to ENE-facing monoclines and NW- to NNW-trending asymmetric folds and suggest a direct link between the Class B and some class D domains (Tables 2 and 3). As part of the same Phase 3 event, the steep east-vergent reverse faults are interpreted to be the direct result of regional scale east-directed compression, while the west-vergent low angle thrusts are interpreted as a product of the folding and resultant space problems accommodated by flexural slip along unit contacts.

The westward vergence of low angle thrusts and other NW- to NNW-trending folds in the NMB (e.g., Snakes Eyes and Galaxy areas; Figures 26 and 28) may show vergence toward the newly-interpreted location of the hinge of a major anticline which is inferred to be the northern extension of the Illipah anticline of the Eastern Nevada Fold Belt (Figures 2 and 45) (D.Schwarz, unpub. written comm., 2012; Long, 2015; K. Raabe, unpub. written comm. 2020). The Illipah anticline axial trace extends ~100 km to the south to the White Pine Range (Figure 1) where it is a tight fold with a moderately dipping western

limb and moderate to steeply dipping eastern limb (Long, 2015). To the south, the Illipah anticline folds rocks as young as Jurassic and Early Cretaceous (Long, 2015). The overall scale, timing, and orientation of faulting and folding in this compressional Phase 3 is consistent with deformation in the Eastern Nevada Fold Belt of the Sevier hinterland from the late Jurassic to the Paleogene (Long, 2015).

Phase 4

A distinct late Middle Eocene sinistral transpressional folding event (Phase 4; Table 4) has been documented by Nutt and Good (1998) through the folding of Eocene sedimentary rocks around NW-trending axes in the southern BMMD. This folding event is constrained in time to being syn- to post-mineralization (~42 Ma) based on the silicification of folded Eocene rocks, and pre-35 Ma based on tilted but unfolded and unmineralized overlying dated volcanics (Nutt and Good, 1998). According to Nutt and Good (1998) this transpressional Eocene folding event may be related to the initial uplift and exhumation of the Ruby Mountain core complex to the north.

The short wavelength, meter-scale, discontinuous NW-trending folds are oriented at a clockwise angle of 30° or less to the WNW-striking faults (Nutt and Good, 1998), and folds of similar orientation and style are also noted in this study within middle Devonian to late Mississippian rocks in the NMB including the Galaxy, Royale, and Winrock areas, described above (Figures 27, 28, 33, 38, and 43). Late strike-slip to oblique sinistral slip and separation is evidenced by mutually cross cutting orientations of NE- and NW-striking faults, oblique-slip slickenlines (Figures 29 and 42) on both silicified and unaltered rock, and on the orientation and slip of interpreted relay faults (Figures 38 and 41). Localized domains of transpression with NE-SW shortening may be segregated by the WNW- to NW-striking sinistral strike-slip faults and lead to the complex cross cutting relationship between apparently late and coeval NE- and NW-striking normal faults throughout the NMB.

Phase 5

Phase 5 is marked by late extensional N- to NE-striking normal faults that range from gently to steeply dipping on both listric and planar geometries (Phase 5; Table 4; Figure 44). This Phase is the result of a gradual shift to a broadly extensional tectonic regime in northern Nevada by ~ 40 Ma (Henry et al., 2011), and it introduces further complexities in cross cutting relationships and the timing of deformational phases. By the late Miocene, widespread extension that continues to form the Basin and Range province was established (Dickinson, 2006; Long, 2019), and the direction of extension rotated from NE-SW to NW-SE in the northern Basin and Range (e.g., Wernicke, 1992). At BMMD, Cenozoic extension is recorded throughout the district as widespread N- to NE-striking normal faults that cut ~36 Ma volcanic rocks (Nutt et al., 2000). This tectonic shift resulted in the reactivation and inversion of many of the compressional structures noted above. Where steeply dipping at the surface, post-mineralization normal faulting results in horst and graben features which often exploit earlier compressional fold and fault trends (Nutt et al., 2000).

Reactivated normal fault separations on are what are interpreted to be originally Phase 1 reverse faults can be significant. In the Little Bald Mountain (LBM) and Dynasty areas (Figure 2) the Dynasty fault dips moderately to steeply to the east and down-drops stratigraphy to the east. It locally juxtaposes the Catlin member of the Cambrian Windfall formation against Ordovician Eureka formation with stratigraphic separation calculated at ~ 1700’ (Figures 4 and 30). In the Dynasty fault exposure and deposit at Little Bald Mountain (LBM) pit, I estimate the fault has at least 1000’ of normal throw with lower Ordovician Pogonip limestones in the footwall and Silurian Laketown dolomite in the hanging wall (Figures 3, 4, and 30). The NNE1 fault at Royale shares similar orientation and apparent normal stratigraphic separation magnitudes with the Dynasty fault. Normal separation on the Dynasty and NNE1 faults, combined with the evidence for Phase 1 reverse slip described above support the interpretation of reactivation during late extension.

Key evidence for timing of Phase 5 normal faults relies on the latest through going orientation in mapped areas and localities where deposits or mineralization-related jasperoids are cut. Some areas like Galaxy (Figure 26) have a clear NE-striking normal fault cross-cutting orientation, whereas other areas like Snake Eyes have limited instances of late NE-striking through going faults which cut all other orientations (NE1) (Figure 20). Additionally, the NE2 fault at Royale appears to cut both the NNE1 fault zone and the NNW3 fault (Figure 31). Abundant post-mineralization slickenlines indicate the reactivation of preexisting structures. In general, fault strike orientations that are at a high angle to NW-SE directed Neogene extension accommodate reactivation with a greater dip-slip component. In this way, late NE-striking faults often exhibit dip-slip components while likely reactivated NW-striking faults have a greater strike-slip component or exhibit more gently raking slickenlines e.g., NW-striking vs. NE-striking normal faults at Galaxy (Figure 29A) and dominantly dip-slip slickenlines on NNE-striking faults at Winrock (Figure 42). This generalization, however, is not consistent throughout the NMB as the presence of multiple sets of slickenlines on some faults may record changes in the incremental slip vector or internal block rotation that varies from the net fault slip.

Low angle normal faults interpreted by other workers to fall within Phase 5 (Nutt and Hofstra, 2007) were not mapped in this study, however they occur elsewhere in BMMD. Timing of low angle normal faulting remains enigmatic. While some low angle detachment faults are documented as being Jurassic (pre-159 Ma) (Mach et al., 2015), others such as the Ruby fault (Figure 5) are definitively Miocene in age with a separation of up to 2.8 km (Nutt and Hofstra, 2007). Mesozoic detachment faulting may be consistent with gravitational spreading and the collapse of thickened crust in fold and thrust belts (Long, 2015). Further study should be done to constrain the kinematics and timing of these detachment faults as they have been demonstrated to cut and translate sections of deposits across the district (Pace, 2009; Mach et al., 2015).

A Comparison with the Rhys et al. (2015) Structural Model of the Northern Carlin Trend

Based on the geographic separation between the northern Carlin trend and BMMD, differences in tectonic influence and resulting structural geometries are to be expected. In this section, observations made in the Rhys et al. (2015) model are compared to observations made at BMMD, and differences in tectonic influence are discussed. Note that in the following discussion of Phases uses Roman numerals for the Rhys et al. (2015) model (Table 1) and Arabic numerals (Table 4) for BMMD Phases discussed above.

It is apparent that the structure at BMMD shares many kinematic and geometric similarities to those noted by Rhys et al. (2015) in the northern Carlin trend, as described below and noted in Tables 1 and 4. Deformation events largely overlap between the two areas, and many of the structural complications and uncertainties discussed by Rhys et al. (2015) including progressive or superposed coaxial events, inconsistent or mutual cross-cutting relationships, evidence for local pre-Cenozoic extension, and the overprinting of kinematic indicators through multiphase reactivation are also noted at BMMD. Primary differences between BMMD and the northern Carlin trend include the following aspects discussed below: 1) A lack of Phase I Roberts Mountains thrust hanging wall structure, 2) differences in the prevalence of Phase II features and Mesozoic deformation of differing styles relating to the proximity of the Eastern Nevada Fold Belt and in the Sevier hinterland, 3) the timing and origin of WNW-striking orientations of basement faults that control intrusive emplacement and bound structural domains in the BMMD, and 4) documented Eocene age folding.

Episodic SE-NW to ESE-WNW shortening at various times throughout the Paleozoic and the lack of RMT and GT hanging wall structure at BMMD make it necessary to combine Rhys et al. (2015) Phases I and II into a single Phase 1 at BMMD. Phase 1 Structures that deform Mc and Mdp (e.g. WTF, and the inferred NMB bounding fault) must be equivalent to Phase II (Table 4; Figure 45). While the presence of the hanging wall of the RMT is a key exploration feature in the northern Carlin trend, the position of BMMD in the Antler foreland basin and the associated siliciclastic infill therein (Mc, Mdp)

appears to be a suitable replacement of the "upper plate" impermeable boundary against which Au-bearing fluids can pool. All the Carlin type deposits in the NMB occur at favorable stratigraphic horizons that feature contrasts in the carbonate and siliciclastic sediment content (e.g., Dg/Mp and Mj/Mc) (Figure 4). Rhys et al. (2015) propose that some displacement of the RMT may have been accommodated in deeper stratabound shear zones that also helped to control later faulting and fluids, however the lack of associated shearing at Bald Mountain indicates that this is not necessary for Carlin-type mineralization.

While the Phase II structures of the Rhys et al. (2015) model are noted to be the most widely developed phase of deformation on the Carlin trend, they are difficult distinguish at BMMD. With the exception of the GAT01 domain (Figure 19), steeply asymmetric east-vergent folds and related east-vergent faults are not readily identified. Roll overs and monoclines at BMMD are generally ENE- to NE-facing, while Phase II folds in the Carlin trend are described as E-to SE-vergent (Rhys et al., 2015). Corresponding to Carlin trend Phase II folds, NNE-trending folds in the NMB are associated with Phase 1 deformation at BMMD. However, Phase 1 folds in the NMB typically occur as anticline/syncline pairs at a discontinuous and smaller decameter-scale, are upright, and are less clearly associated with reverse fault propagation when compared to Phase II folds in the Carlin trend. This apparent difference in the prevalence of Phase II features between the Carlin trend and BMMD may be due to the longitudinal separation between the two areas and diminished strain the east of the location of the Golconda allochthon (Figure 1). Additionally, Rhys et al. (2015) state that localized areas in the Carlin trend that feature anomalous NNW-trending Phase II folds also feature more pronounced development of Phase III structures. As Phase III deformation is centered further to the east during the Sevier and Laramide orogenies, it follows that corresponding Phase II deformation at BMMD may be more overprinted by Mesozoic shortening (Phase III, Phase 3) at BMMD in addition to being less developed.

The origin of the Phase 2 WNW-striking structures at BMMD (Figures 44, 45) is difficult to constrain, and they may in part be inherited from faults that predate both Phases 1 and Phase I. In the Jurassic, the Bida trend became a strike-slip pull-apart structure that controlled the emplacement of the

Late Jurassic Bald Mountain stock, associated dikes, and intrusive related gold mineralization during east directed Mesozoic contraction (Nutt and Hofstra, 2007). The BMMD Phase 2 WNW-striking structures (Table 3; Figures 44, 45), which are associated with the Bida trend and the emplacement of the Bald Mountain stock, necessarily predate 159 Ma but are otherwise of unknown age. While WNW (N060-070W) trends are considered above to postdate Phase 1 tectonics based on cross cutting relationships (Table 3), this relationship may be complicated by reactivation, and it is possible that the WNW trend actually predates all other orientations. Geophysical evidence suggests that that Bida trend is a deep-seated, through-going basement structure (Wannamaker and Doerner, 2002) and additional major WNW-striking structures have been noted by other workers in the northern Carlin trend (Muntean et al., 2007). WNW-striking structures in both the northern Carlin trend and within the BMMD are associated with facies transitions in Paleozoic rocks, unit thicknesses, the distribution and style of later Mesozoic compressional structures, and the distribution of Tertiary alteration systems (Cox and Otto, 1995; Nutt et al., 2000; Muntean et al., 2007). Various workers have interpreted these regional WNW-striking faults as normal faults which formed either during incipient rifting of the continent in the Neoproterozoic (Muntean et al., 2007) or as a series of trough and highland structures resulting from SE-directed compression on a NE-trending continental margin during the upper Paleozoic Antler orogeny (Cox and Otto, 1995). Evidence for WNW-striking Paleozoic syn-sedimentary growth faults and repeated phases of normal and reverse reactivation is debated (Embso et al., 2006; Muntean and Coward, 2007; Rhys et al., 2015). An alternative explanation of the major WNW-striking faults may be formation during the Late Paleozoic Humboldt orogeny. Workers (e.g., Thorman et al., 1991; Price, 2010) have proposed a rotation of the regional stress field to N-S compression during the Pennsylvanian-Permian Humboldt orogeny in Nevada. Humboldt orogeny fold and thrust trends range from WNW to WSW and are noted in the northern Carlin trend (Price, 2010). Kilometer-scale WNW trending anticline and syncline sets have been mapped in the southwest area of the BMMD in Permian and older rocks west of the Vantage deposit (Figures 5, 17), however they are not apparent in the northern BMMD.

Nutt and Good (1998) document an early to middle Eocene event that resulted in sinistral strike-slip motion on W- to NW-striking faults and the creation of local NW-trending folds in Tertiary rocks in the southern BMMD. This deformation may be spatially constrained to the margins of the Ruby Mountain metamorphic core complex as it is inferred to be related to transpression at the initial stages of exhumation of the core complex (Nutt and Good, 1998), however the extent of the deformation is unspecified. Large scale NW-trending folds are also documented in Eocene aged strata to the north and west of the RMCC near Elko (Figure 2) (Ketner and Alpha, 1988). Rhys et al. (2015) state that the relationship of the Eocene folds at BMMD (Phase 4) to the Phase III NW-trending folds in the Carlin trend remains unclear. The possibility of some Eocene structure being misinterpreted as Mesozoic Phase III structure remains, and there may be some functional difference with regard to gold targeting and exploration efforts if later Eocene deformation did include a significant strike-slip component.

Conclusion and Future Work

This project sought to lend insight to the structural history of BMMD by identifying distinct structural geometries and their associated deformation events (Table 3). Historical mapping and structural data were collected and compiled into a geodatabase (Supplement 1) which was used to do a dip domain analysis and identify distinct structural features. Once structural domains were classified (Table 1 and 2), follow up work on areas of interest in the NMB included new mapping and cross section analysis. The resulting suggested structural history determined by the geometry, kinematics, and timing of structures at BMMD (Table 3) was compared to the Rhys et al. (2015) structural model developed around the Carlin deposit in north-central Nevada (Table 4). The comparison suggests broad similarities between the two models with notable differences consistent with their geographic separation and tectonic influence.

In order to continue to gain understanding of the structural history at BMMD, future work may focus on the collection of kinematic indicator data on both pre- and post-mineralization rocks. Detailed kinematic analysis may lend further specifics to the structural Phases discussed above. As noted by Rhys et al (2015), in the northern Carlin trend slip vectors tend to transition from dip-slip to oblique-slip, to strike-slip as normal fault orientations rotate from NE- to N- to NW-striking. This may be an important factor to take into account with continuing exploration in the BMMD. Offsets of deposits have the potential to be traced along the dip of mineralizing faults, however when strike-slip offset post-dates mineralization, deposits may be translated significant distances from mineralization conduits. Detailed study of the kinematics of faults within known deposits will lend insight to both pre-mineralization frameworks favorable to Au-bearing fluids and the potential post-mineralization offset of mineralized bodies. Further work to add value to targeting and exploration should place an emphasis on identifying major WNW- to E-W striking faults. These faults apparently bound major structural domains and knowledge of these structural boundaries along with how structural styles change between them will help to constrain targeting. For example, efforts to trace mineralizing structures along strike directly across the WNW-striking faults may prove to be largely unsuccessful, as they have been between the Galaxy deposit and Snake Eyes (Figure 26). The determination of slip vectors by offset linear piercing points such as fold hinges across the WNW-striking faults will give insight to subsurface geometries and potential mineralization offsets. Additionally, further study of why and how the orientation of primary through-going structures may change across the WNW-striking faults will aid in the understanding of the Bald Mountain Mining District's complex deformation history and the role that strike-slip faulting played in the current structural framework.

References Cited

Allmendinger, R.W., Cardozo, N., and Fisher, D., 2011, Structural Geology Algorithms: Vectors and Tensors in Structural Geology: New York, Cambridge University Press, 304 p.

Bald Mountain - Operations - Kinross Gold Corporation, https://www.kinross.com/operations/#americas-baldmountain (accessed February 2022).

Carlin Complex-Major Mines and Projects, Mining Data Online, https://miningdataonline.com/property/2967/Carlin-Complex.aspx (accessed February 2022).

Cashman, P.H., and Sturmer, D.M., 2021, Paleogeographic reconstruction of Mississippian to Middle Pennsylvanian basins in Nevada, southwestern Laurentia: Palaeogeography, Palaeoclimatology, Palaeoecology, v. 584, p. 1-23, doi:10.1016/j.palaeo.2021.110666.

Cox, B.E., Otto, B.R. 1995. Interim report for the Bald Mountain-Alligator Ridge regional geologic mapping project. Unpublished Placer Dome US internal report, 22 p.

Cline, J.S., Hofstra, A.H., Muntean, J.L., Tosdal, R.M., and Hickey, K.A., 2005, Carlin-Type Gold Deposits in Nevada Critical Geologic Characteristics and Viable Models, Society of Economic Geologists, v. One Hundredth Anniversary, p. 451-484, doi:10.5382/AV100.15.

Constenius, K.N., 1996, Late Paleogene extensional collase of the Cordilleran foreland fold and thrust belt. Geological Society of America Bulletin: Geological Society of America Bulletin, v.108, n.1, p. 20-39, doi: https://doi.org/10.1130/0016-7606(1996)108<0020:LPECOT>2.3.CO;2

Currie, J.B., Patnode, H.W., and Trump, R.P., 1962, Development of Folds in Sedimentary Strata: Geological Society of America Bulletin, v. 73, p. 655-673, doi:10.1130/0016-7606(1962)73[655:DOFISS]2.0.CO;2.

DeCelles, P.G., and Coogan, J.C., 2006, Regional structure and kinematic history of the Sevier fold-and-thrust belt, central Utah: Geological Society of America Bulletin, v. 188, p. 841–864, doi:10.1130/B25759.1.

Dickinson, W.R., 2006, Geotectonic evolution of the Great Basin: Geosphere, v. 2, p. 353-368, doi:10.1130/GES00054.1.

Druschke, P., Hanson, A.D., and Wells, M.L., 2009, Structural, stratigraphic, and geochronologic evidence for extension predating Palaeogene volcanism in the Sevier hinterland, east-central Nevada: International Geology Review, v. 51, p. 743–775, doi:10.1080/00206810902917941.

Emsbo, P., Groves, D.I., Hofstra, A.H., and Bierlein, F.P., 2006, The giant Carlin gold province: a protracted interplay of orogenic, basinal, and hydrothermal processes above a lithospheric boundary: Mineralium Deposita, v. 41, p. 517–525, doi:10.1007/s00126-006-0085-3.

Griesel, G., Valli, F., Essman, J., Rhys, D., Hart, E., Phillips, A., and Berg, E. Five Years Later: Progressing the Rhys Model of Fold and Fault Geometry on the Carlin Trend via Integration of Mapping, Sequence Stratigraphy and Lithogeochemistry, Geological Society of Nevada Conference-Vision for Discovery: Geology and Ore Deposits of the Basin and Range, Geological Society of Nevada, p. 137–155.

Henry, C.D., McGrew, A.J., Colgan, J.P., Snoke, A.W., and Brueseke, M.E., 2011, Timing, distribution, amount, and style of Cenozoic extension in the northern Great Basin, *in* Geologic Field Trips to the Basin and Range, Rocky Mountains, Snake River Plain, and Terranes of the U.S. Cordillera, Geological Society of America, p. 27–66, doi:10.1130/2011.0021(02).

Hitchborn, A.D., Arbonies, D.G., Peters, S.G., Connors, K.A., Noble, D.C., Larson, L.T., Beebe, J.S., McKee, E.H., Coyner, A.R. and Fahey, P.L., 1996, Geology and gold deposits of the Bald Mountain mining district, White Pine County, Nevada. *I*n Geology and ore deposits of the American cordillera: Reno, Geological Society of Nevada, Symposium proceedings, p. 505-546.

Hammond, K.J., and Evans, J.P., 2003, Geochemistry, mineralization, structure, and permeability of a normal-fault zone, Casino mine, Alligator Ridge district, north central Nevada: Journal of Structural Geology, v. 25, p. 717–736, doi:10.1016/S0191-8141(02)00060-3.

Harbaugh, D.W., 1980, Depositional Facies and Provenance of the Mississippian Chainman Shale and Diamond Peak Formation, Central Diamond Mountains, Nevada [Doctoral Dissertation]: Stanford University.

Ilchik, R.P., 1990, Geology and geochemistry of the Vantage gold deposits, Alligator Ridge-Bald Mountain mining district, Nevada: Economic Geology, v. 85, p. 50–75, doi:10.2113/gsecongeo.85.1.50.

Ketner, K., and Alpha, A., 1988, Mesozoic and Tertiary rocks near Elko, Nevada; evidence for Jurassic to Eocene folding and low-angle faulting: U.S. Geological Survey Bulletin 1988–C, 20 p., doi:10.3133/b1988C.

Kleinhampl, F.J. and Ziony, J.I., 1985, Geology of northern Nye County, Nevada*:* Nevada Bureau of Mines and Geology Bulletin A, 99, p.172-195.

Long, S.P., 2015, An upper-crustal fold province in the hinterland of the Sevier orogenic belt, eastern Nevada, U.S.A.: A Cordilleran Valley and Ridge in the Basin and Range: Geosphere, v. 11, p. 404–424, doi:10.1130/GES01102.1.

Long, S.P., 2018, Geometry and magnitude of extension in the Basin and Range Province (39°N), Utah, Nevada, and California, USA: Constraints from a province-scale cross section: GSA Bulletin, v. 131, p. 99–119, doi:10.1130/B31974.1.

Long, S.P., Henry, C.D., Muntean, J.L., Edmondo, G.P., and Cassel, E.J., 2014, Early Cretaceous construction of a structural culmination, Eureka, Nevada, U.S.A.: Implications for out-of-sequence deformation in the Sevier hinterland: Geosphere, v. 10, p. 564–584, doi:10.1130/GES00997.1.

Long, S.P., Thomson, S.N., Reiners, P.W., and Di Fiori, R.V., 2015, Synorogenic extension localized by upper-crustal thickening: An example from the Late Cretaceous Nevadaplano: Geology, v. 43, p. 351–354, doi:10.1130/G36431.1.

Long, S.P., 2019, Geometry and magnitude of extension in the Basin and Range Province (39°N), Utah, Nevada, and California, USA: Constraints from a province-scale cross section: GSA Bulletin, v. 131, p. 99–119, doi:10.1130/B31974.1.

Marshak, S., Karlstrom, K., and Timmons, J.M., 2000, Inversion of Proterozoic extensional faults: An explanation for the pattern of Laramide and Ancestral Rockies intracratonic deformation, United States: Geology, v. 28, p. 735–738.

Mach, C., Wright, B., Bettles, K., Loranger, B., Ankomah, J., Pace, D., and Rehn, W., 2015, Geology of the Redbird Gold Deposit, Bald Mountain Mining District, White Pine County, Nevada: Geological Society of Nevada, 28 p.

McGrew, A.J., and Snee, L.W., 1994, 40Ar/39Ar thermochronologic constraints on the tectonothermal evolution of the Northern East Humboldt range metamorphic core complex, Nevada: Tectonophysics, v. 238, p. 425–450, doi:10.1016/0040-1951(94)90067-1.

Miller, E. L., Miller, M. M., Stevens, C. H., Wright, J. E., Madrid, R., 1992, Late Paleozoic paleogeographic and tectonic evolution of the western US Cordilleran *in* The Geology of North America, The Geological Society of America, The Cordilleran Orogen: Conterminous U.S., v. G-3, p. 57-107.

Mitra, S., 2002, Structural models of faulted detachment folds: AAPG Bulletin, v. 86, p. 1673-1694, doi:10.1306/61EEDD3C-173E-11D7-8645000102C1865D.

Mortensen, J.K., Thompson, J.F., Tosdal, R.M., Cluer, J.K., Price, J.G., Struhsacker, E.M., Hardyman, R.F. and Morris, C.L., 2000, U-Pb age constraints on magmatism and mineralization in the northern Great Basin, Nevada. Geological Society of Nevada, p. 419-438.

Muntean, J.L., Cline, J.S., Simon, A.C., and Longo, A.A., 2011, Magmatic–hydrothermal origin of Nevada's Carlin-type gold deposits: Nature Geoscience, v. 4, p. 122–127, doi:10.1038/ngeo1064.

Muntean, J.L., Coward, M.P., and Tarnocai, C.A., 2007, Reactivated Palaeozoic normal faults: controls on the formation of Carlin-type gold deposits in north-central Nevada: Geological Society, London, Special Publications, v. 272, p. 571–587, doi:10.1144/GSL.SP.2007.272.01.29.

Nelson, C., 1990, Comparative geochemistry of jasperoids from Carlin-type gold deposits of the western United States: Journal of Geochemical Exploration, v. 36, p. 171–195.

Nutt, C.J., and Good, S.C., 1998, Recognition and Significance of Eocene Deformation in the Alligator Ridge Area, Central Nevada: Contributions to the Gold Metallogeny of Northern Nevada, Open-File Report 98-338, 10 p., doi:10.3133/ofr98338B.

Nutt, C.J., Hofstra, A.H., Hart, K.S., and Mortensen, J.K., 2000, Structural Setting and Genesis of Gold Deposits in the Bald Mountain-Alligator Ridge Area, East-Central Nevada: Geology and Ore Deposits 2000: The Great Basin and Beyond Proceedings, v. I, p. 513-537.Nutt, C.J., and Hofstra, A.H., 2003, Alligator Ridge District, East-Central Nevada: Carlin-Type Gold Mineralization at Shallow Depths: Economic Geology, v. 98, p. 1225–1241.

Nutt, C.J., and Hofstra, A.H., 2007, Bald Mountain Gold Mining District, Nevada: A Jurassic Reduced Intrusion-Related Gold System: Economic Geology, v. 102, p. 1129–1155, doi:10.2113/gsecongeo.102.6.1129.

Otto, B., 1994, Summary Report and Drill Proposal for Vantage Basin, Alligator Ridge Mine, White Pine County, Nevada. Internal Report for Placer Dome U.S., 37 p.

Pace, D., 2009, Relationship Between Magmatism and Mineralization in the RBM Gold Deposit, White Pine County, Nevada: [MS thesis]: University of Nevada, Reno, 181 p.

Perry, R., and Visher, M., 2019, Major Mines of Nevada 2018-Mineral Industries in Nevada's Economy: The Nevada Division of Minerals, v. 30, 35 p.

Poole, F.G., 1974, Flysch Deposits of the Antler Foreland Basin, Western United States: *in* Tectonics and Sedimentation. Dickinson, W.R. ed., SEPM (Society for Sedimentary Geology), p. 58-82, doi:10.2110/pec.74.22.

Poole, F.G. and Sandberg, C.A., 1977, Mississippian paleogeography and tectonics of the western United States: Society for Sedimentary Geology Pacific Section, Field Trip Guide, p. 67-85.

Poole, F. G., Stewart, J. H., Palmer, A. R., Sandberg, C. A., Madrid, R. J., Ross Jr, R. J., and Wrucke, C. T., 1992, Latest Precambrian to Latest Devonian time; Development of a Continental Margin *in* The Geology of North America, Geological Society of America, v. G-3, The Cordilleran Orogen: Conterminous U.S., p. 9-57.

Price, S., 2010, The Battle Mountain—Eureka trend: Evidence for a collapsed Mesozoic to early Tertiary compressional uplift: Geological Society of Nevada, 2015 Symposium, p. 549-584.

Ressel, M.W., 2006, Igneous Geology of the Carlin Trend, Nevada: Development of the Eocene Plutonic Complex and Significance for Carlin-Type Gold Deposits: Economic Geology, v. 101, p. 347–383, doi:10.2113/gsecongeo.101.2.347.

Rhys, D., Valli, F., Burgess, R., Heitt, D., Griesel, G., and Hart, K., 2015, Controls of Fault and Fold Geometry on the Distribution of Gold Mineralization on the Carlin Trend: Geological Society of Nevada, 2015 Symposium, p. 333–389.

Rigby, J., 1960, Geology of the Buck Mountain-Bald Mountain area, southern Ruby Mountains, White Pine County, Nevada, *in* Guidebook to the Geology of East Central Nevada, Intermountain Association of Petroleum Geologists, 11th Anniversary Field Conference, p. 173–180.

Saller, A.H., and Dickinson, W.R., 1982, Alluvial to marine facies transition in the Antler overlap sequence, Pennsylvanian and Permian of North-central Nevada: Journal of Sedimentary Research, v. 52, p. 925–940, doi:10.1306/212F8094-2B24-11D7-8648000102C1865D.

Speed, R.C. and Sleep, N.H., 1982. Antler orogeny and foreland basin: A model: Geological Society of America Bulletin, v.93, p.815-828.

Taylor, W.J., Bartley, J.M., Martin, M.W., Geissman, J.W., Walker, J.D., Armstrong, P.A., and Fryxell, J.E., 2000, Relations between hinterland and foreland shortening: Sevier orogeny, central North American Cordillera: Tectonics, v. 19, p. 1124–1143, doi:10.1029/1999TC001141.

Teal, L., and Jackson, M., 2002, Geologic Overview of the Carlin Trend Gold Deposits. *In*: Gold deposits of the Carlin trend (Thompson, T.B., Teal, L., Meeuwig, R. O., eds.). Nevada Bureau of Mines and Geology Bulletin 111, p. 9–19.

Thorman, C.H., Ketner, K.B., Brooks, W.E. and Snee, L.W., Schafer, RW, and Wilkinson, WH, 1991, Geology and Ore Deposits of the Great Basin, Symposium Proceedings: The Geological Society of Nevada, p. 25-45.

Thorman, C.H., Sandberg, C.A., Henry, C.D., Zuza, A.V., and Ressel, M.W., 2020, The Late Middle Jurassic Elko Orogeny—An Update: The Geological Society of Nevada, 6 p.

Trexler, J.H., Cashman, P.H., Snyder, W.S., and Davydov, V.I., 2004, Late Paleozoic tectonism in Nevada: Timing, kinematics, and tectonic significance: Geological Society of America Bulletin, v. 116, p. 525-538, doi:10.1130/B25295.1.

Wannamaker, P.E., and Doerner, W.M., 2002, Crustal structure of the Ruby Mountains and southern Carlin Trend region, Nevada, from magnetotelluric data: Ore Geology Reviews, v. 21, p. 185–210, doi:https://doi.org/10.1016/S0169-1368(02)00089-6.

Wyld, S.J., 2002, Structural evolution of a Mesozoic backarc fold-and-thrust belt in the U.S. Cordillera: New evidence from northern Nevada: Geological Society of America Bulletin, v. 114, p. 1452–1468.

Wernicke, B., 1992, Cenozoic Extensional Tectonics of the U.S. Cordillera, *in* The Geology of North America, Geological Society of America, v. G-3, The Cordilleran Orogen: Conterminous U.S., p. 553–581.

Whitmore, R., 2011, Mid- to Late-Paleozoic Deformation on Buck Mountain, Nevada [MS thesis]: University of Nevada, Reno, 70 p.

Table 1 -Summary of the Rhys et al. (2015) deformation model phases

Phase	Structure	Orientation	Tectonic Event
I	Roberts Mountain Thrust	Low angle W dipping	Dev-Miss Antler Orogeny
II	Thrusts + inclined to recumbent folds	Shallow W to NW thrusts + N to NE trending folds	Miss-Jur Sonoma + Elko Orogenies
III	Steep reverse faults + upright, open folds	NW striking, steeply SW dipping + NW trends	K-Eocene Laramide + Sevier Orogenies
IV	Extensional faulting	NW to NE striking, steeply dipping	Oligocene-present Basin and Range

Table 2-Summary of Domain Classes

Domain Class	Description
A	Gently to moderately dipping homoclines
B	NW- to NNW-trending, horizontal to gently plunging, upright, gentle, km-scale, cylindrical to sub-cylindrical folds and anticline/syncline pairs
C	N to NNE- trending, horizontal to gently plunging, upright to moderately inclined axial plane, close to tight, km-scale, asymmetric folds
D	E- to NE- facing monoclines or with abrupt limb rollover at a decameter to kilometer scale

Table 3- Selected Domain Classes discussed in the text with reference to location and corresponding figure.

Domain Class	Domain Codes	Area	Figures
A	SWB01, SEB01, TOP01/02	North District	11,13,15
B	BUC05, BUC06, SNK03	Buck Pass, N. Mooney	17,18
C	GAT01	S. Alligator Ridge	19
D	SNK04, GAL01, RYL01, WIN01	Royale, Snake Eyes, Galaxy, Winrock	20,27,31,38

Table 4-Overview of assigned deformation phases at BMMD and correlation to the Rhys et al. (2015) phases in the Carlin Trend.

Phase	Structure	Scale	Orientation	Kinematics	Tectonic Event	Phase in Rhys et al. (2015)
1	• reverse faults • open to overturned folds	• km • m to km	• NNE to NE strike • NNE to NE trend	ESE to SE vergent	Permian to Late Jurassic, Sonoma, and Elko Orogenies	I+II
2	• strike-slip and tear faults	• km	• WNW to NW strike	Formation of strike-slip transtensional system on NW-striking faults	Late Jr to K back-arc plutonism and Laramide + Sevier onset	N/A
3	• gently plunging open folds • steep reverse faults • low angle thrusts	• m to km • m to km • dm to km	• NNW to NW trend • NNW to NW strike • N strike	ENE-WSW shortening	Late K to Eocene Sevier hinterland CNTB and ENFB	III
4	• close to tight folds • strike-slip faults	• m to dm • dm to km	• NW trend • W to NW strike	NE-SW shortening, sinistral transpression on NNW-striking faults	mid Eocene to Oligocene RMCC exhumation	N/A
5	• listric to planar normal faults • detachment faults	• m to km • km	• N to NE strikes • N strike	NW-SE extension	mid Eocene to contemporary Basin and Range extension	IV

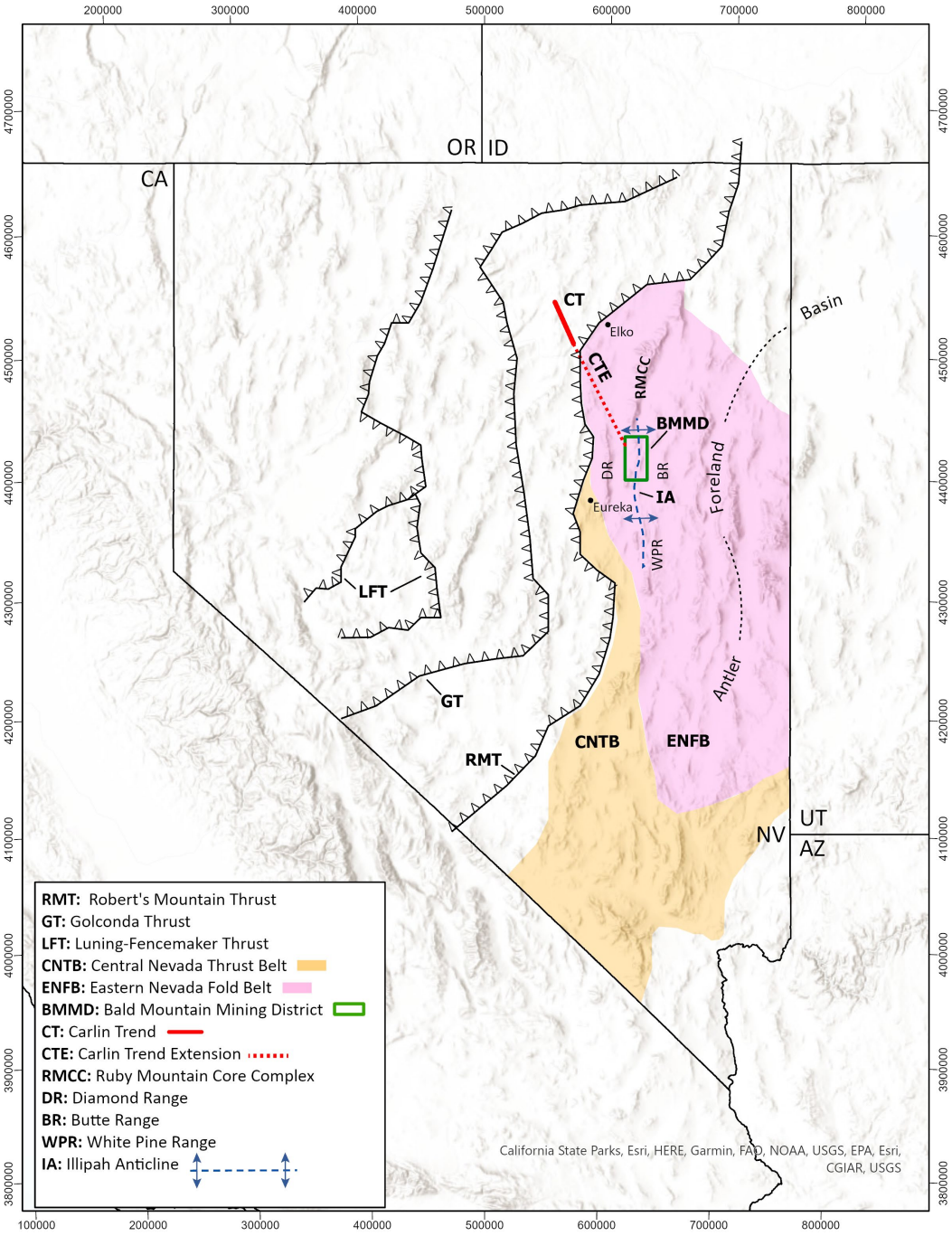

Figure 1- Regional tectonic and geographic location map with the toothed lines showing the approximate locations of regional thrust traces. The dotted black lines shows the approximate center of the Antler Foreland Basin of the RMT. The pink polygon encompasses the Eastern Nevada Fold Belt (ENFB), and the orange polygon encompasses the Central Nevada Thrust Belt (CNTB) along with other areas of Sevier-related thrusting in Nevada (Long, 2015). Grid coordinates on all maps are in UTM NAD 27 zone 11N.

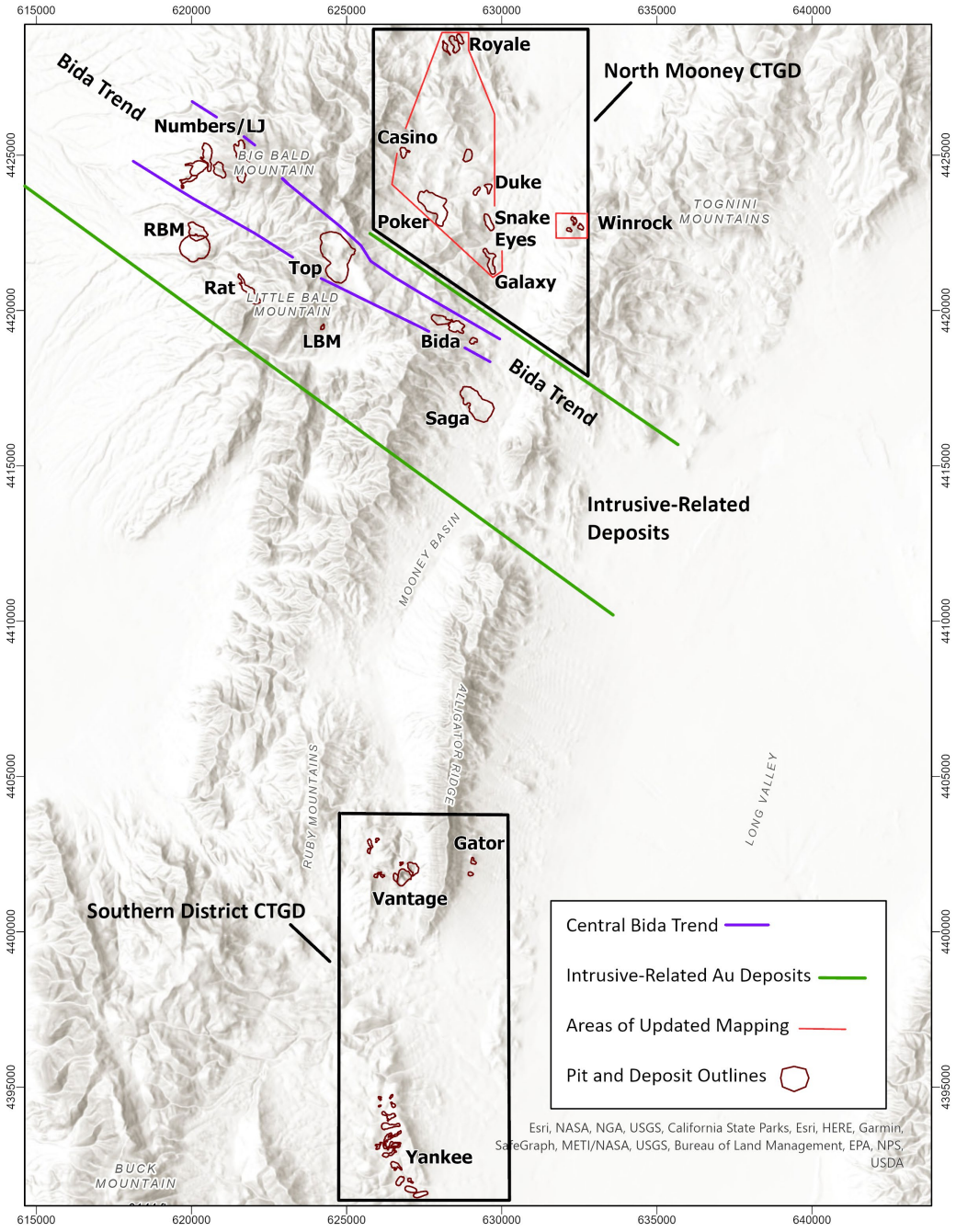

Figure 2-District overview figure zoomed in on the green box from Figure 1. Brown polygons and adjacent names denote deposits. The southern black box outlines the southern district Carlin-type gold deposits (CTGD), also known as the Alligator Ridge District. The purple outlines the core of the Bida trend, while the northwest trending green box outlines intrusive-related deposits associated with the Bald Mountain stock and an area sharing some parallel structural fabric with the Bida trend (Nutt et al., 2000). The northern black polygon outlines the North Mooney Basin study area, and the red polygons within denote areas of updated mapping for this study.

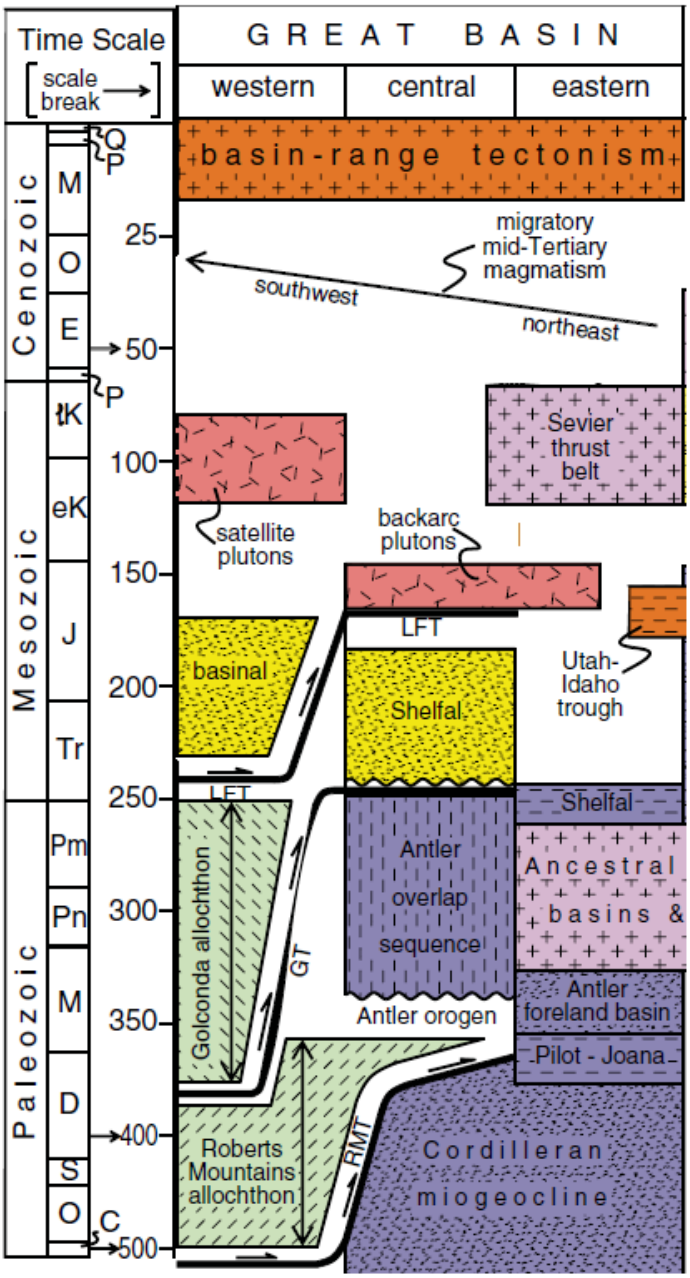

Figure 3-A space-time diagram of tectonic events in the Great Basin. GT= Golconda Thrust, RMT= Roberts Mountain Thrust, LFT=Luning-Fencemaker Thrust. Modified from Dickinson (2006).

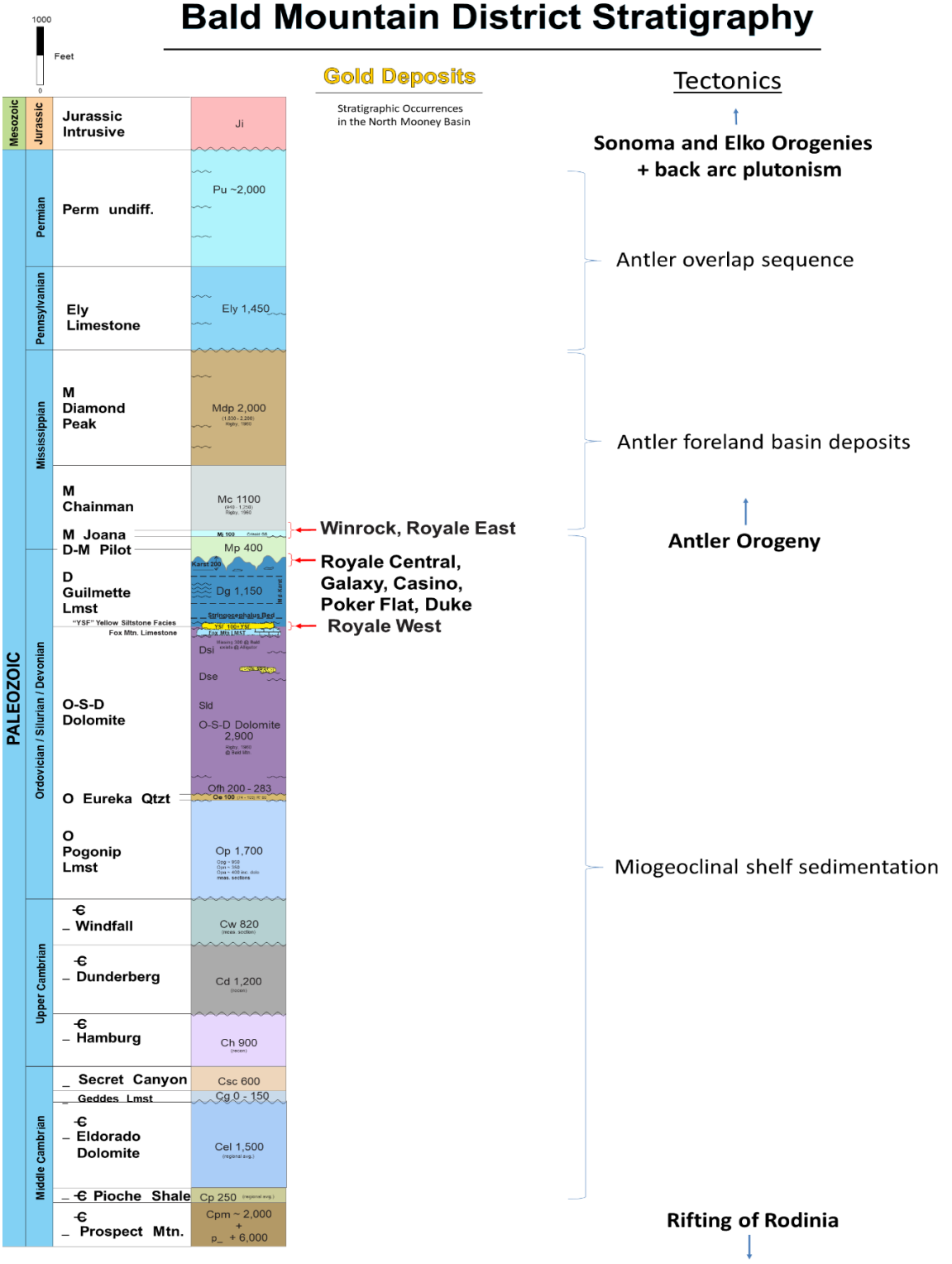

Figure 4- Stratigraphy of BMMD, modified from Barrick Gold Corp. geologists (written comm., D.L. Schwarz et al., 2012). High resolution image can be electronically magnified for detail. Stratigraphic locations of Au deposits in the NMB are noted on the left. Corresponding tectonic and sedimentation events are noted on the right. Average stratigraphic thicknesses of units are variable and based on locally measured sections and regional averages. Note the scale bar in the upper left corner, all thicknesses are stated in feet.

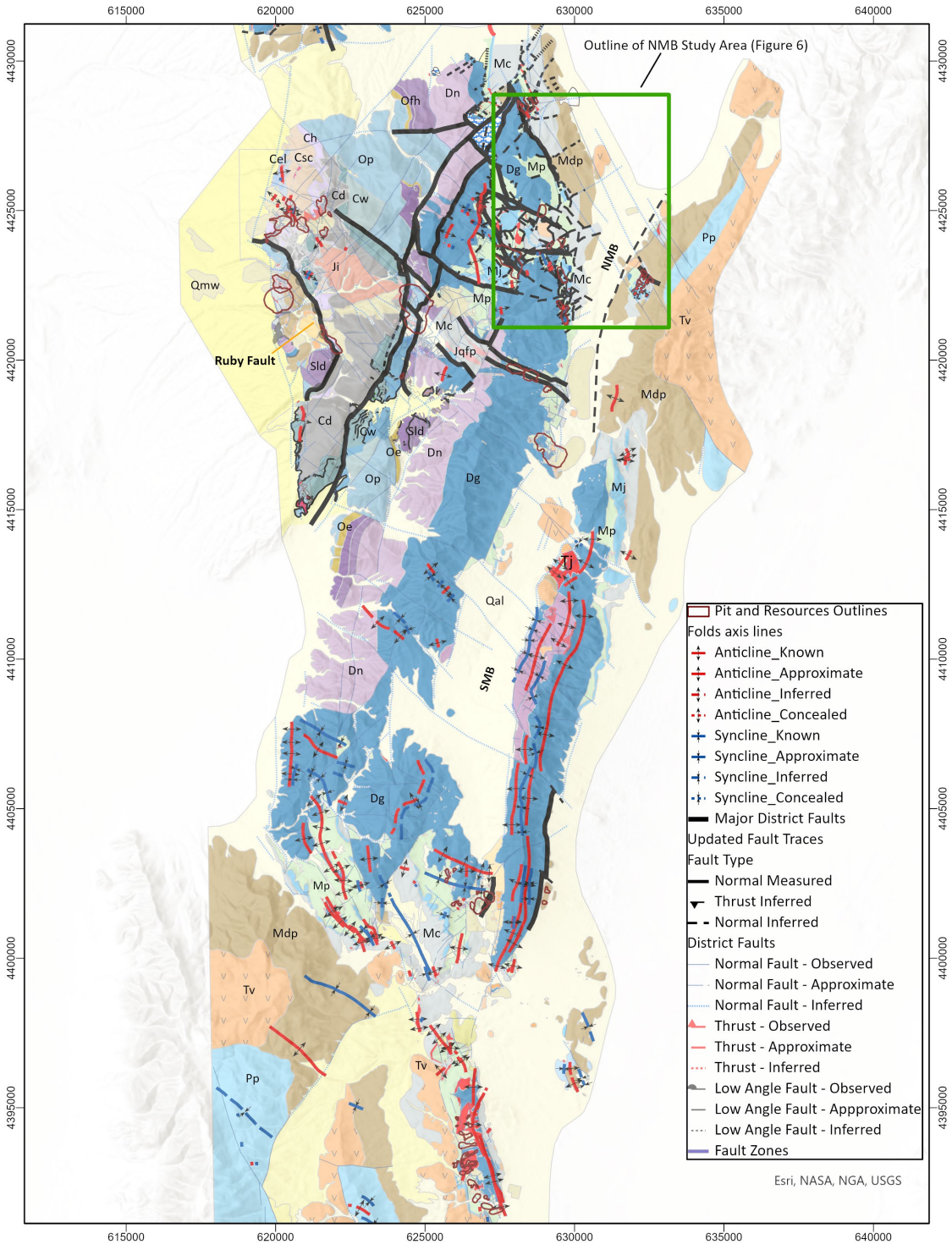

Figure 5 -An overview map of the BMMD geology with major folds and faults. The bold black lines represent selected major faults discussed in the text. Light blue lines represent historically mapped faults (unpublished internal mapping). Complete legend of geologic units on Figures 4 and 7, complete legend of structure symbols on Figure 8. The green box highlights the North Mooney Basin (NMB) study area of Figure 6. NMB marks the geographic North Mooney Basin and SMB the South Mooney Basin. See Data Supplement 1 for ArcGIS data.

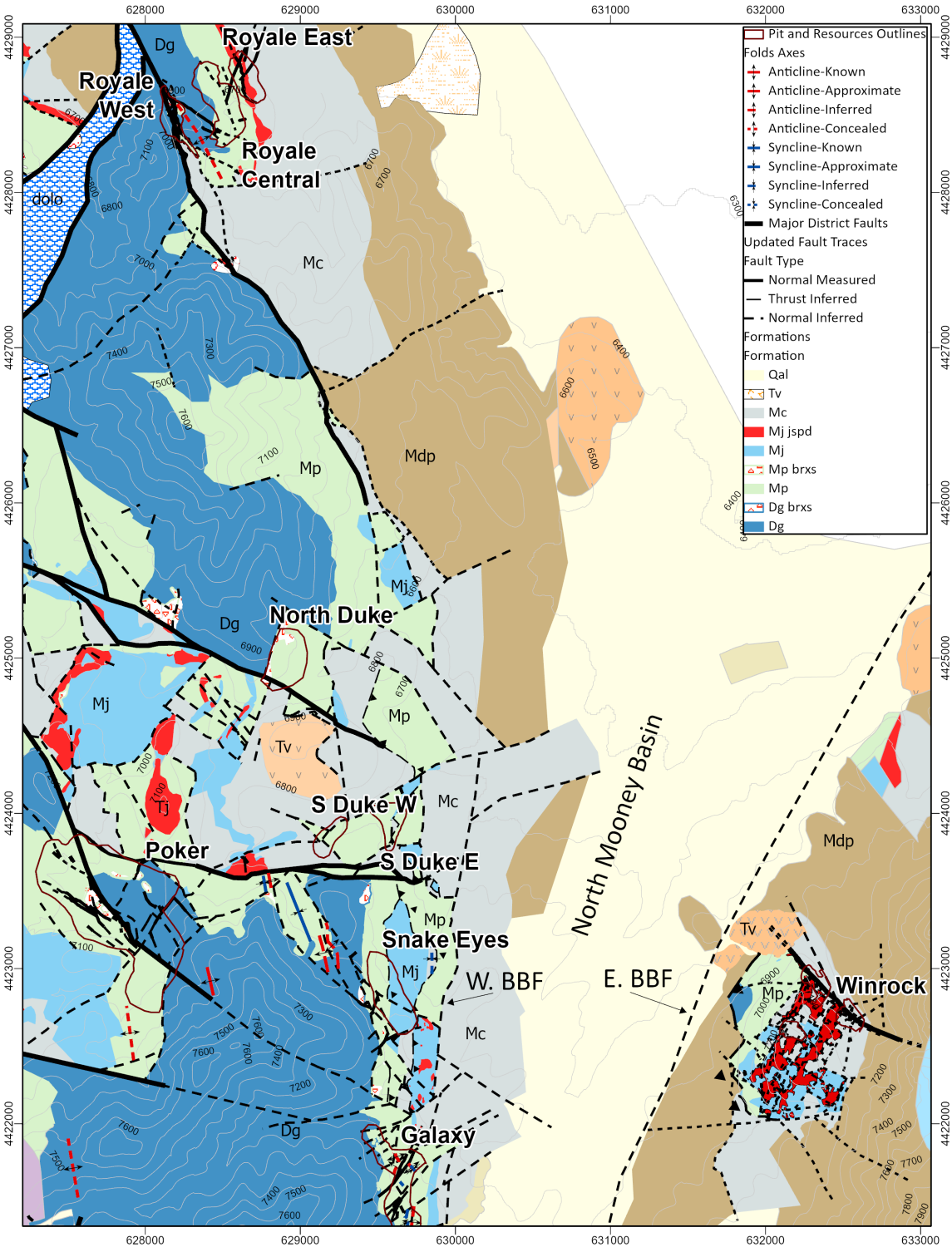

Figure 6- An overview geology map of the North Mooney Basin study area. Location shown by green box in Figure 5. “E. BBF” and “W. BBF” mark the east and west Mooney Basin bounding faults, respectively. Complete legend of geologic unit colors on Figure 7- “jspd” = jasperoid, “brxs” = silicified breccia. Complete structural legend on Figure 8.

Bald Mountain Lithologic Units Map Legend

Figure 7-Legend of geologic map units. Includes original mapping lithologies (Kinross Gold Corp., Barrick Gold Corp., unpublished internal mapping). Geologic units included in the legend span the entire BMMD.

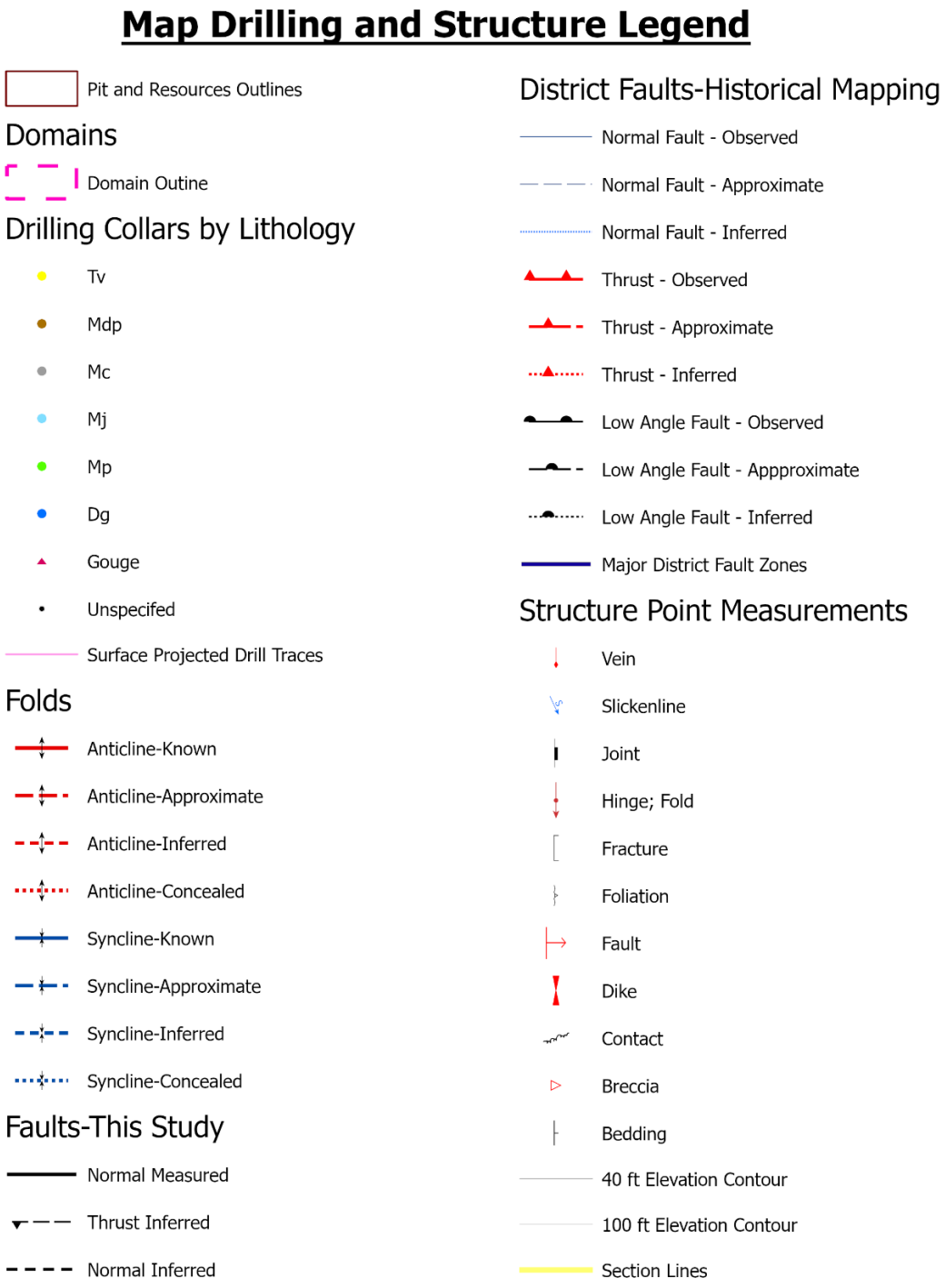

Figure 8- Mapping Symbology Legend. The District Faults- Historical Mapping heading displays symbols used by Barrick Gold Corp and Kinross Gold Corp. Different symbols under the Faults-This Study heading are used in this study to highlight edits and variations with respect to historical mapping.

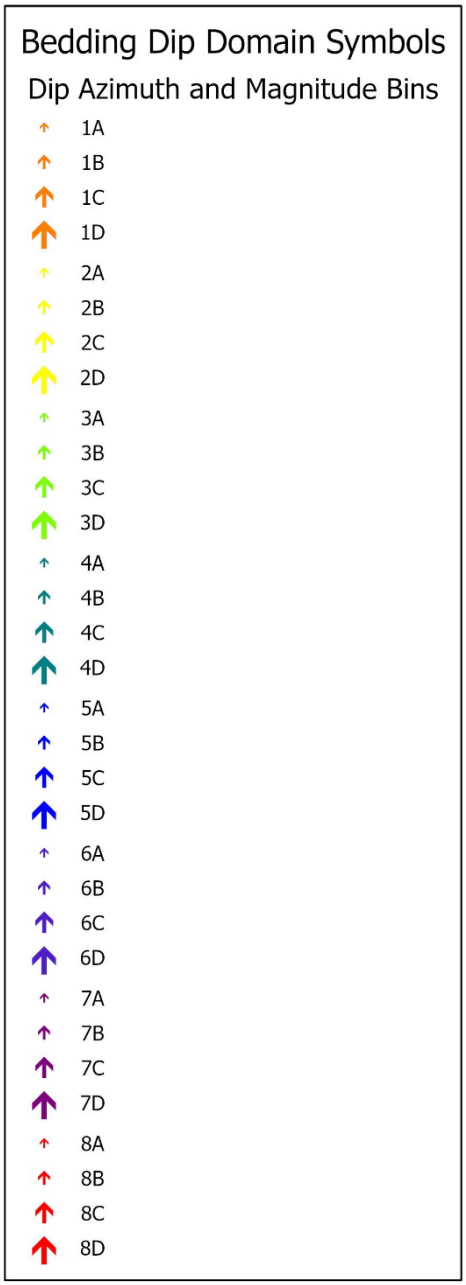

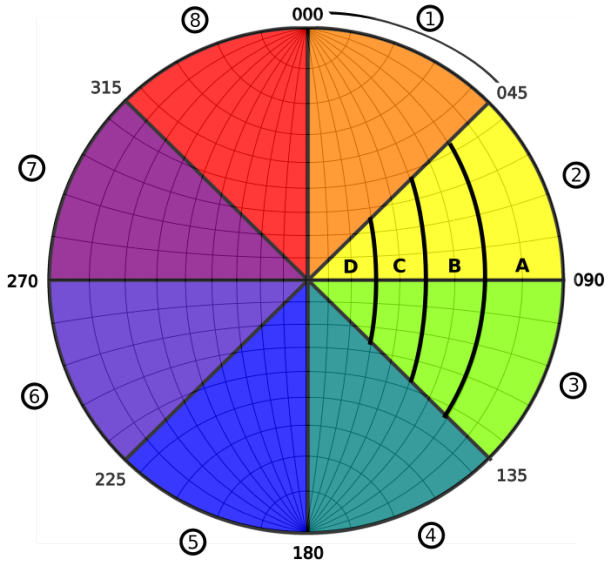

Figure 9 -Dip bin symbology: Colored slices represent 45-degree dip azimuth ranges in sub-bins 1-8. Letters represent dip magnitude sub-bins, A: 0°- 20°, B: 20°- 40°, C: 40°- 60°, and D: 60°- 90°. Arrow symbology on map is represented by color and size, with high magnitude dips displayed largest, and arrows are rotated to display dip direction on the maps.

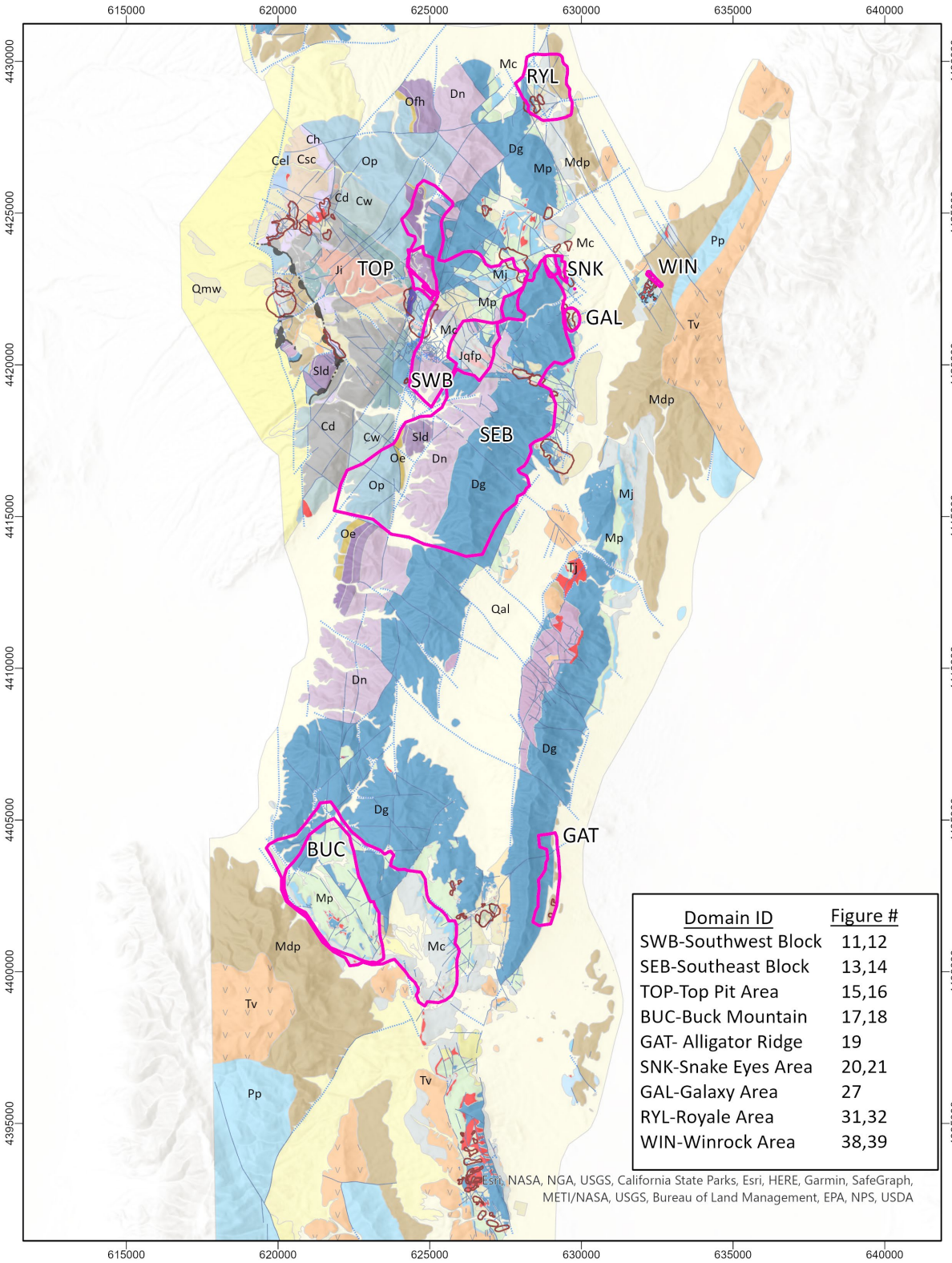

Figure 10- Map of the Bald Mountain mining district from unpublished Kinross Gold Corp. databases. Three-letter abbreviations label the structural domains noted in Tables 2 and 3. Units are defined in Figure 7. Structures are defined in Figure 8. Plate 1 and Data Supplement 1 show complete data compiled for this study.

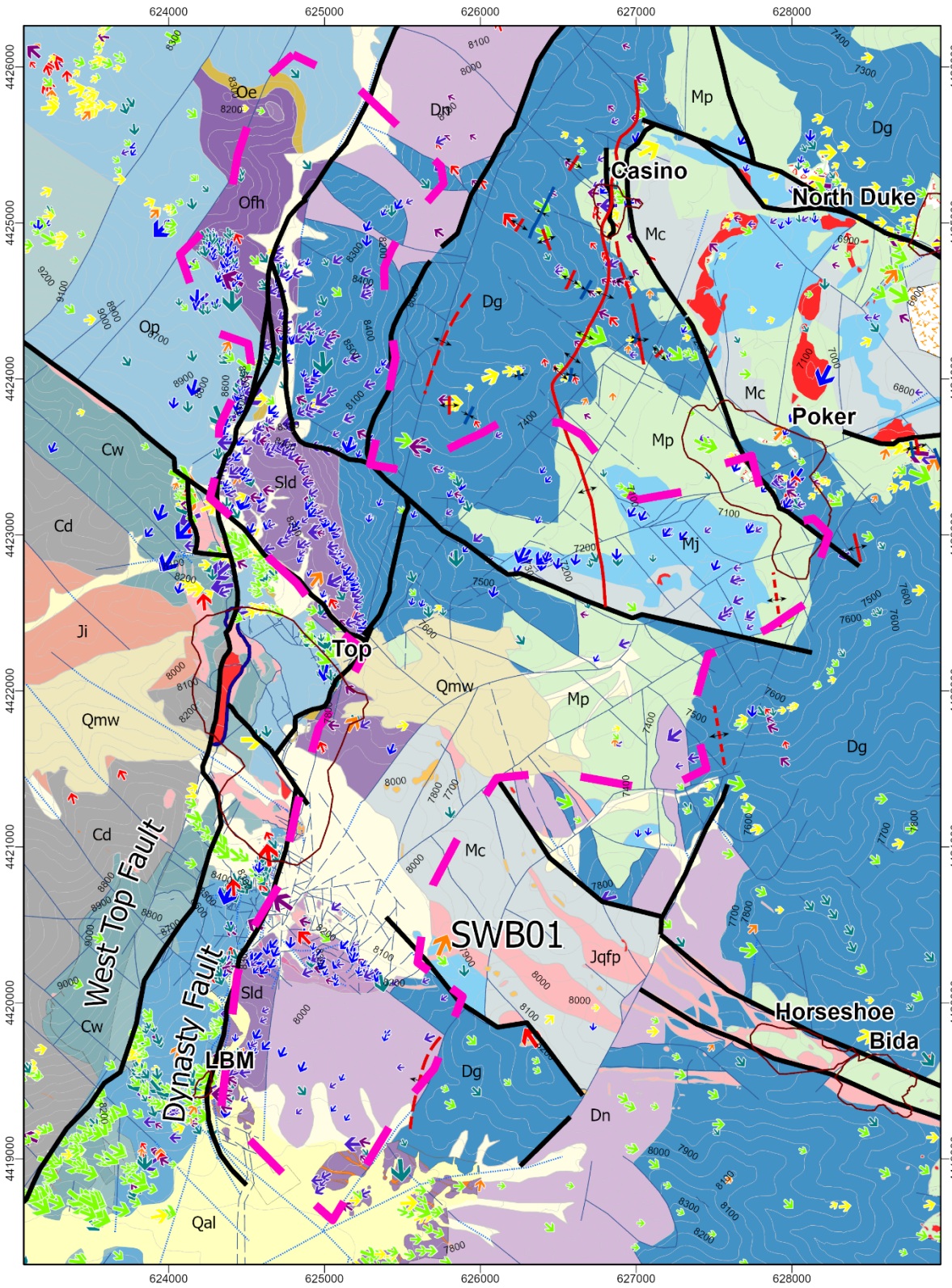

Figure 11- Geologic map of SWB01 from Domain Class A displays a broad SW dipping homoclinal block. Units and symbols are defined in Figures 7, 8, and 9.

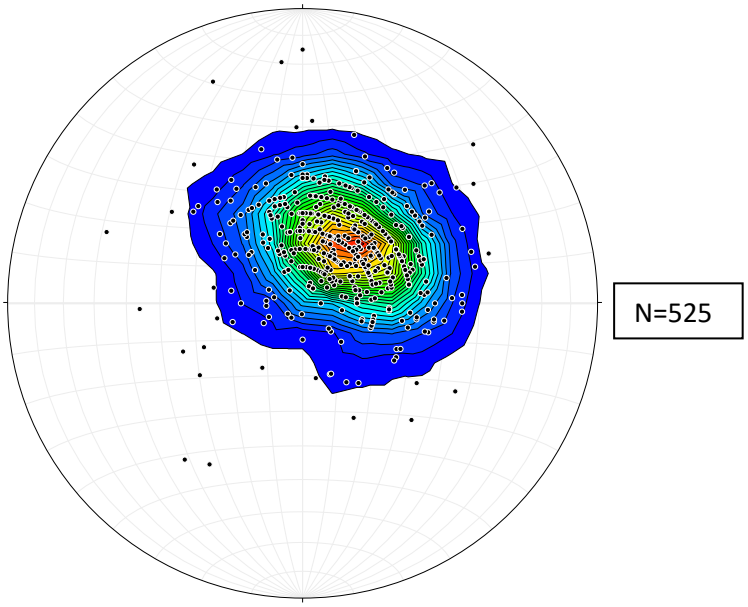

Figure 12- Equal area stereographic projection of poles to bedding planes in the Class A Domain SWB01. Colors display smoothed Kamb contours with an interval of two and twenty grid nodes. Average bedding measurement = 127/19 (s/d).

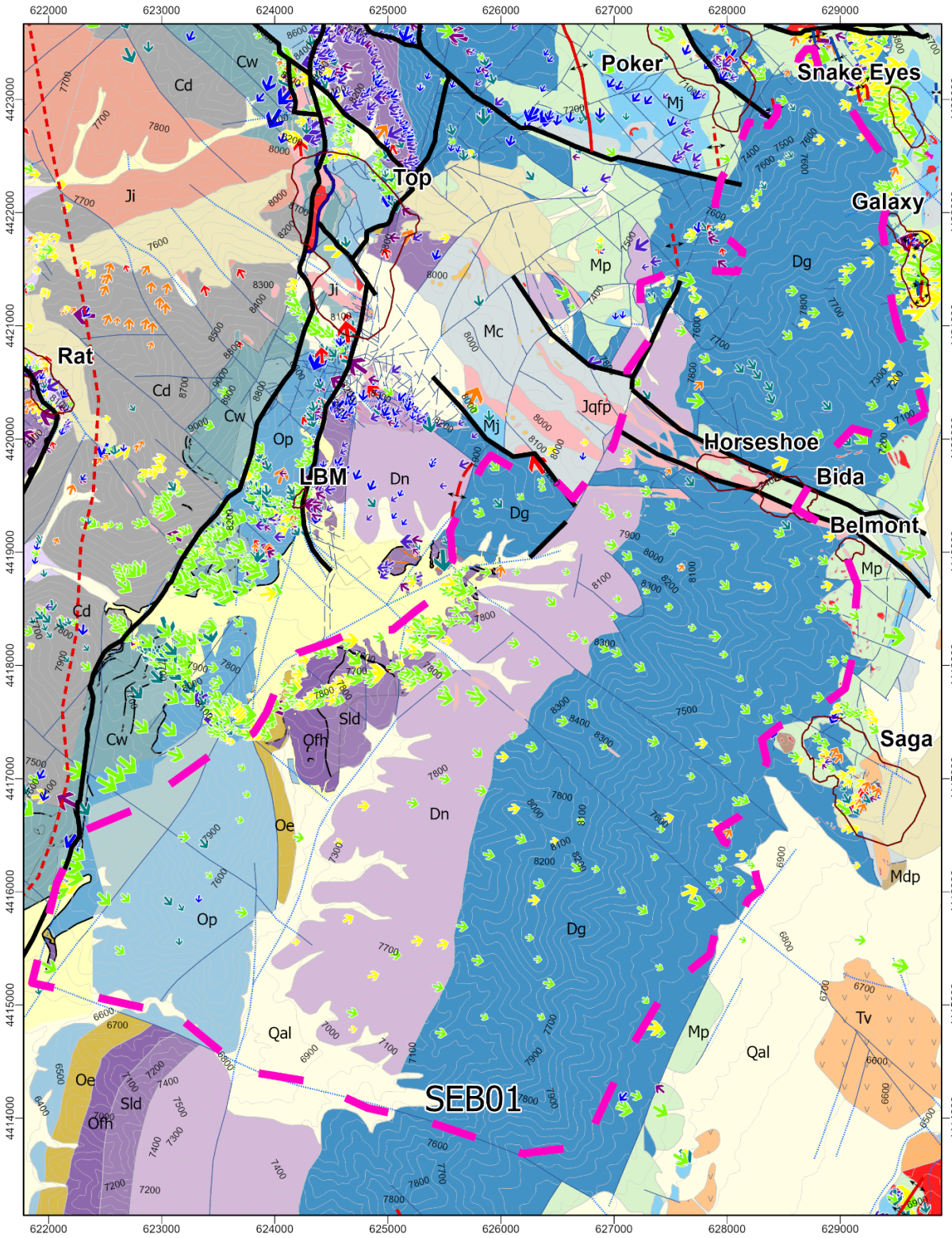

Figure 13 -Geologic map displaying the SEB01 domain of Domain Class A as a broadly grouped homocline of east to east-southeast dipping bedding in the central Bald Mountain district. Units and symbols are defined in Figures 7, 8, and 9.

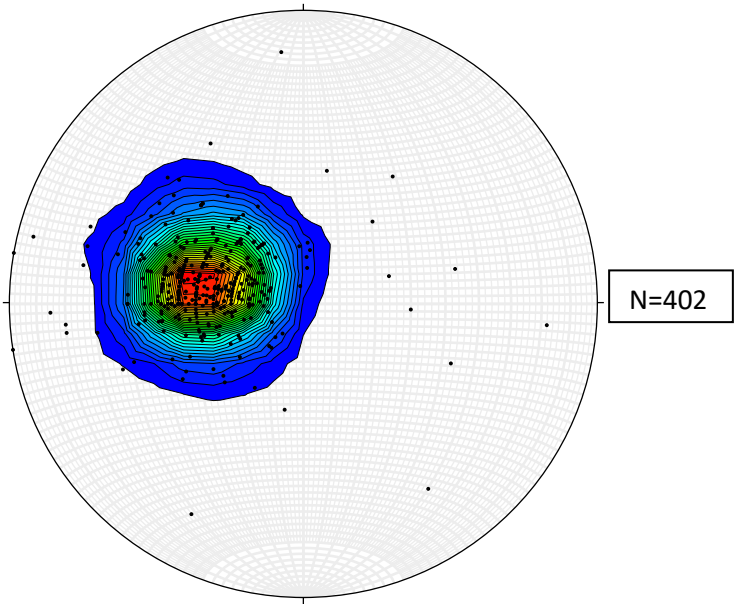

Figure 14- Equal area stereographic projection of poles to bedding planes in the Domain Class A SEB01. Figure 12 includes Kamb contour specifications. Average bedding measurement = 014/28 (s/d).

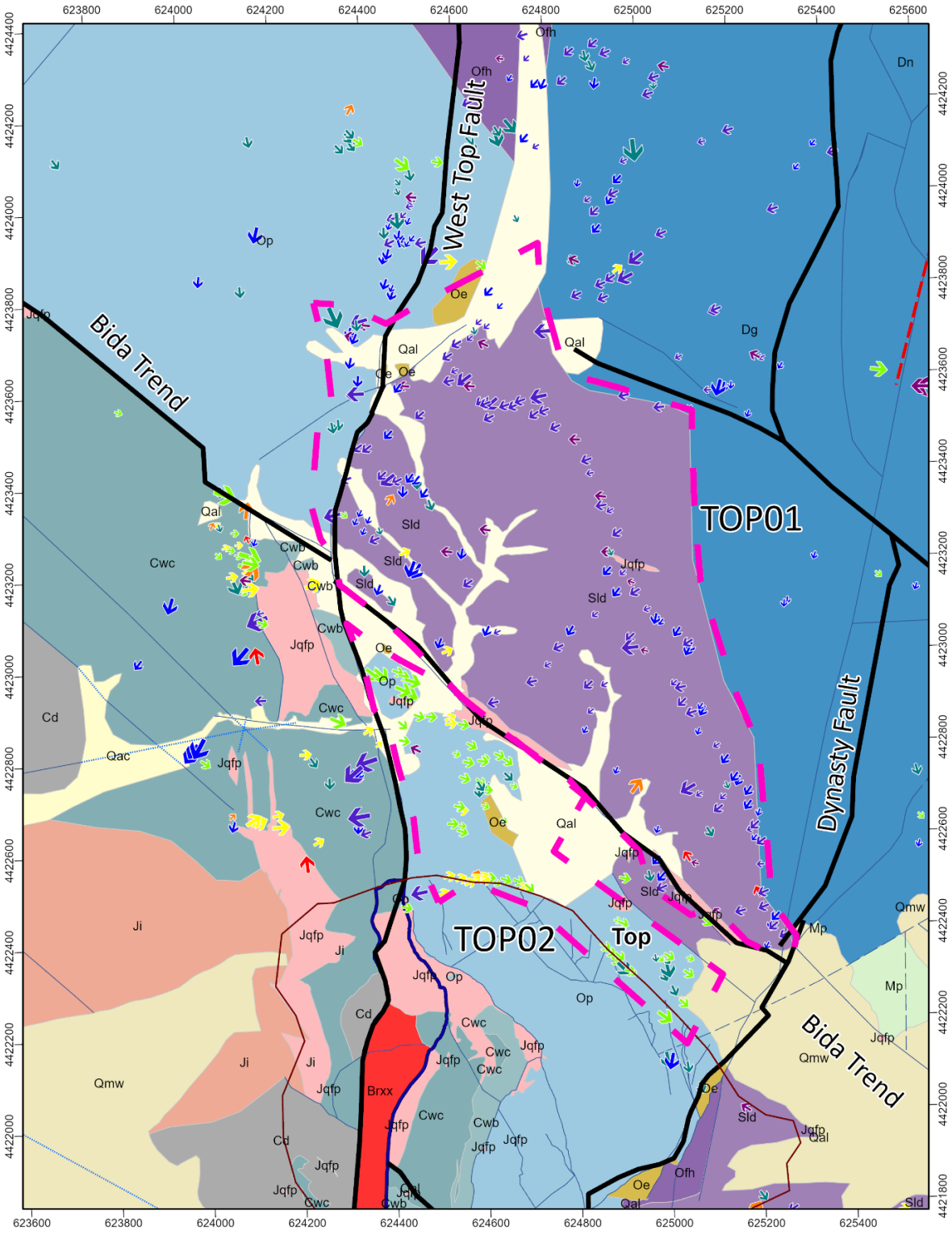

Figure 15-Geologic map displaying the Class A domains of TOP01 and TOP02, located directly north of the Top deposit and at the intersection of the Bida trend, West Top Fault, and Dynasty fault. Units and symbols are defined in Figures 7, 8, and 9.

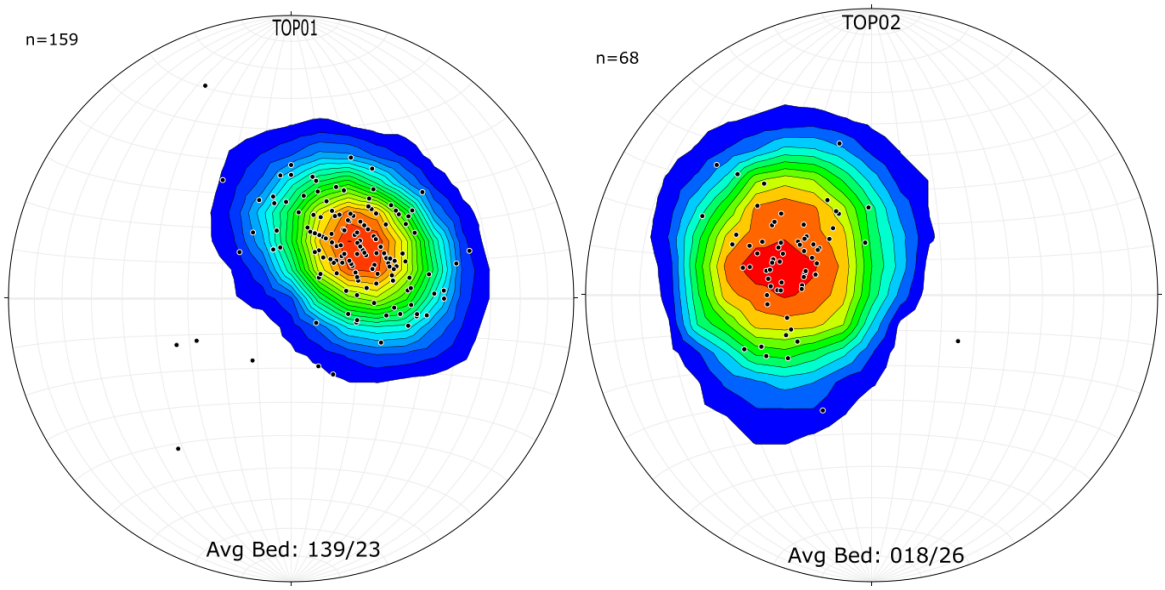

Figure 16-Stereonet plots of poles to bedding planes within the Class A TOP01 and TOP02 domains. Kamb contour interval specifications are included on Figure 12.

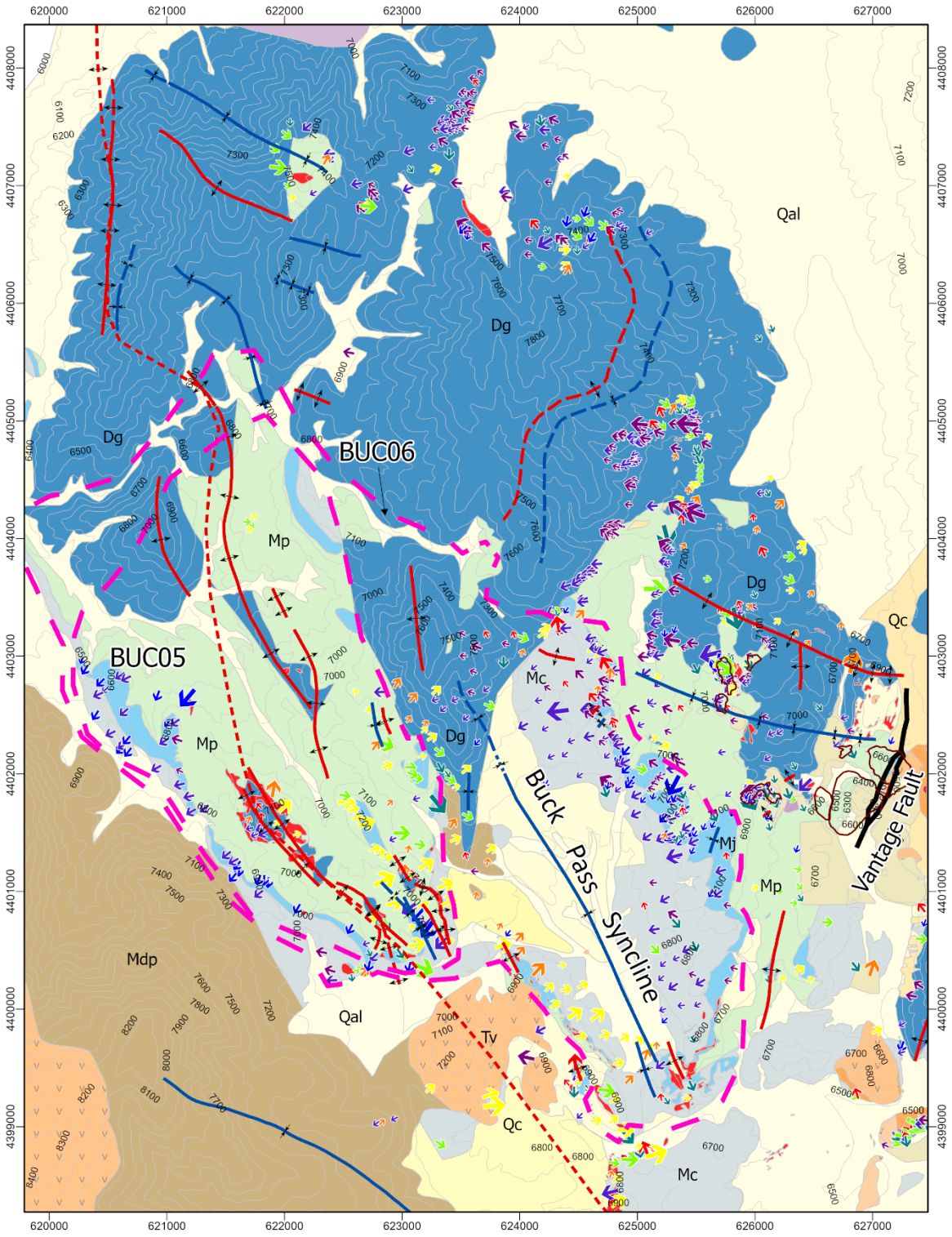

Figure 17- Domains BUC05 and BUC06 in the southern district Buck Pass area, from Domain Class B. BUC05 contains multiple anticline/syncline pairs that are parasitic to the broader NW-trending fold pattern contained by BUC06. Units and symbols are defined in Figures 7,8 and 9.

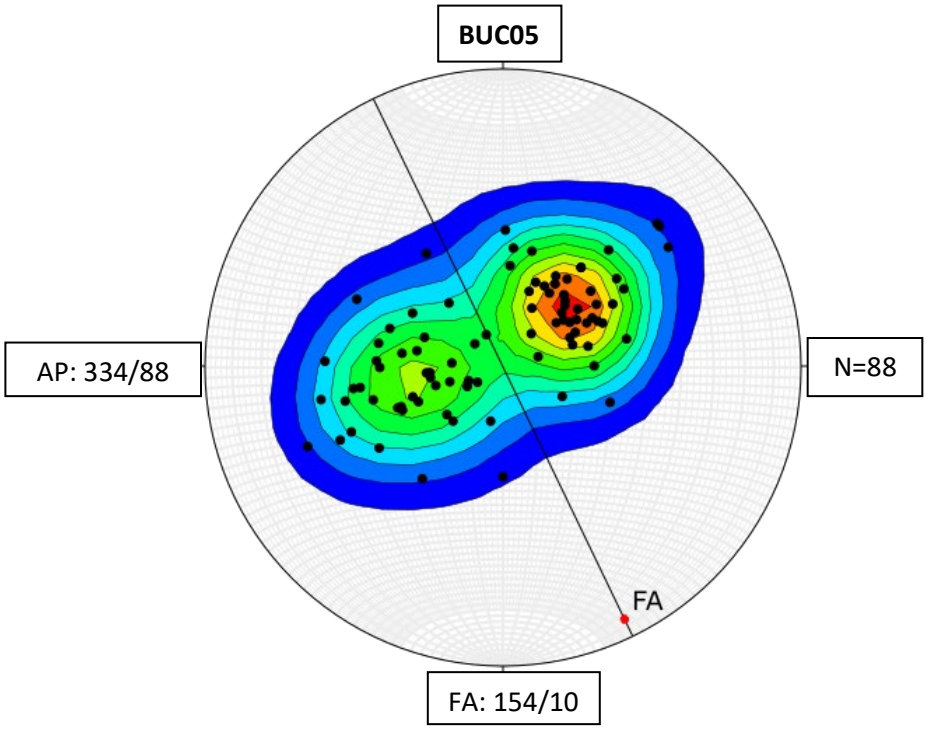

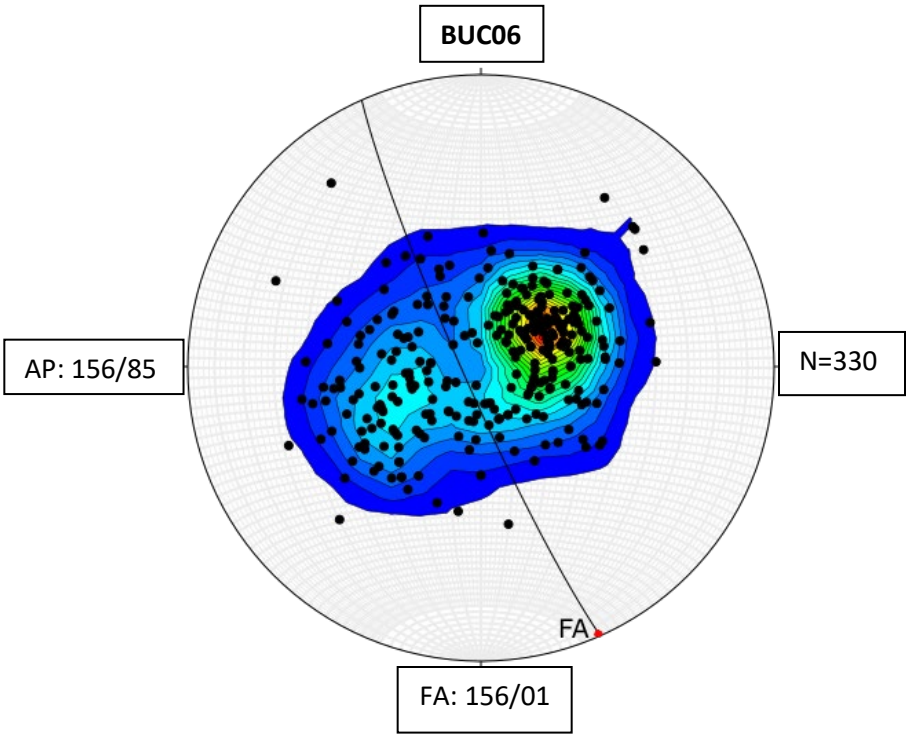

Figure 18-Stereonets displaying poles to bedding corresponding to Class B Domains BUC05 and BUC06. Red point marks the fold axis (FA), black line marks the axial plane (AP). Kamb contour interval specifications are included on Figure 12.

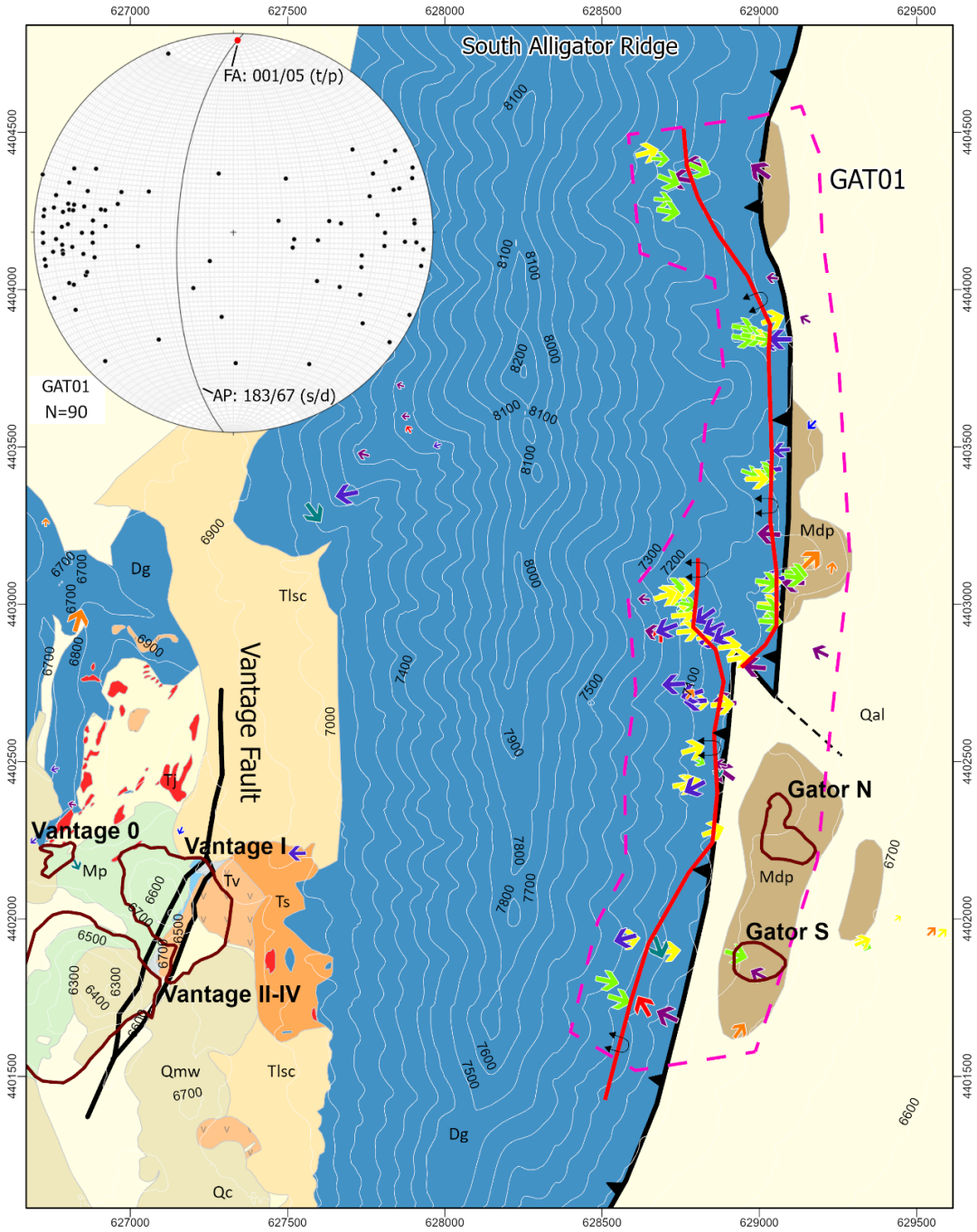

Figure 19- Geologic map of the southern Alligator Ridge area displaying GAT01 which contains a thrust fault and steep fold limb as part of the Domain Class C. Stereonet for the GAT01 bedding is included, FA= fold axis (trend/plunge), AP=axial plane (strike/dip). Note that steeply west dipping (large red and purple arrows) along the fault margin (bold black line within domain) are overturned bedding. Units and symbols are defined in Figures 7-9.

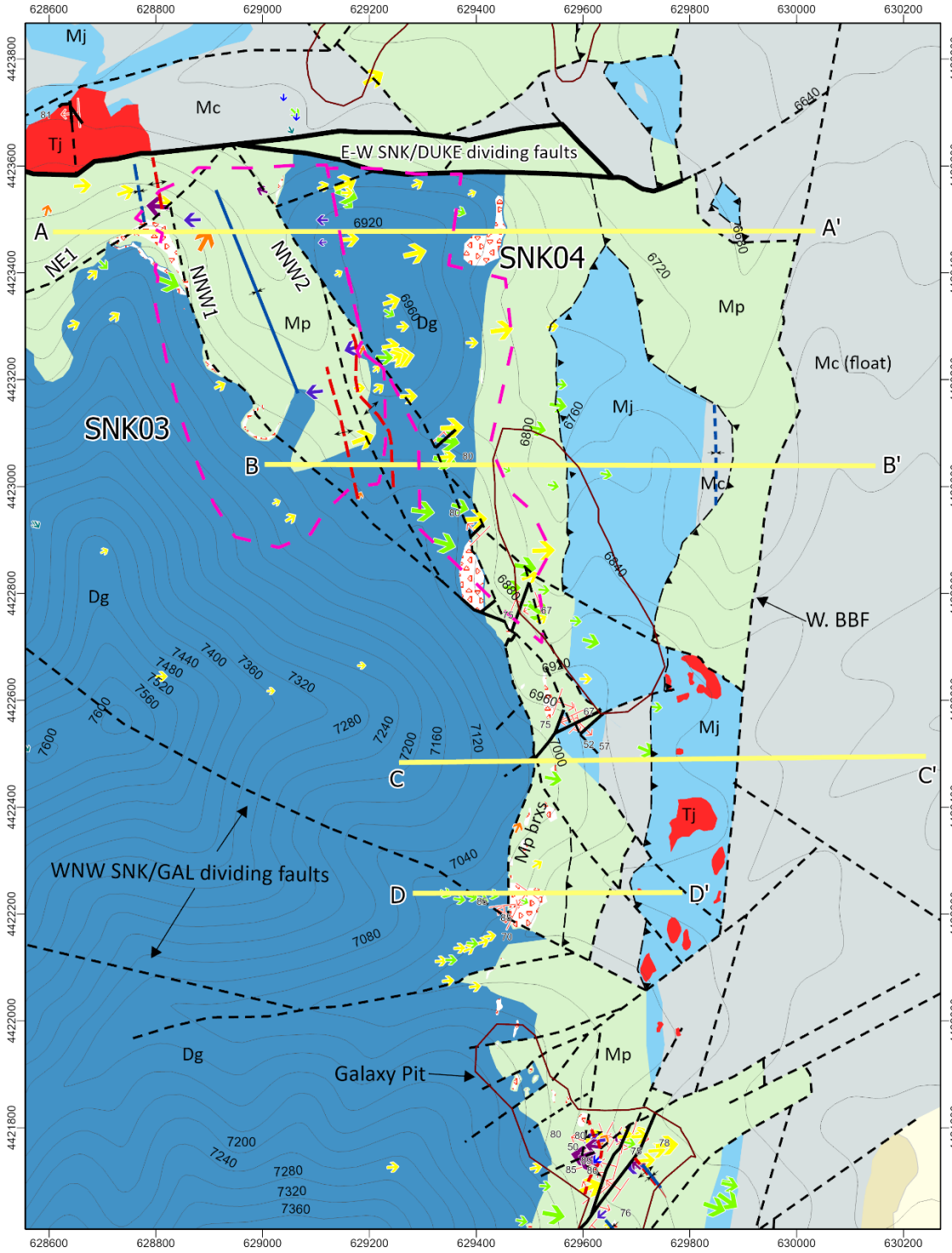

Figure 20- Snake Eyes Overview Map-includes Class B domain SNK03 and Class D domain SNK04. Note that medium weight dashed black lines are inferred faults, medium solid black lines are measured faults, and heavy weight black lines are major faults with district-scale strike lengths and significant apparent stratigraphic offsets. W BBF labels the west basin bounding fault. Units and symbols are defined in Figures 7-9.

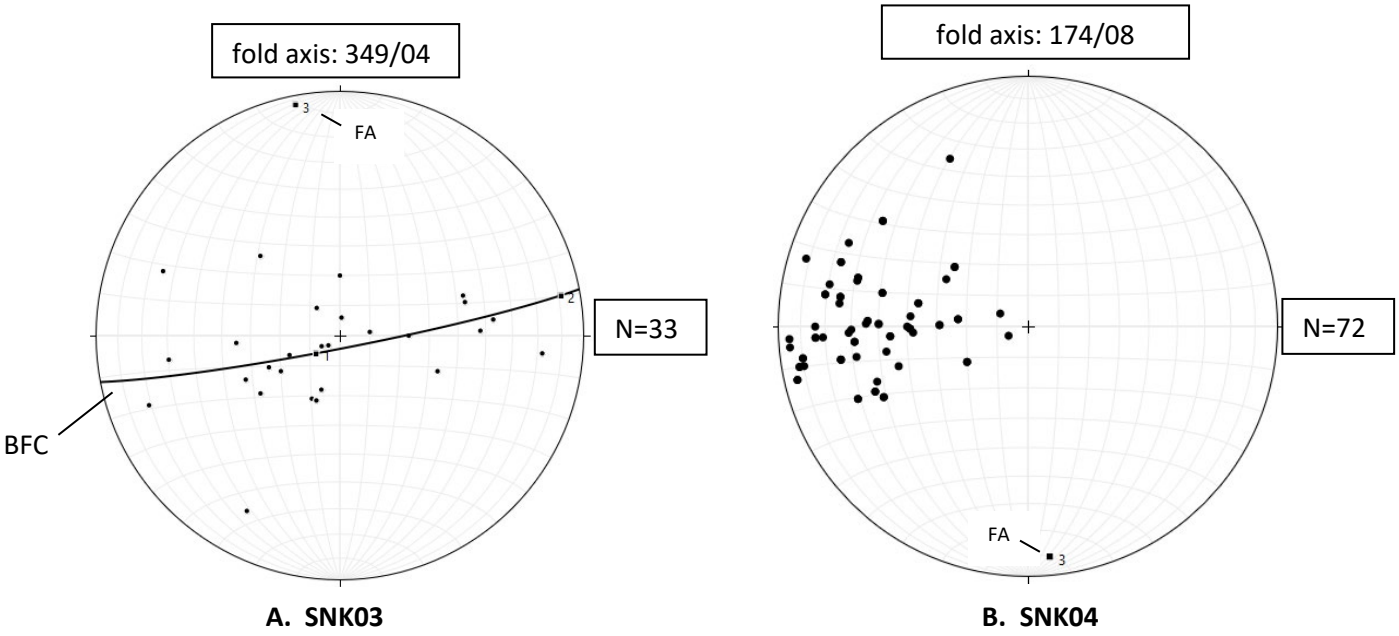

Figure 21- Stereonets containing data from chosen domains SNK03 and SNK04. 21A. Plot of Domain Class B SNK03 shows poles to bedding plane measurements and the corresponding Bingham Analysis of the poles with a best fit great circle (BFC) and fold axis (Bingham axis 3) labeled FA (trend/plunge). 21B. Plot of Domain Class D SNK04 shows poles to measured bedding planes and the fold axis (FA) of the monocline.

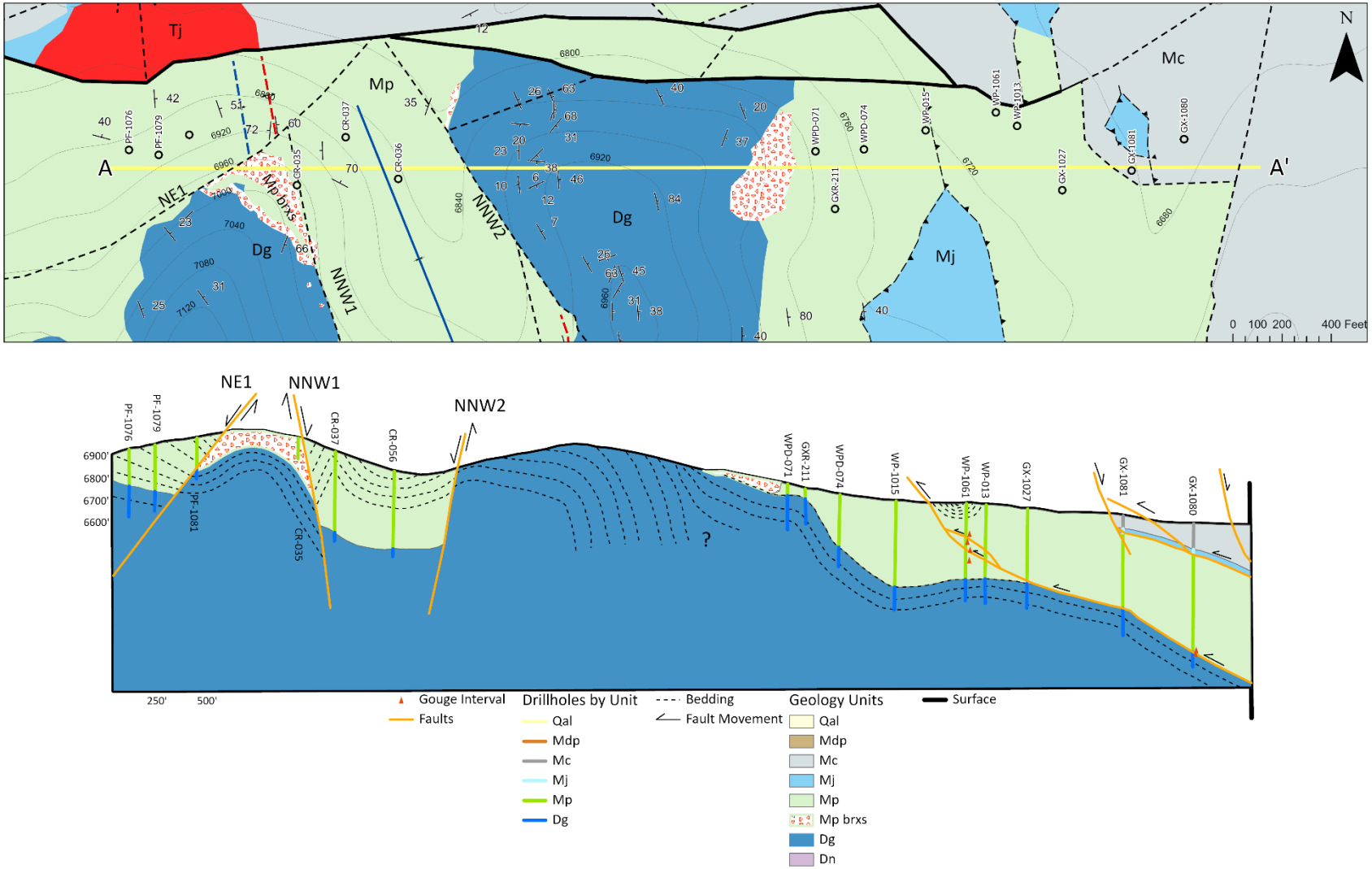

Figure 22- Snake Eyes cross section A-A'. Legend is the same for all subsequent cross sections. See Figures 7 and 8 for map legends.

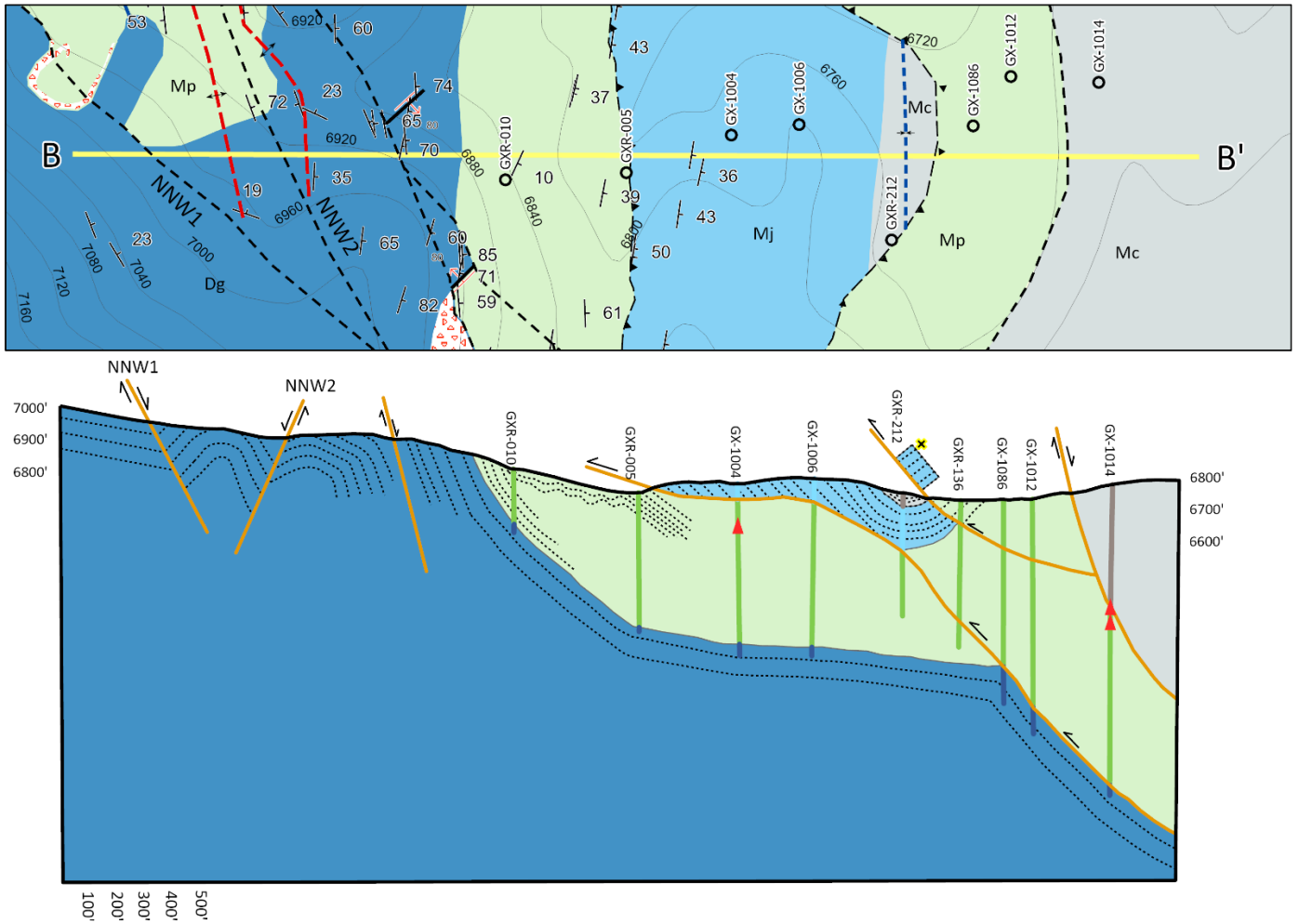

Figure 23- Snake Eyes cross section B-B'. Note black and yellow 'x' and above surface block of Mj represents the interpreted syncline truncation by the thrust. Cross section legend included on Figure 22 and map legend included on Figures 7 and 8.

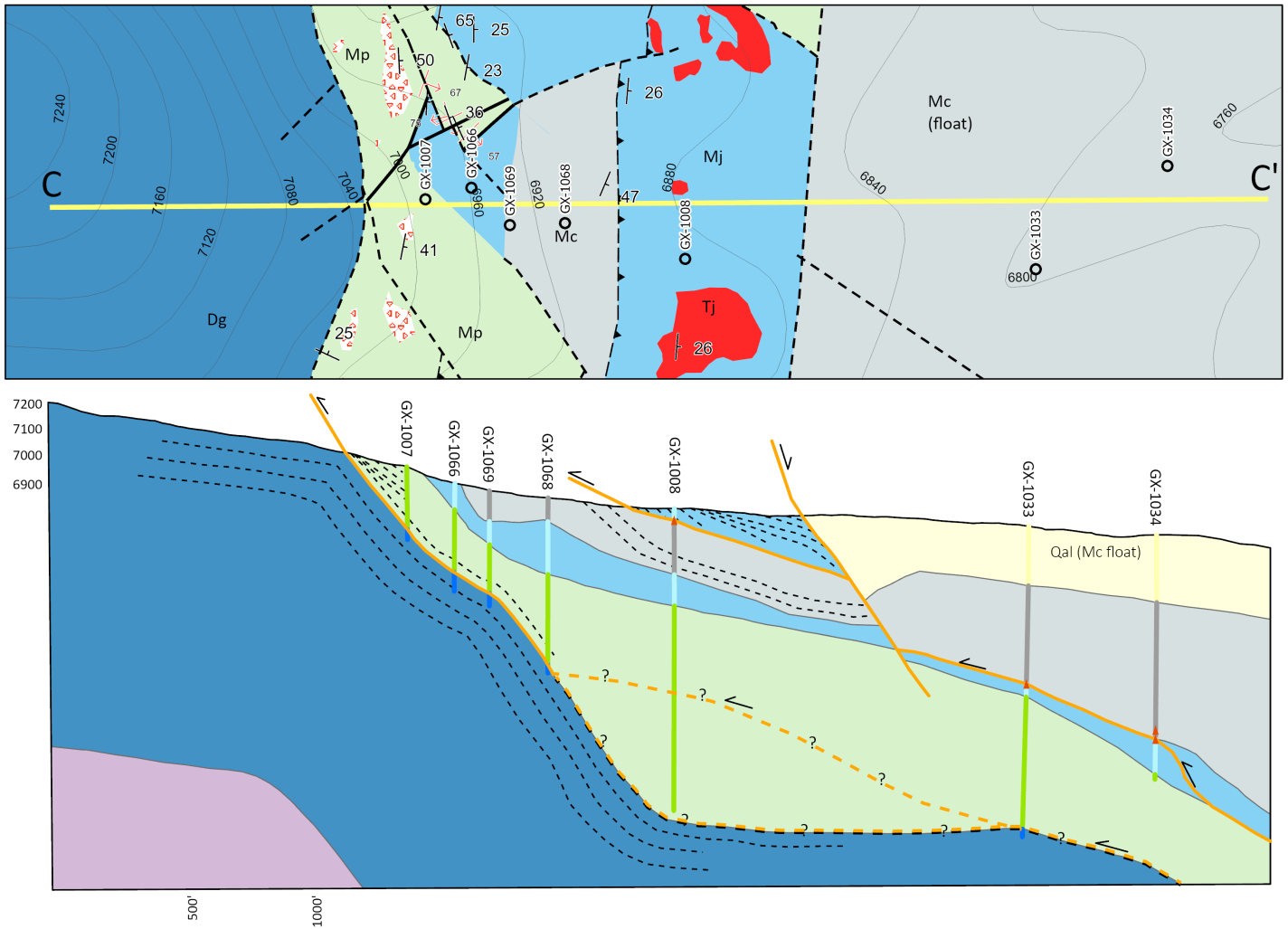

Figure 24- Snake Eyes cross section C-C'. Queried fault lines and contacts indicate alternative interpretations for thickened Mp section via duplexing or a karsted Dg/Mp contact. Cross section legend included on Figure 22 and map legend on Figure 7 and 8.

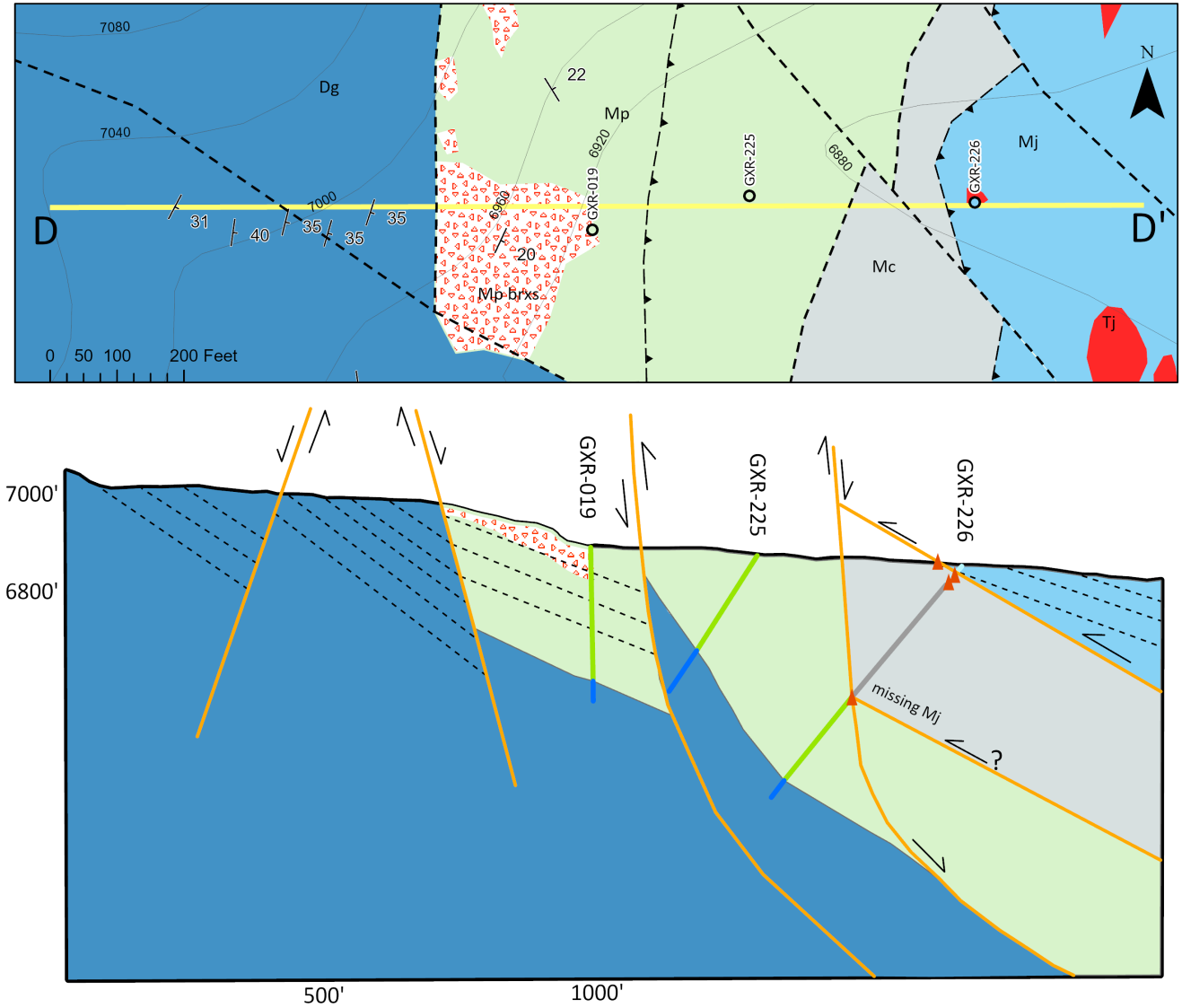

Figure 25- Snake Eyes Cross Section D-D'. Cross section legend included on Figure 22 and map legend on Figures 7and 8.

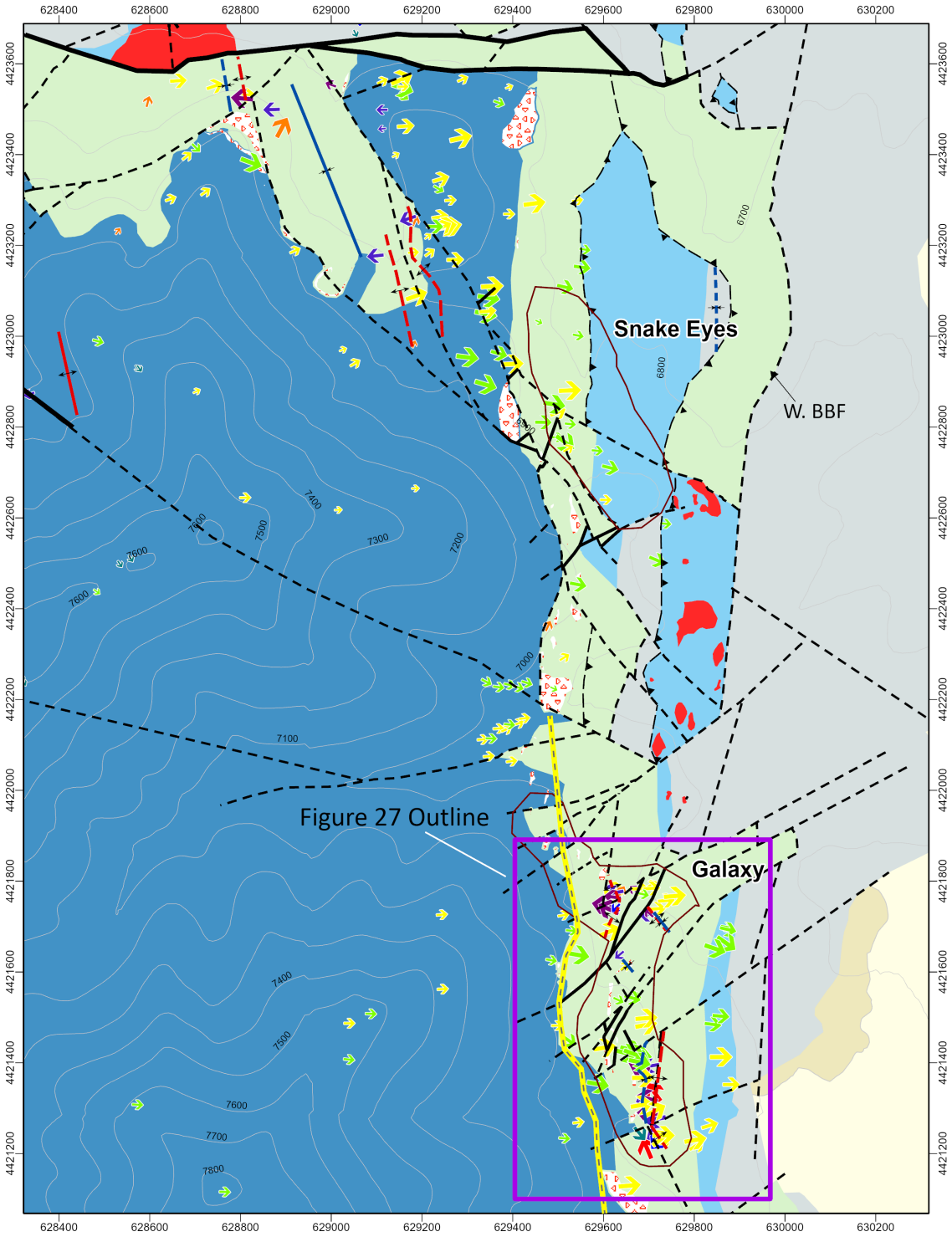

Figure 26- Snake Eyes and Galaxy updated mapping (this study) overview. The yellow line marks where rollover of the GAL01 domain occurs. “W. BBF” indicates the location of the west basin bounding fault in the Snake Eyes area. Purple box indicates the extent of Figure 27. Units and symbols are defined in Figures 7-9.

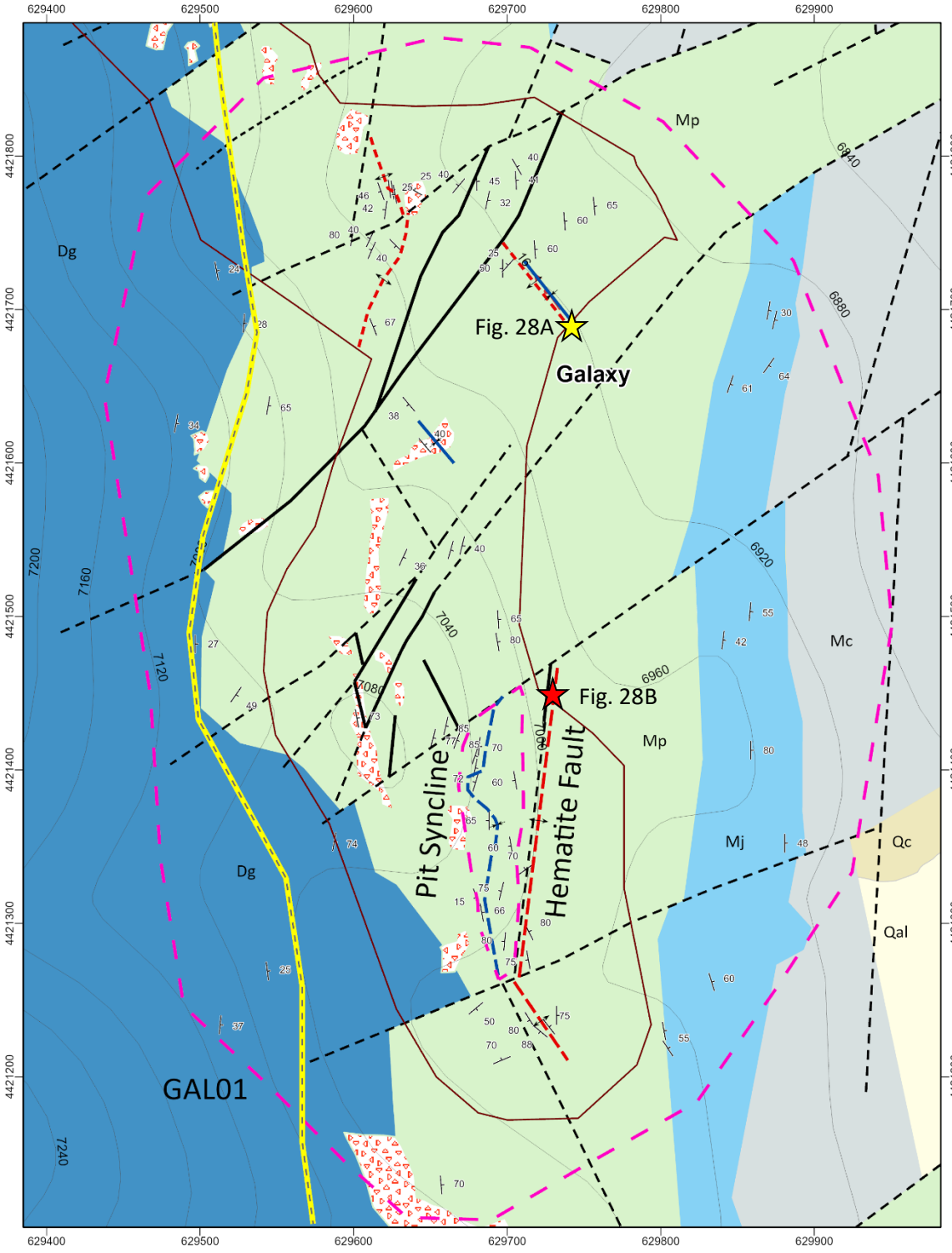

Figure 27- Updated mapping (this study) figure of the Galaxy Pit. The brown outline represents the pit walls. The outer dashed pink polygon contains the GAL01 and in the inner dashed pink contains measurements of the pit syncline plotted in Figure 29. The yellow star marks the location of the Figure 28A, the red star the location of Figure 28B. The yellow line marks where bedding roll over occurs. Units and symbols are defined in Figures 7 and 8.

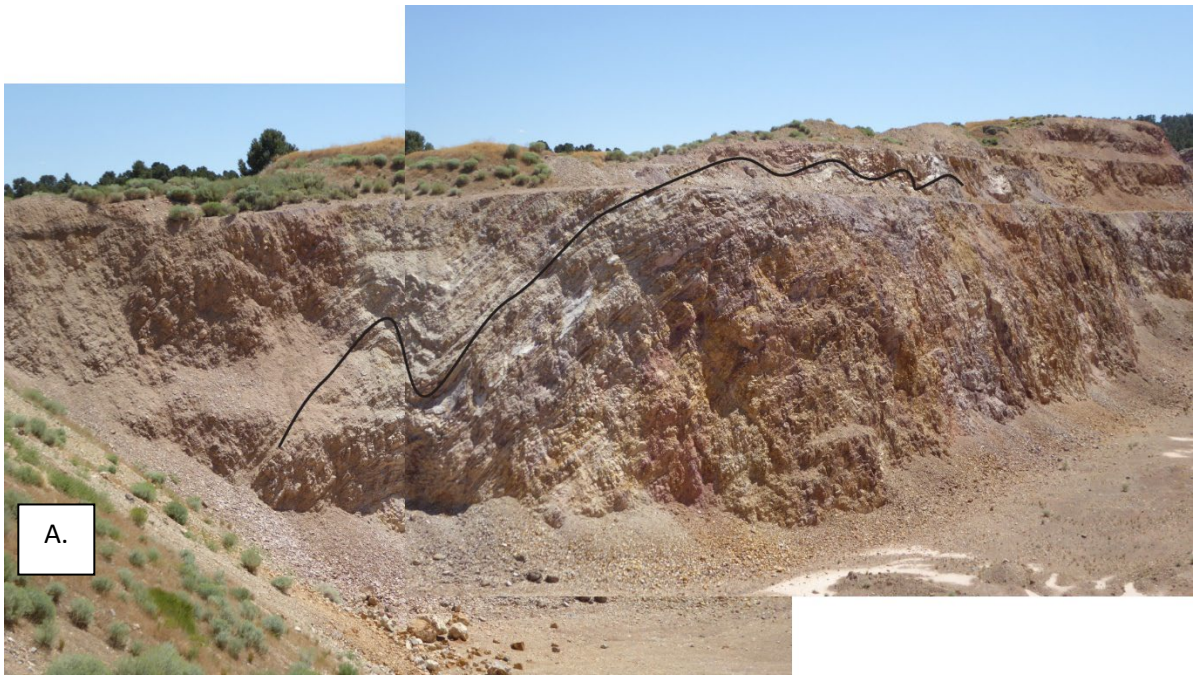

Figure 28A.- Looking to the SSE; a tight, angular to open, gentle buckle folds in Mp with the synclinal hinge measuring (325/16) (trend/plunge) and vergence to the southwest. - Photo by Liz Schermer

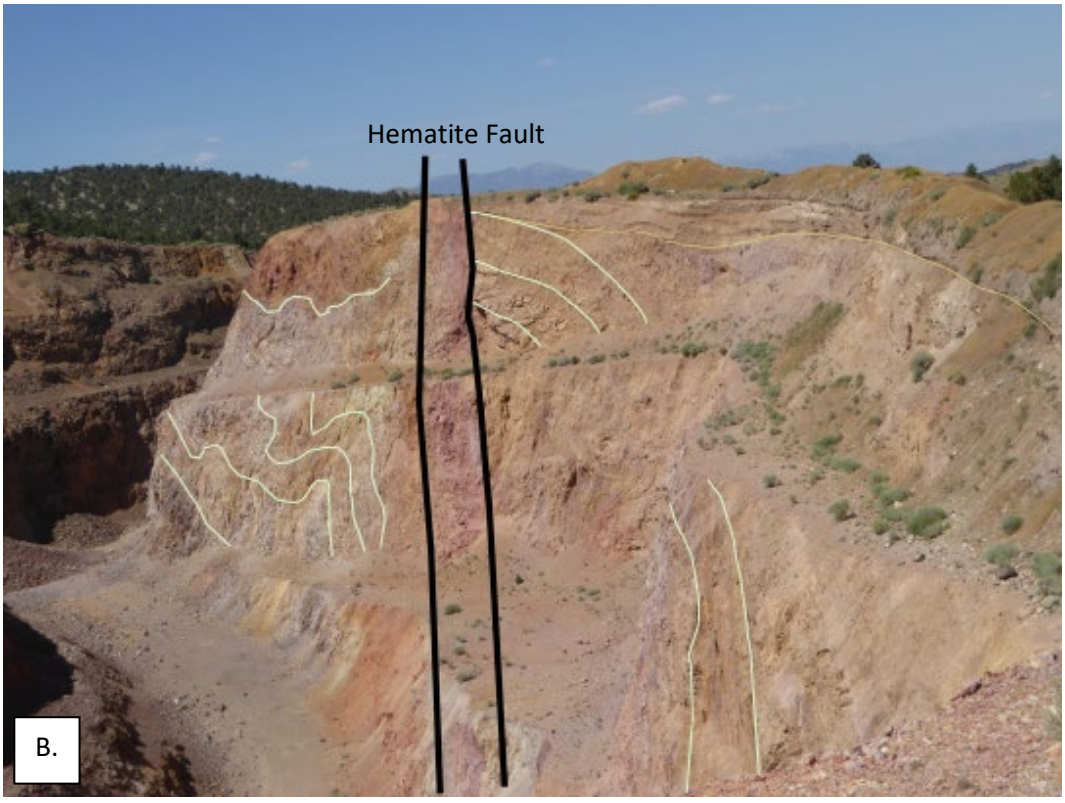

28B.-Looking to the NNW; at the NNE-striking Hematite Fault (shear zone outlined in black) which cuts an anticlinal fold hinge in the SE Galaxy pit area. Light green lines highlight Mp bedding. -Photo by Liz Schermer.

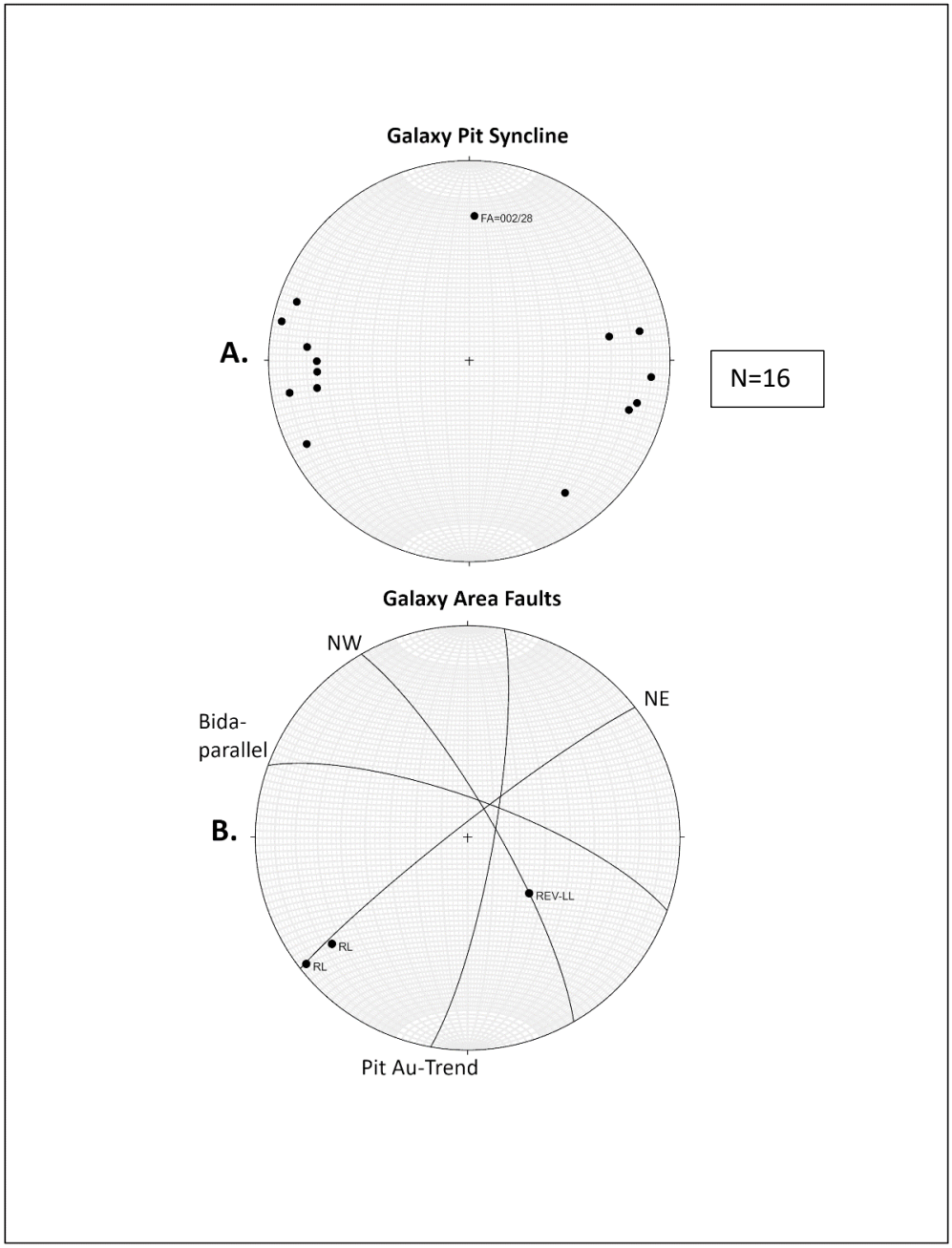

Figure 29- Stereonet plots of structural measurements and trends in the Galaxy area. 29A. Galaxy Pit Syncline Fold Domain, Fold Axis= (FA). 29B. Selected fault measurements referenced in text. “Bida-parallel” and “Pit-Au Trend” planes represent generalized fault orientations in the area, and the NW and NE planes plot measured faults with corresponding slickenlines. REV-LL = reverse left lateral and RL = right lateral slickenlines.

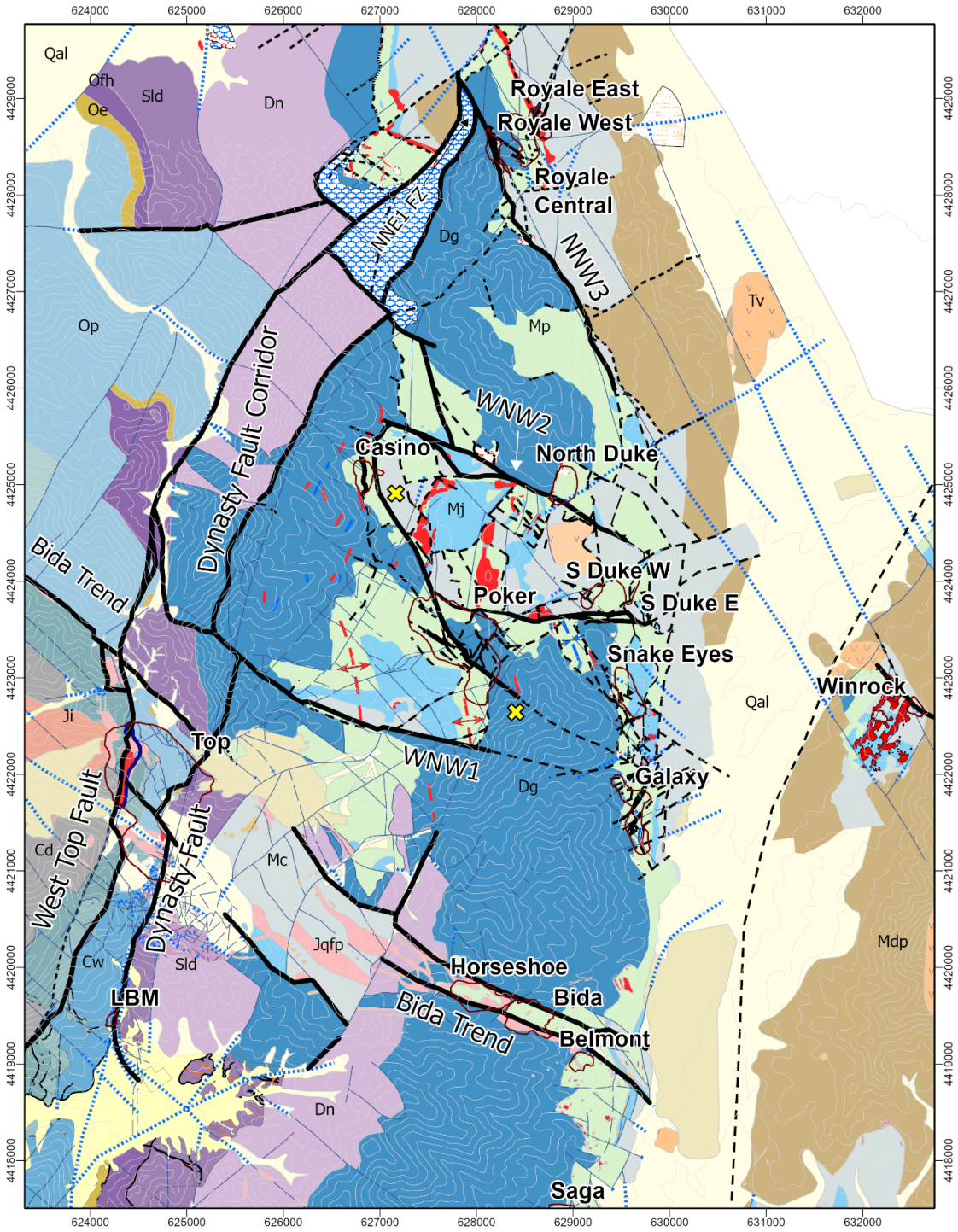

Figure 30- Geologic map displaying major district-scale faults of northern BMMD, traced in heavy black lines. The West Top, Dynasty, Bida trend, NNE1 fault zone, WNW1, WNW2, and NNW3 faults are labeled. The yellow X's mark the location of NW- to WNW-bending fault between Casino and Poker that intersects the area between the Snake Eyes and Galaxy areas. Units and symbols are defined in Figures 7 and 8.

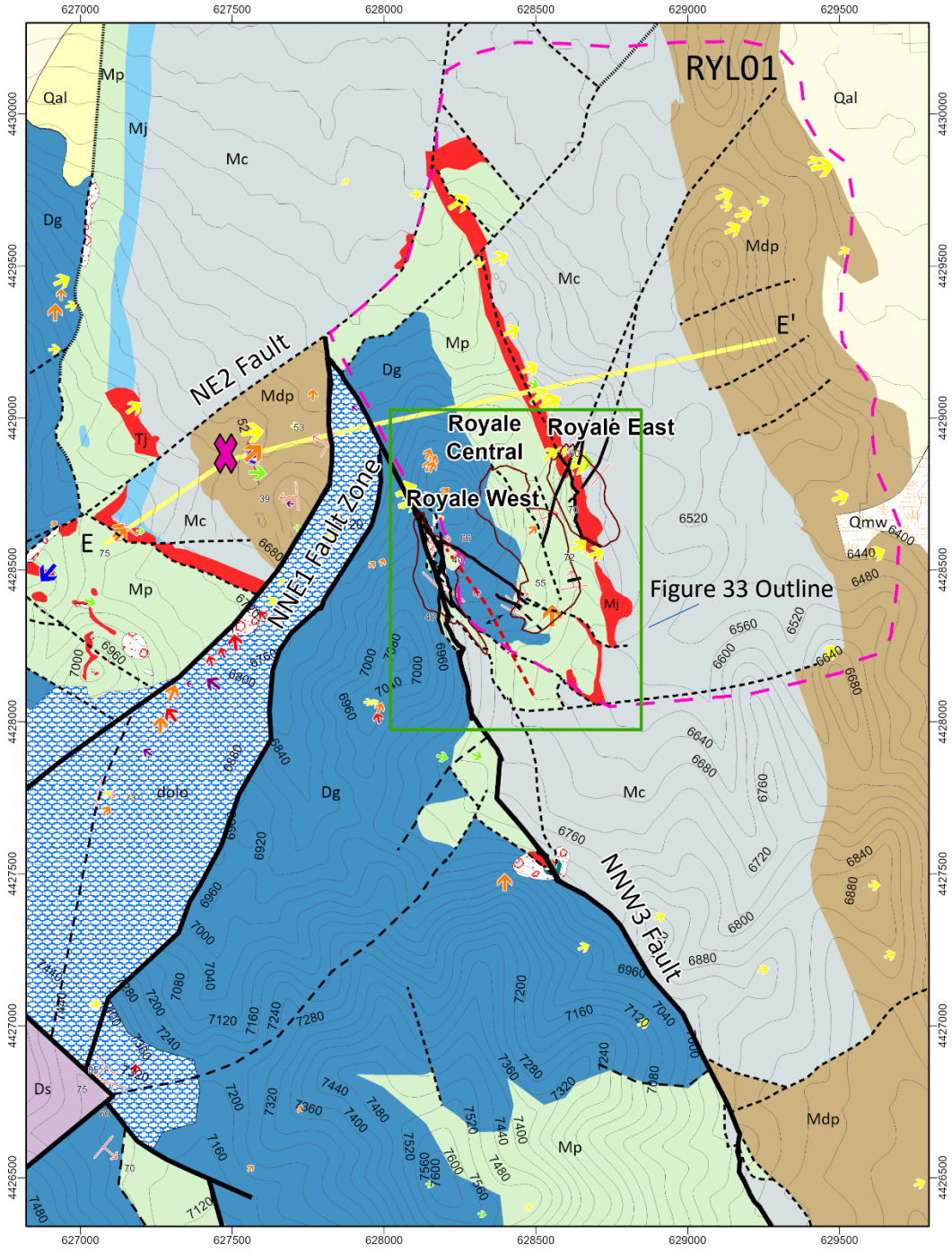

Figure 31- Overview of updated mapping (this study) in the Royale area containing cross section E-E'. The dashed pink outline surrounds the RYL01 Class D domain area. The cross hatched light blue polygon containing the NNE1 fault zone label denotes the area of secondary dolomitic alteration. The green box outlines the extent of Figure 33. The pink X represents the location of the measured fold in Figure 36. Units and symbols are defined in Figures 7-9.

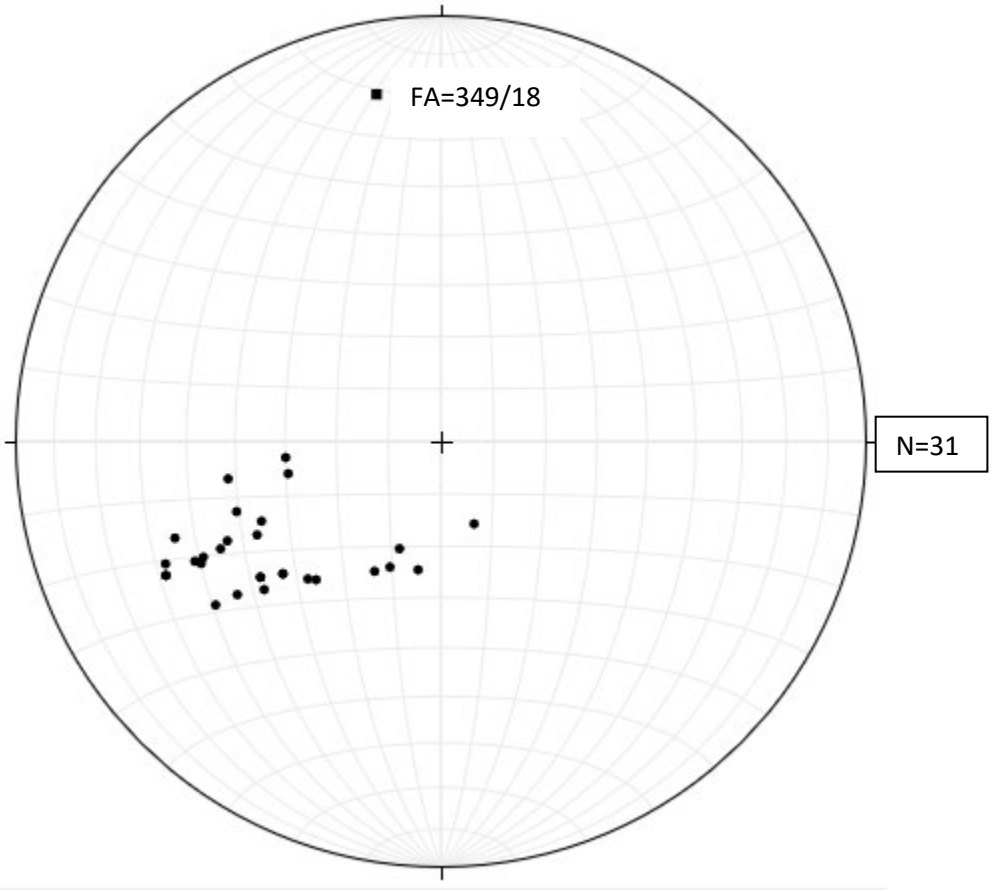

Figure 32- Poles to bedding of domain RYL01 roll over. FA=fold axis measuring (349/18).

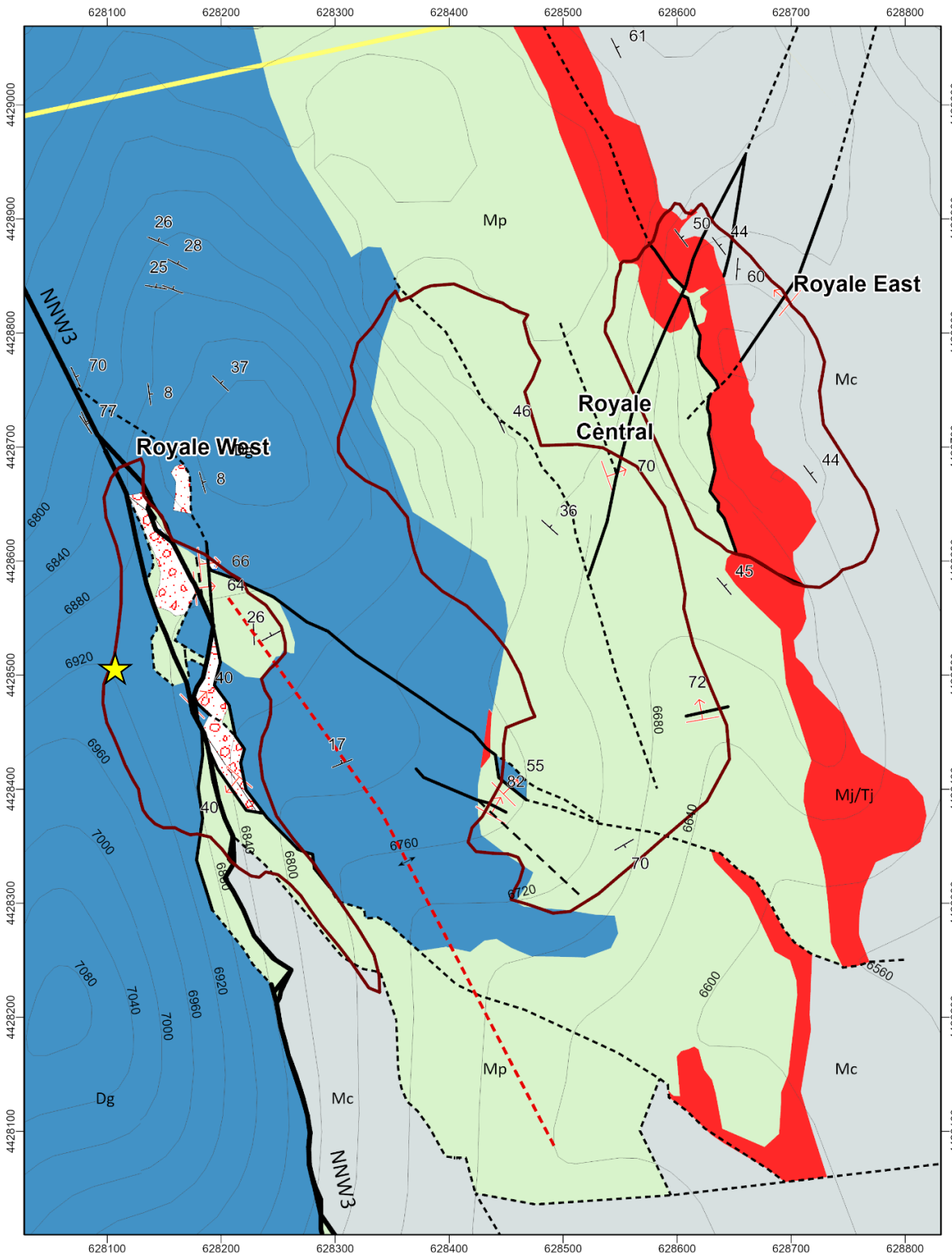

Figure 33- Map of the three Royale pits with location shown by green box on Figure 31. The dashed red line represents a NNW-trending fold hinge along which the Central and East deposits lie on the east limb and the West deposit lies on the west limb at the intersection with the NNW3 fault. The yellow star represents the location of Figure 37. Units and symbols are defined in Figures 7 and 8.

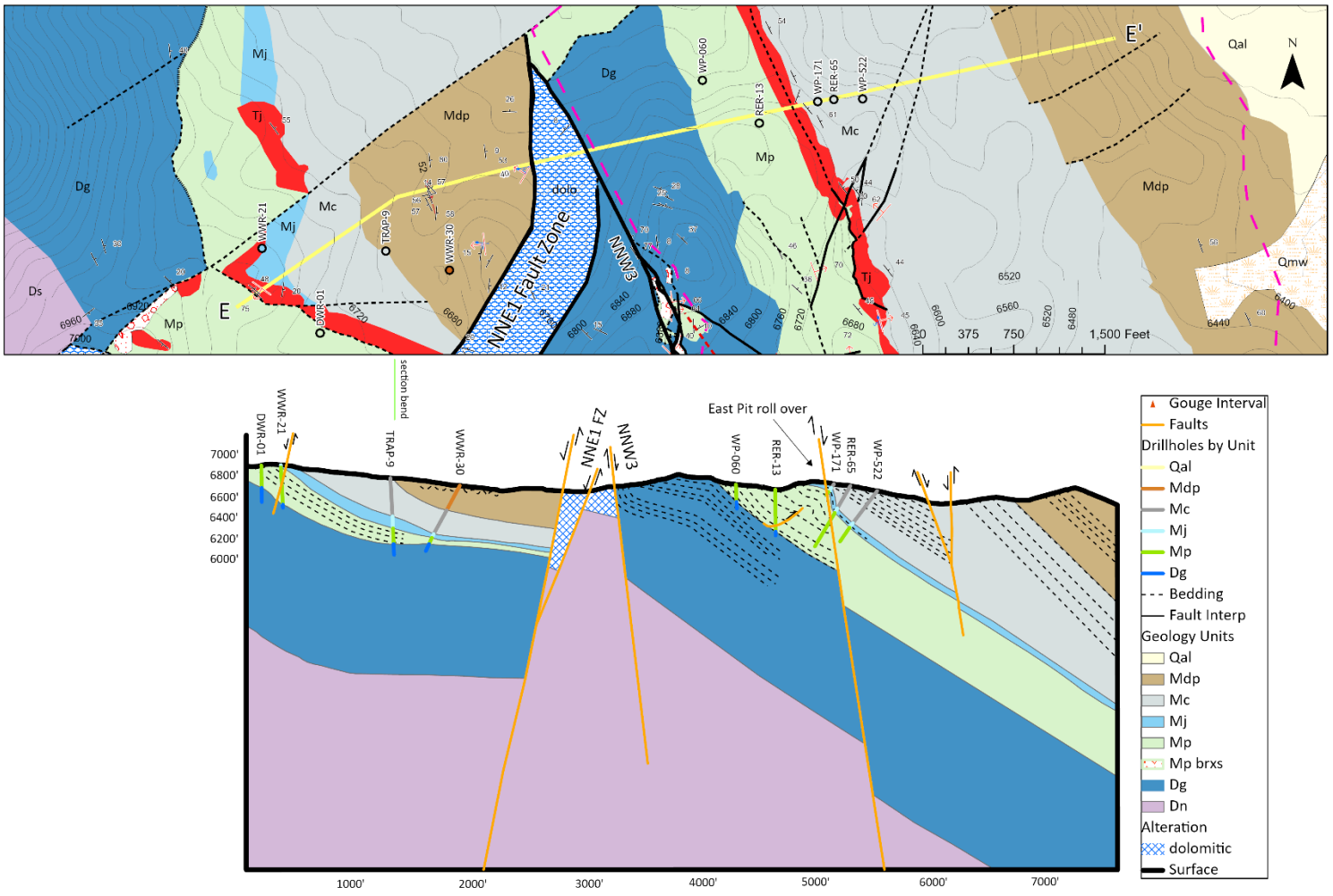

Figure 34-Royale Cross Section E to E'. Location on Figure 31. Red jasperoid units (Tj) in map view are interpreted as the light blue Joana (Mj) unit in cross section. Map legend on Figures 7 and 8.

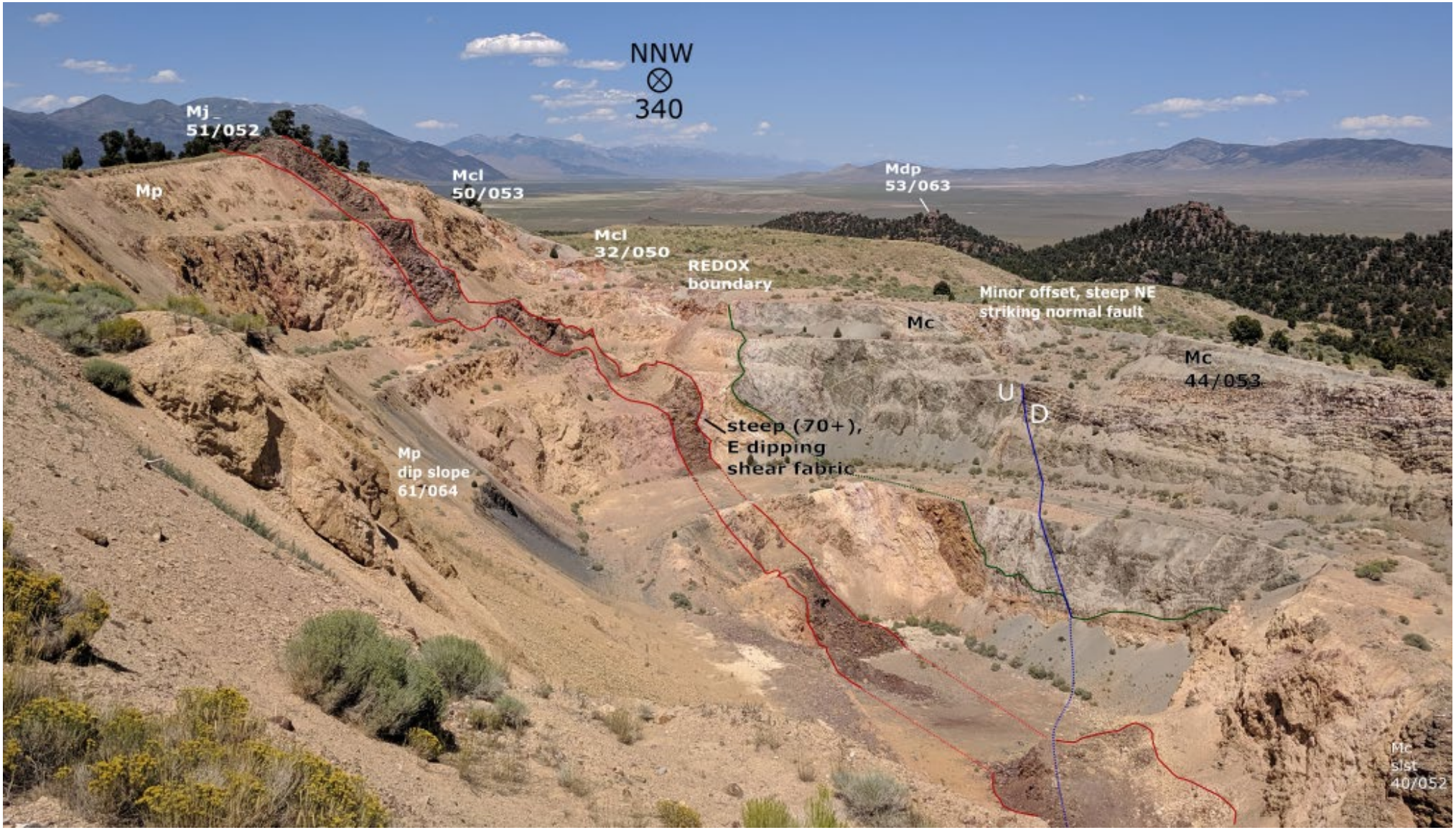

Figure 35- Photo of the Royale East Pit, looking NNW with the southern Ruby Mountains core complex on the horizon. Geologic units and local bedding measurements are noted by dip/dip direction.

Figure 36-Looking northwest, photo of the upper benches of the west wall of the Royale West pit showing moderately west-dipping beds of Dg limestone. Location of photo shown in Figure 33. Photo by Liz Schermer.

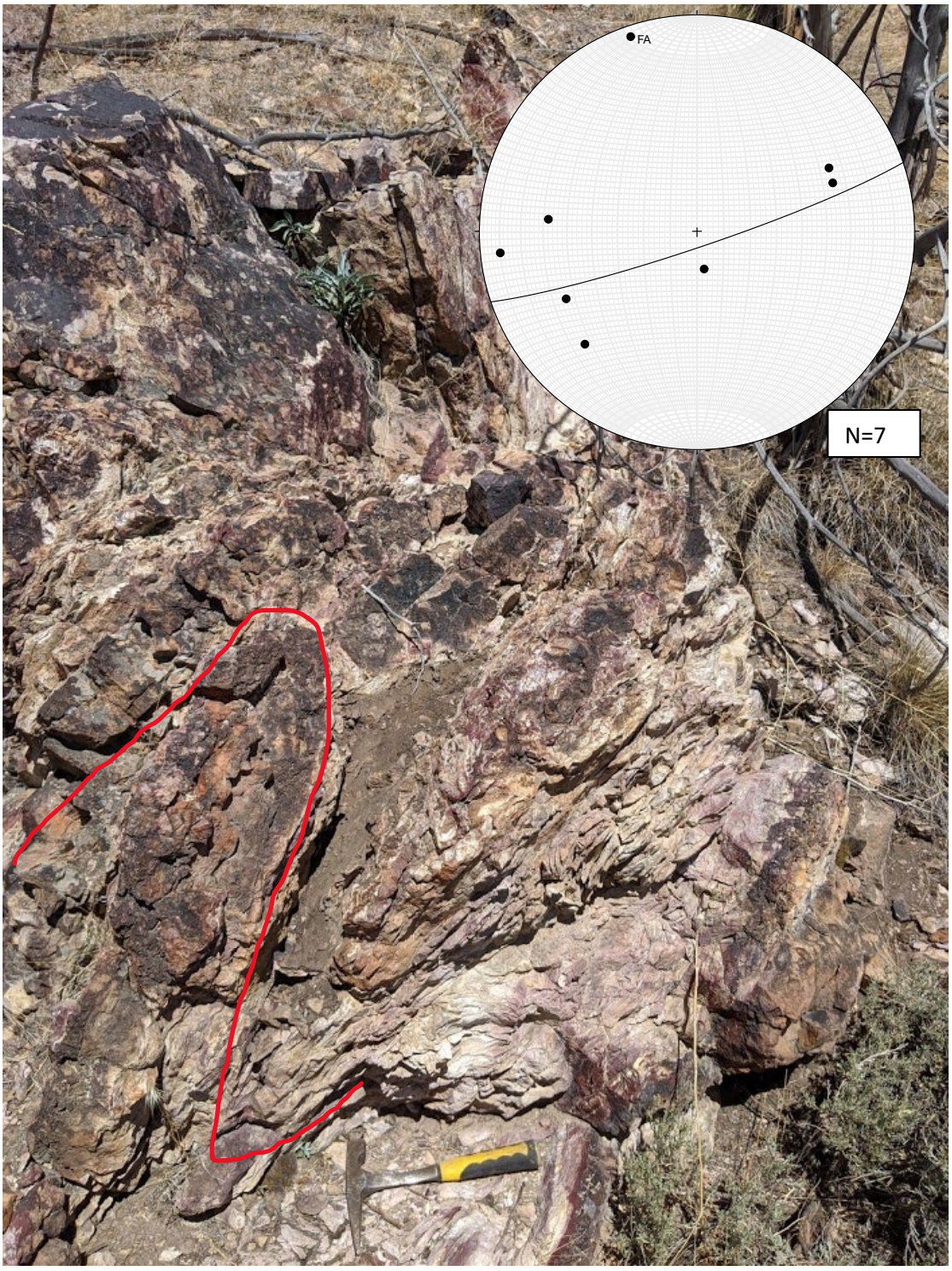

Figure 37- Folded Mc or Mdp siltstone in west Royale, looking along the brecciated fold hinge trend to the NNW—the measured anticlinal hinge is gently NNW plunging (341/06) (trend/plunge), has a tight interlimb angle, is upright, and occurs in a patchy silicified, brecciated, and oxidized Mdp or Mc siltstone. Stereonet displays poles to bedding planes in the fold.

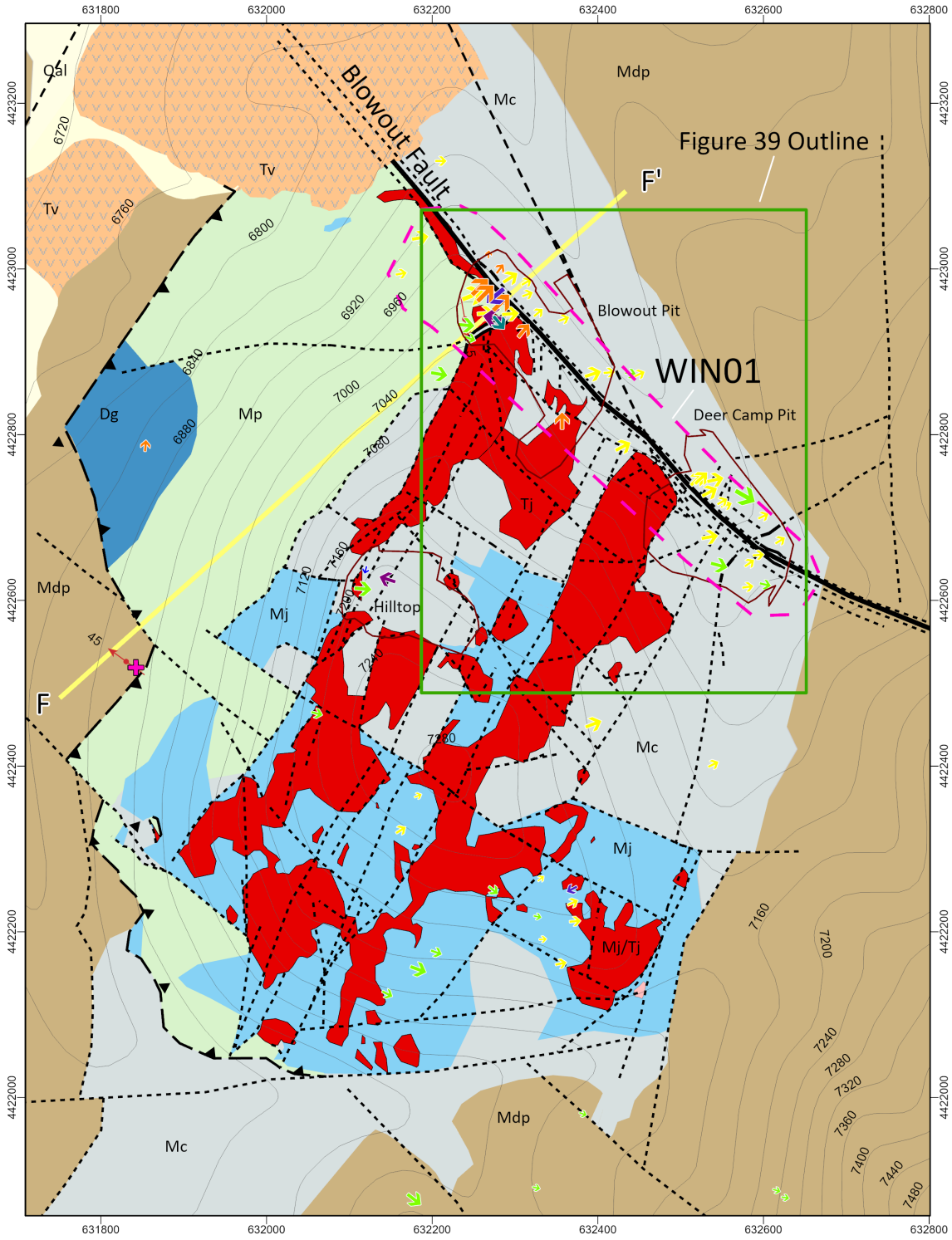

Figure 38- Geologic map of the Winrock area (revised from R. Conelea, 2004) showing pit, cross section, and WIN01 domain locations. The green box outlines the extent of Figure 39. The pink cross shows the location of the Mdp syncline photo in Figure 43. Units and symbols are defined in Figures 7-9.

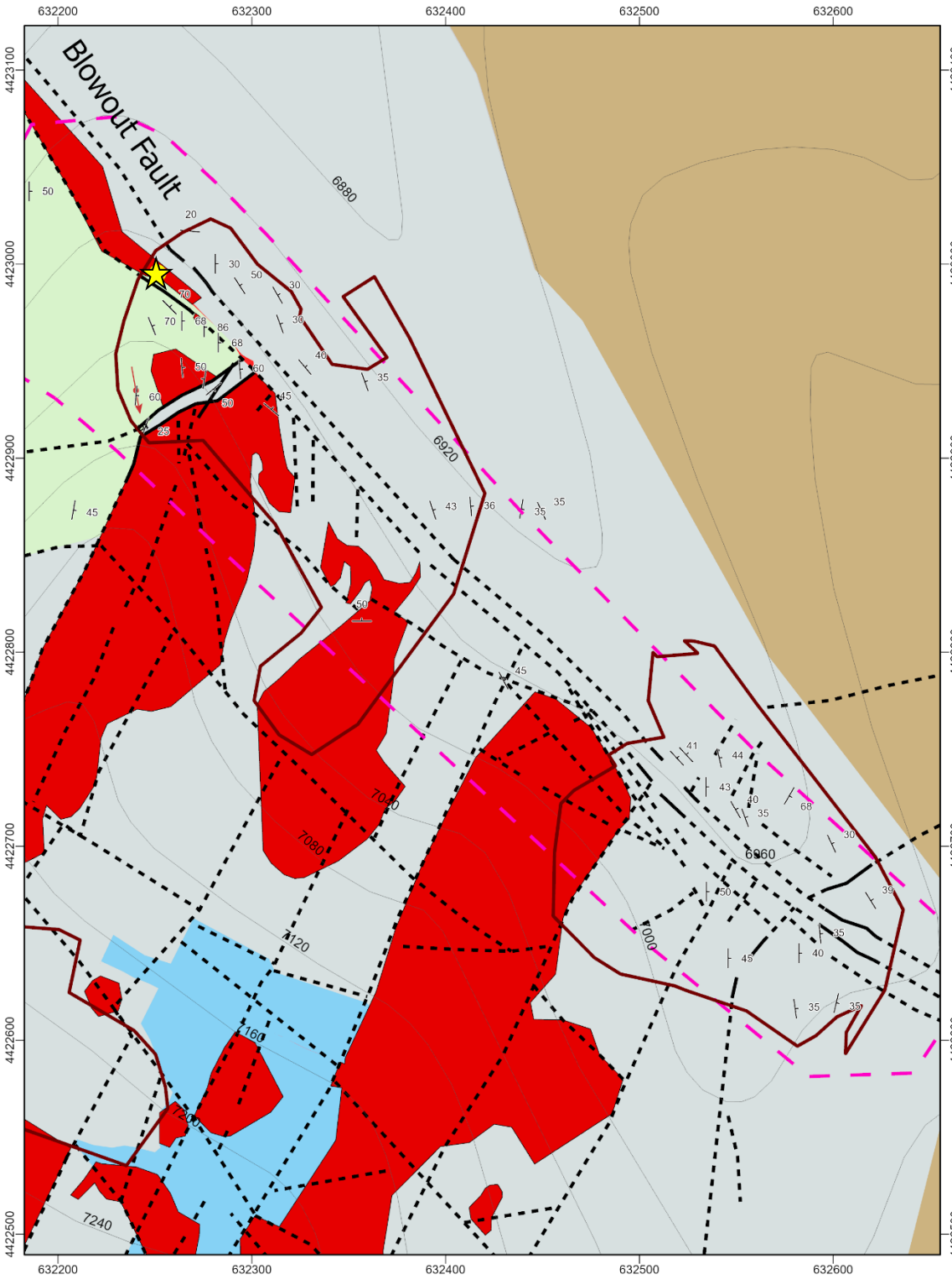

Figure 39- Overview map of the northeast Winrock and Blowout fault area. The yellow star marks the location of the photo in Figure 41. Units and symbols are defined in Figures 7 and 8.

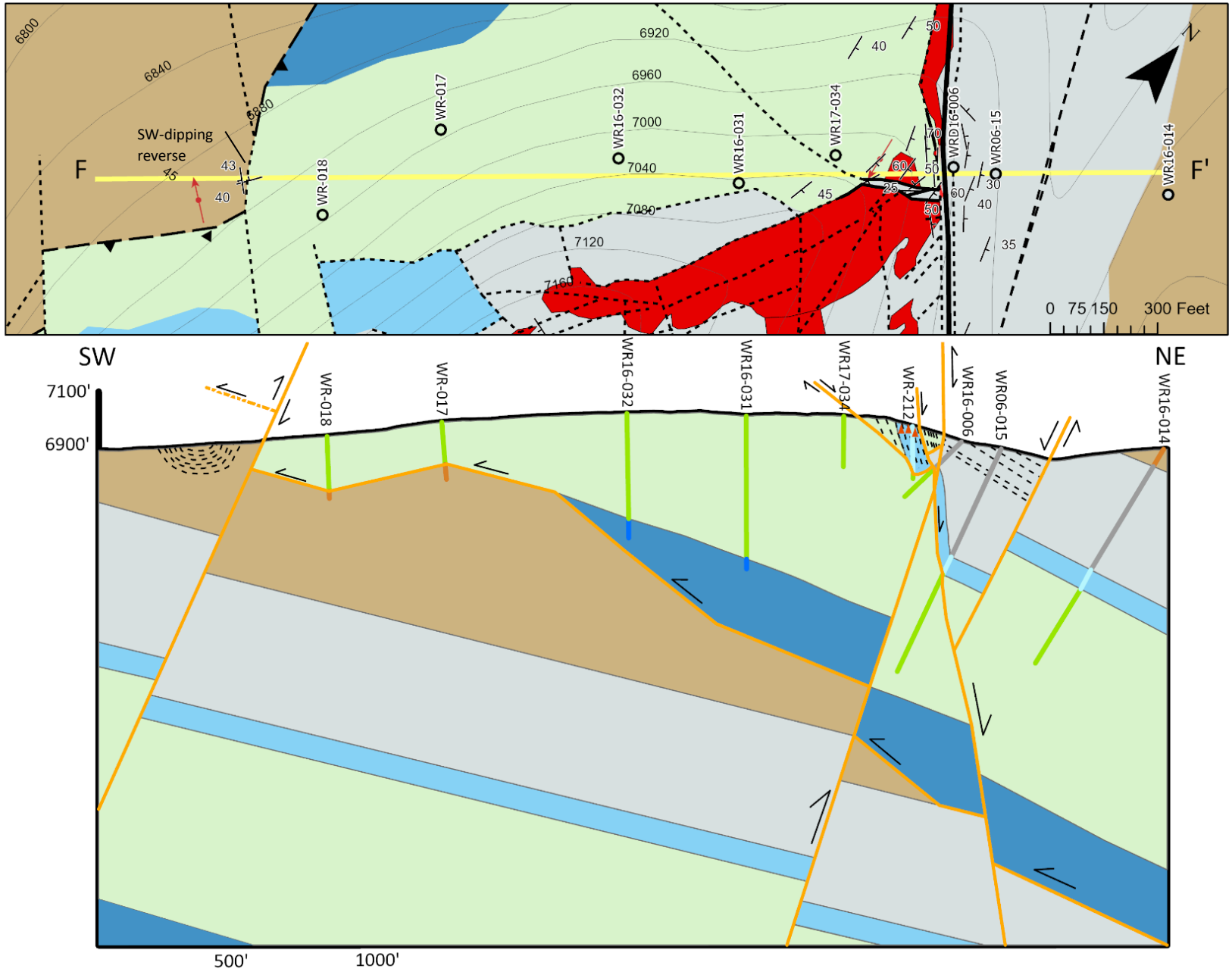

Figure 40– Winrock Cross Section F to F', looking NW. Note that red jasperoid units in map view are interpreted as the light blue Mj unit in cross section. Cross section legend on Figure 22.

Figure 41- Winrock Blowout Pit, North Wall, looking north. Location of photo is shown by the yellow star in Figure 39. Photo shows a fold with steep to locally overturned bedding in the Mp, Mj, and Mc units of the Blowout fault footwall. Note that the photo angle give the fault an apparent west dip, however in reality is it vertical to steeply NE-dipping. Unit abbreviations on Figure 7. FW= footwall, HW= hanging wall

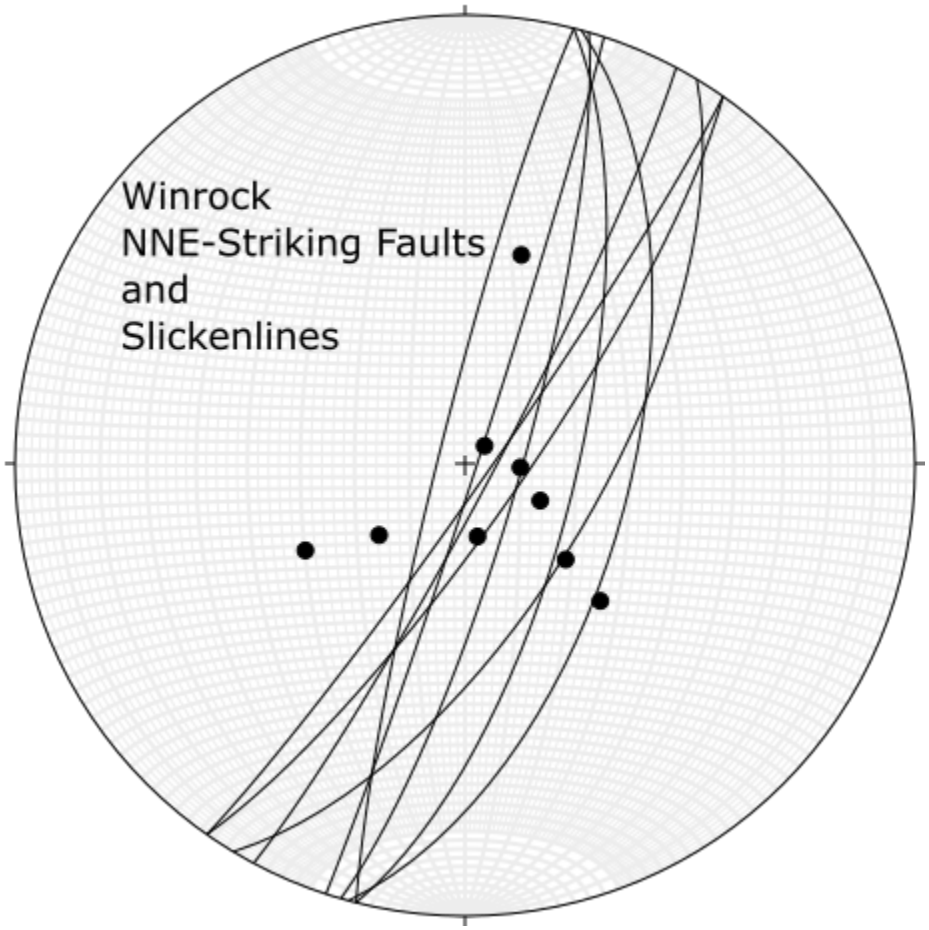

Figure 42-Stereonet plot of select NNE-striking faults and corresponding slickenlines in the Winrock area. Slickenlines have a Fisher mean vector of 142/83 (trend/plunge).

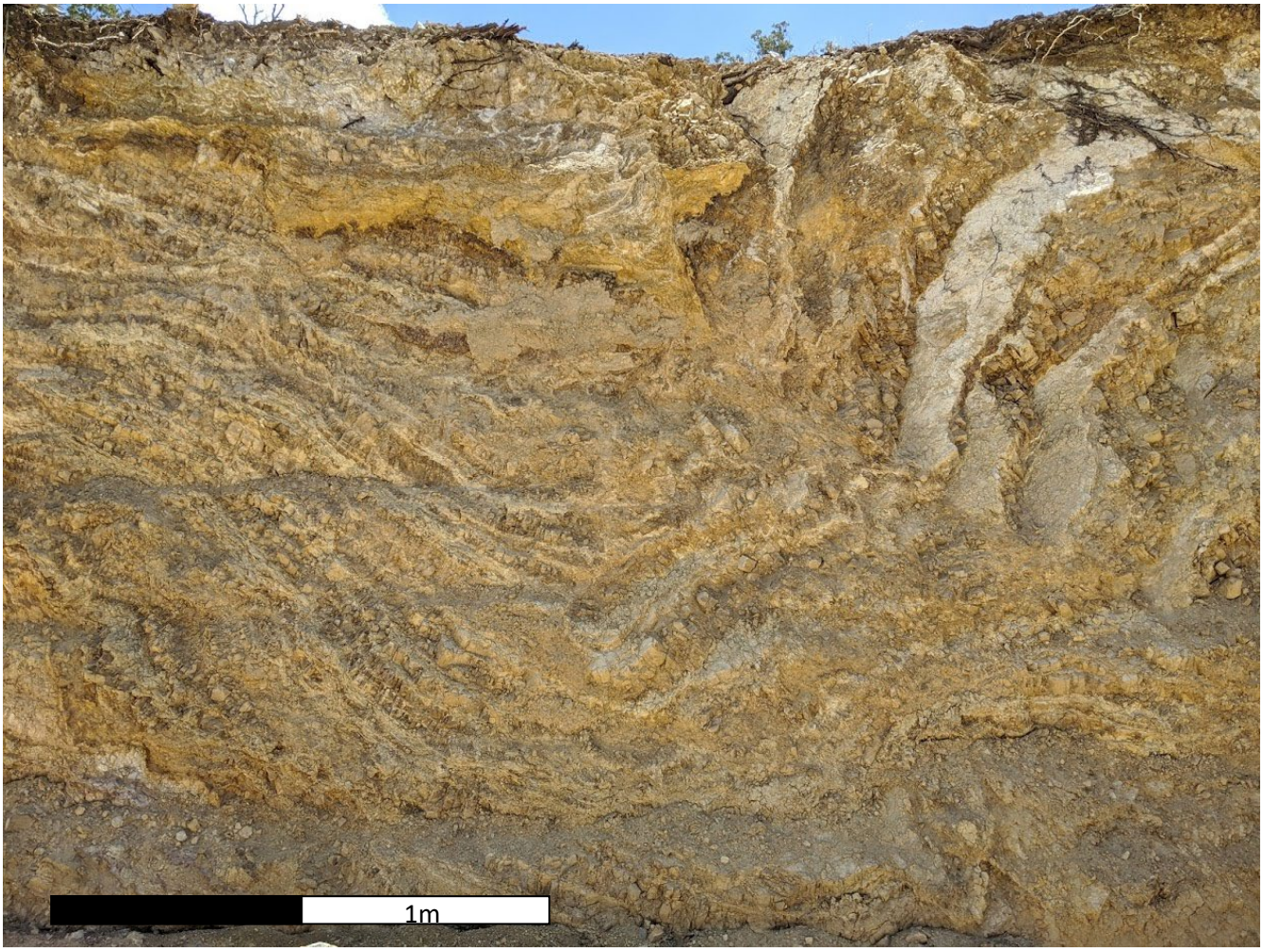

Figure 43- Photo of a syncline (306/45) in the Winrock area in the Mdp unit exposed in the recent (2020) haul road cut to the Hilltop deposit. Pink cross on Figure 38 shows the photo location. Scale bar is 2 meters long

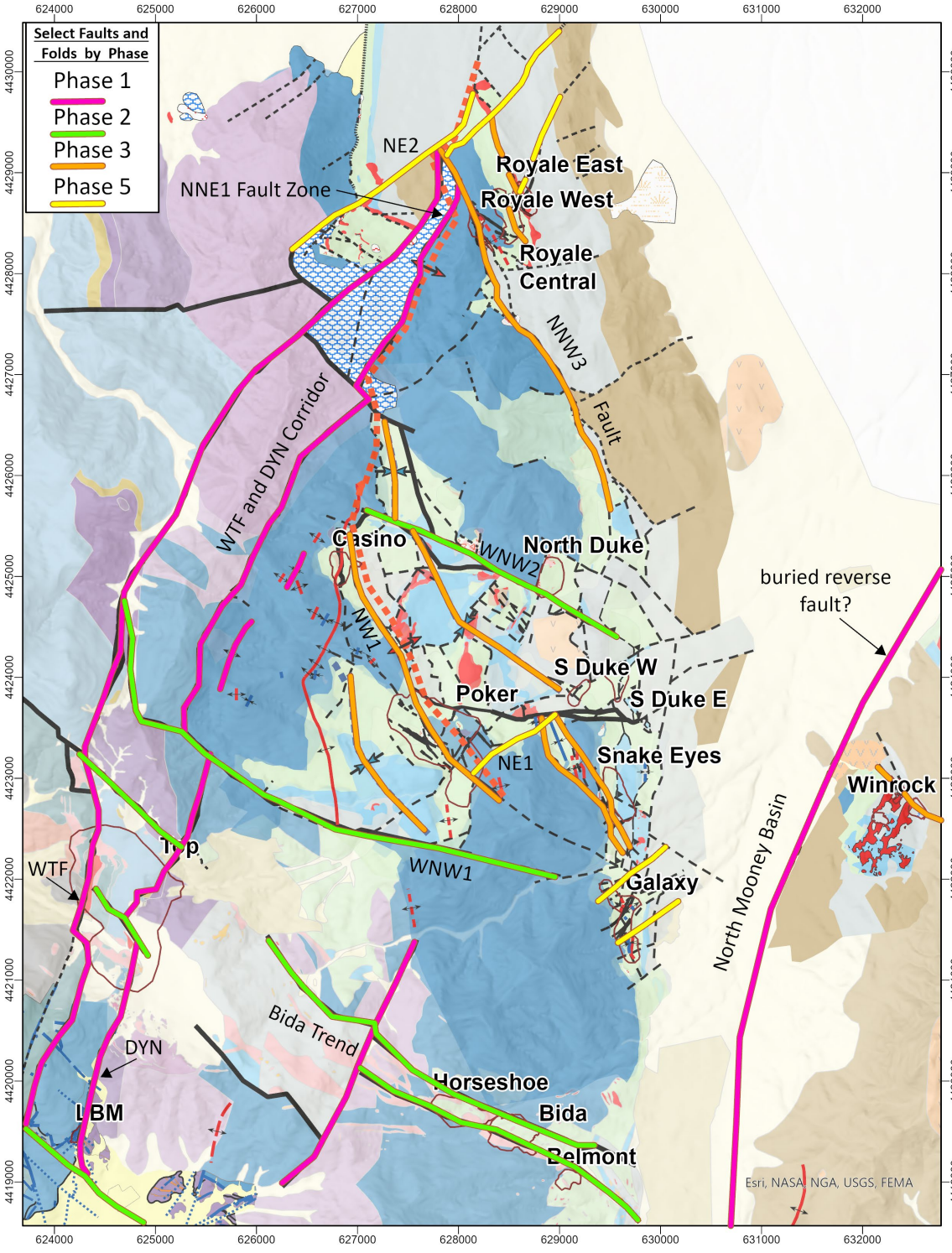

Figure 44- Overview geologic map of the north district highlighting discussed BMMD structures by Phase number. Historical and newly interpreted fold traces are also shown. Note that minor Phase 4 structures are not visible at this map scale. WTF= West Top Fault, DYN= Dynasty Faults. Units and symbols are defined in Figures 7 and 8.

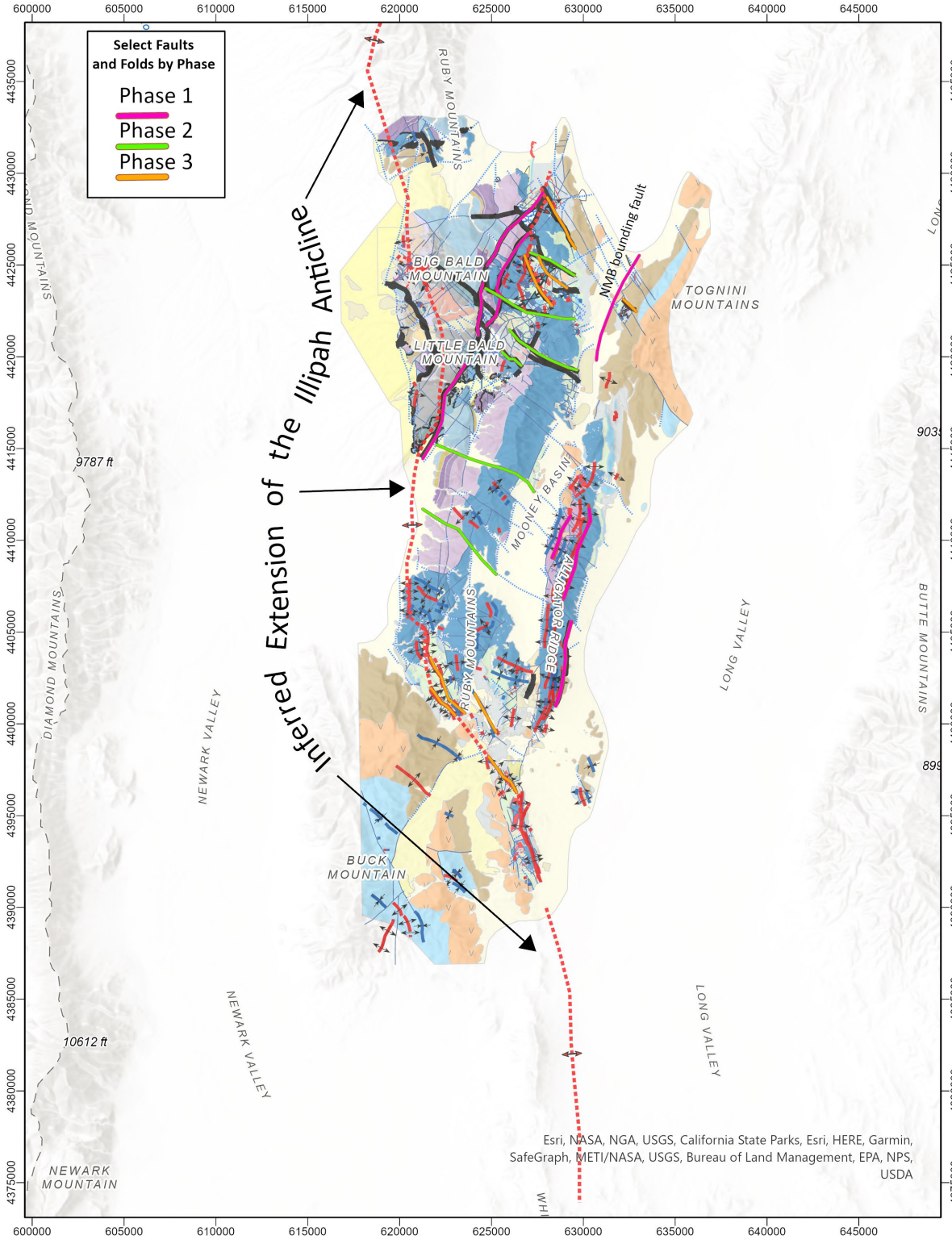

Figure 45-District-scale overview geologic map displaying the newly interpreted trace of the Illipah anticline through the BMMD (D. Schwarz. written comm., 2012; Long, 2015; K. Raabe, written comm., 2021). Select folds and faults are highlighted by Phase number. Units and symbols are defined in Figures 7 and 8.

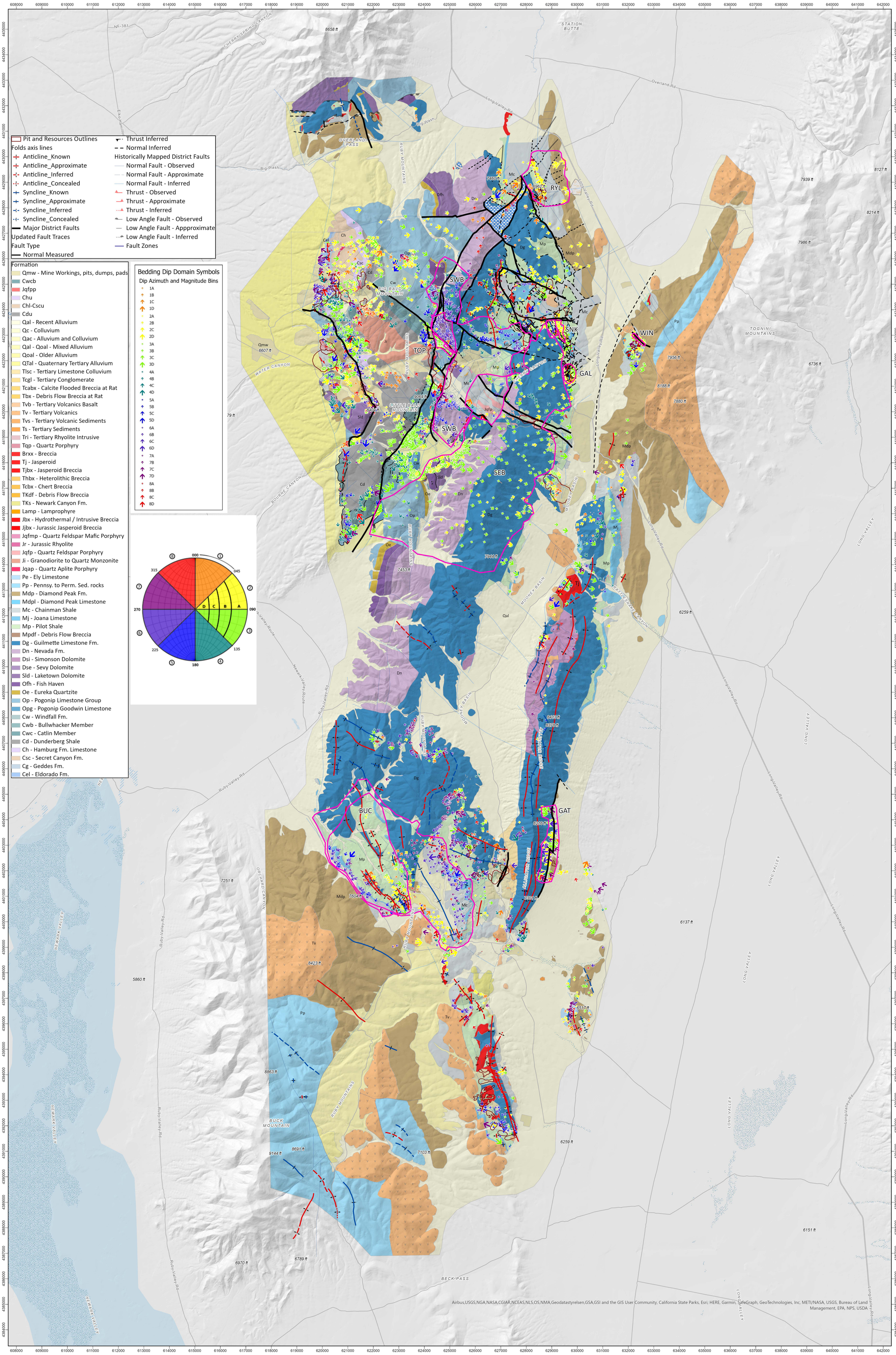

Plate 1-Overview geologic map of BMMD displaying structural domain boundaries and bedding measurements symbolized according to Figure 9. Historical geologic mapping from unpublished Kinross Gold Corp. databases. Plate is formatted to be plottable on a 24"x36" page. Coordinate system is referenced in UTM NAD 27, zone 11.

Appendix 1

Stratigraphy of the North Mooney Basin

The stratigraphic section that comprises the North Mooney basin is approximately 4,750' (1,448 m) thick, however Carlin type gold mineralization always occurs within a narrow 600' (183 m) band (Figure 4). Favorable stratigraphy in conjunction with structure is necessary in controlling Carlin-type mineralization. Additionally, rheological contrasts between thick bedded limestone and shale units and the development of jasperoids influence structural development. Note that the mining industry in the United States typically uses the Imperial system of measurement which this study includes as unit thicknesses measured in feet.

Guilmette, Dg, (1150') (350.5 m)

The Devonian Guilmette limestone forms resistant topographic highs and is variably mineralized at its upper contact throughout the NMB At the base of the Guilmette a marker bed of 50' (15.2 m) of a regressive, slope-forming, yellow weathering siltstone to sandstone facies with a dolomitic matrix has been noted by various workers (R. Thorson, Internal Report, 2004; D. Schwarz, Internal Report, 2012) (Figure 4) and may outcrop in the West Royale pit (Figure 6). The middle Guilmette consists primarily of thick bedded to massive grainstones that are dark gray in color. The upper unit becomes increasingly thinly bedded, micritic, and brecciated in the upper 200' (61 m) (Rigby, 1960). The uppermost Guilmette has an irregular, conformable contact with the lower Pilot that consists of approximately 200' (61 m) of complex, multi-generational breccias which were initially karst breccias and were later modified by hydrothermal fluids. In the North Mooney Basin, the Dg/Mp contact is commonly brecciated in a 200'+ (60 m +) transitional zone with varying degrees of silicification (Thorson, unpublished written

communication, 2004). In mapping, silicified and brecciated units near the Dg/Mp contact are designated *Mp brxs* if predominantly siltstone and *Dg brxs* if predominantly limestone.

Pilot (Mp) (400') (122 m)

The Upper Devonian and Lower Mississippian Pilot formation is medium to dark gray to yellowish gray in color, thin to medium-bedded, platey, variably calcareous shale to siltstone with local thin-bedded limestone and rare chert interbeds. Weathered surfaces commonly display Liesegang banding (Rigby, 1960). Drill intercepts encounter zones that can be strongly carbonaceous or strongly argillized. The lower contact is commonly brecciated and silicified (Mp brxs), while the upper unit becomes increasingly calcareous and fossiliferous as it grades into the Joana limestone.

Joana (Mj) (100') (30.5 m)

The Joana unit is a medium gray coarse grainstone that weathers light grey to tan in color. Beds are 3" to 8" (7.6 to 20.3 cm) thick and locally contains up to 20% dark gray to black chert nodules and ribbons that are parallel to bedding. Crinoid fragments are common (Kleinhampl and Ziony, 1985). Complete sections measure approximately 100' (30.5 m) thick, however outcrops and drilling often record variable thicknesses (Rigby, 1960). In the North Mooney Basin area, the Joana limestone is often pervasively silicified and brecciated by replacement-style hydrothermal alteration and mapped as a jasperoid unit, Tj (see below).

Chainman (Mc, Mcl) (1100') (335.3 m)

The lowest Chainman unit, Mcl, is a 30' to 50' (9.1 to 15.24 m) thick transgressive unit above a weathered and weakly karsted upper Mj surface and consists of dark gray wackestone to micrite with diagnostic cross laminations and Nereites worm burrows. The middle and upper units become increasingly silty and thinly bedded with variably sandy and calcareous interbeds (Thorson, Internal

Report, 2004). This is a recessive formation and often occurs in the area as platy to blocky float fragments with smooth rounded edged and corners. The formation is variably silicified and organic rich.

The Chainman and Diamond Peak formations are largely part of the same major gradational depositional sequence (Harbaugh, 1980), however current Kinross geologists and my mapping reserve the Chainman formation designation for sequences dominated by shale and siltstone, while the Diamond Peak formation is dominated by sandstone and conglomerate.

Diamond Peak (Mdp) (2000') (610 m)

The Diamond Peak Formation at Bald Mountain contains arkosic sandstone to coarse pebble conglomerates with quartzite and chert clasts. It is poorly sorted and generally normally graded. The formation is a resistant ridge former, outcropping to the east of the Royale and Winrock deposits

Jurassic Bald Mountain stock (Jbm)

The Bald Mountain stock is dated at 159 Ma (Mortenson et al., 2000), composed of quartz monzonite porphyry, and has an associated dike swarm that is rarely noted within the North Mooney Basin. (Nutt and Hofstra, 2007).

Tertiary Jasperoid (Tj)

Jasperoid breccias are product of hydrothermal alteration where Paleozoic carbonates are pervasively silicified and dissolved by fluids associated with epithermal and Carlin-type gold systems. Jasperoids in the North Mooney basin are typically altered Mj, however they can also be calcareous horizons in the upper Mp or Mcl. The altered unit is commonly a ferruginous red color but can also be light to dark gray and variably brecciated. Sampled district and regional jasperoid units are always anomalously high in the suite of epithermal system elements (As, Sb, Hg, Ba, and Tl), but do not necessarily contain anomalous gold values (Nelson, 1990). Jasperoids are typically spatially associated with faults that act as conduits for hydrothermal fluids.

Tertiary Volcanics (Tv)

Early Oligocene through Miocene tuffs and intermediate composition flows occur throughout the district (Nutt and Good, 1998) and one widespread unit has been dated at 36 Ma (Nutt et al., 2000). Tertiary volcanics and volcaniclastics unconformably overlie Paleozoic rocks in the Duke and Winrock areas of North Mooney Basin. They are likely Miocene in age (Nutt et al., 2000), post-date mineralization, and have the greatest thicknesses in the structural graben of the central Mooney Basin.